REPORT DOCUMENTATION PAGE

AFRL-SR-AR-TR-04-

0391

1. REPORT DATE *(DD-MM-YYYY)*	2. REPORT TYPE	3. DATES COVERED *(From - To)*
29-05-2004	Final	3-06-2003 - 29-05-2004

4. TITLE AND SUBTITLE	5a. CONTRACT NUMBER
Analytical Systems Engineering Advanced Mathematics	F49620-03-C-0035
	5b. GRANT NUMBER
	5c. PROGRAM ELEMENT NUMBER

6. AUTHOR(S)	5d. PROJECT NUMBER
LaBarre, Robert, E.	
Banaszuk, Andrzej	5e. TASK NUMBER
	5f. WORK UNIT NUMBER

7. PERFORMING ORGANIZATION NAME(S) AND ADDRESS(ES)	8. PERFORMING ORGANIZATION REPORT NUMBER
United Technologies Research Center 411 Silver Lane East Hartford, CT 06108	

9. SPONSORING/MONITORING AGENCY NAME(S) AND ADDRESS(ES)	10. SPONSOR/MONITOR'S ACRONYM(S)
USAF, AFRL AF Office of Scientific Research 4015 Wilson Blvd Room 713 Arlington VA 22203-1954	AFOSR / DARPA
	11. SPONSOR/MONITOR'S REPORT NUMBER(S)

12. DISTRIBUTION/AVAILABILITY STATEMENT

Distribution Statement A. Approved for public release; distribution is unlimited.

13. SUPPLEMENTARY NOTES

14. ABSTRACT

This effort was concerned with identifying and assessing the primary technical barriers and risks that must be overcome to establish fast computational methods for uncertainty analysis in large models of interconnected components where the shape of system-level dynamics is important. The results of this study show tremendous promise for computationally efficient methods for propagating uncertainty. Numerous approaches were investigated on application problems from the control of afterburner combustion instabilities to modeling organic molecules and DNA. This contract also resulted in a highly successful workshop on the Design of Dynamical Systems Robust to Uncertainty, engaging experts from international communities.

15. SUBJECT TERMS

Uncertainty Propagation, Graph Decomposition, Spectral Balance, Dynamical Systems, Symmetry-breaking

16. SECURITY CLASSIFICATION OF:			17. LIMITATION OF ABSTRACT	18. NUMBER OF PAGES	19a. NAME OF RESPONSIBLE PERSON
a. REPORT	b. ABSTRACT	c. THIS PAGE	SAR	66	Dr. Andrzej Banaszuk
U	U	U			19b. TELEPHONE NUMBER *(Include area code)* (860) 610-7381

Standard Form 298 (Rev. 8/98)
Prescribed by ANSI Std. Z39.18

20040617 061

Analytical Systems Engineering
Advanced Mathematics

Contract #: F49620-03-C-0035

Contract Execution Date: 06/03/03

Principal Investigator: Dr. Andrzej Banaszuk

United Technologies Research Center
411 Silver Lane
East Hartford, Connecticut 06108

Table of Contents

United Technologies Research Center

1.0 Objectives

The objective of the effort as described in the proposal to DARPA/DSO was *to identify and assess the primary technical barriers and risks that must be overcome to establish fast computational methods for uncertainty analysis in large models of interconnected components where the shape of system-level dynamics is essential.* This objective was addressed through the following:

1. *Validate the technical hypothesis* that measure-theoretic algorithms (for network congestion in large systems of interconnected model components) could be used to radically accelerate the numerical simulation, identification of dynamic stability boundaries, model reduction and propagation of uncertainty during product design.
2. *Apply preliminary results to selected challenge problem applications* in (i) the design of organic molecules where shaping the conformational dynamics is essential to engineering their exploitable properties; and (ii) the control of afterburner combustion instabilities in gas turbine propulsion systems designed for advanced military aircraft.
3. *Champion advanced computational methods for the management of uncertainty* in large, interconnected systems where the control of dynamics is essential. Engage international communities of experts in mathematics and engineering to sharpen and articulate an actionable, mathematically rigorous approach for the development of *Analytic Systems Engineering* with the potential of broad impact on both the military and commercial sectors.

Table 1 describes our results and accomplishments during the contract period on each of the required contract task elements designed to achieve these objectives.

United Technologies Research Center

Table 1 – Task elements for contract F49620-03-C-0035

Task	Description	Status
Task A	Establish the correct technical framework for model-based uncertainty analysis using the interconnection (graph) structure between components.	**Completed** (see Publications 5, 6, and 7)
Task B	The analytical framework described in Task A will be used to access (i) the potential of the graph-theoretical methods for accelerating computational methods for estimating the propagation of uncertainty measure in interconnected model systems; and (ii) the technical obstacles and risks involved in designing, implementing, and testing numerical algorithms for model-based uncertainty management in the design of complex systems.	**Completed** (i) Addressed in Publications 5,6,7 (ii) Addressed in Publications 3,4
Task C	In collaboration with the DARPA/DSO program manager, specific model systems will be selected to investigate *where the connection structure arises from the physical proximity between the subunits.* The primary application domain will be the design and control of conformation dynamics in large organic molecules, although related problems will be considered.	Addressed in Section 3.7.1 and Publication 8
Task D	In collaboration with the DARPA/DSO program manager, specific model systems will be selected to investigate *where the connection structure arises from the virtual relationships between the subunits.* This will be a model of combustion instability that occurs in the augmentor in a high performance gas turbine engine for advanced military aircraft.	Addressed in Publication 2
Task E	For the selected model systems selected in Tasks C-D above, we will establish the computational complexity bounds as they scale with model size (e.g., as size of a model protein length or with the number of coupled interacting modes in a combustion system).	Addressed in part in Monte Carlo, Polynomial Chaos, and DNA work
Task F	Host a DARPA/DSO sponsored Workshop involving recognized experts in various areas of Mathematics and Engineering to evaluate the state-of-the-art and potential for fast techniques supporting uncertainty analysis in large, multi-scale dynamical systems with applications in computational biology, design of advanced weapon systems and information technology.	**Completed** Workshop held Jan. 15-16, 2004 at UTRC

United Technologies Research Center

2.0 Work Performed

A multi-faceted effort into the propagation of uncertainty in complex networked systems was conducted. This effort included:

1. Graph theoretic decomposition schemes for converting a large monolithic system of differential-algebraic equations into a collection of weakly coupled subsystems of strongly coupled equations. Computational benefits are achieved by solving less stiff systems in parallel.
2. Spectral balance methods for large coupled limit cycling systems for applications in aeroengine augmentor instability control.
3. Determination of density mapping techniques for propagation probability density functions through large systems of interconnected component models.
4. Uncertainty propagation schemes utilizing polynomial chaos methods for nonlinear systems with nontrivial dynamics.
5. Symmetry-breaking schemes, where we deliberately introduce spatial variations in the system parameters in order to change the stability properties.
6. Uncertainty propagation in dynamical systems involved in computational chemistry and molecular modeling.
7. DNA modeling, where we investigated dynamical systems where the connection structure arises from the physical proximity between the subunits.
8. Uncertainty in the dynamics of conservative maps, focusing on the standard map and a discrete Duffing oscillator in $\mathbf{R}^2$.

3.0 Accomplishments and New Findings

In the paragraphs that follow, we detail the key technical work done in conjunction with this contract. The work touched on a number of seemingly diverse topics, that, when taken in their entirety, form the basis for an analytic understanding of uncertainty propagation through large, interconnected systems.

3.1 Literature Search

An extensive literature search was performed in the area of uncertainty propagation with emphasis on dynamical systems that can be modeled as interconnected structures. Information was gathered in the areas of large, multiscale, highly interconnected systems where dynamics plays an important role. Papers were identified covering graph theoretic methods to preserve structure dictated by the local dynamics. Papers on spectral methods for invariant measure computations in dynamical systems were collected. Monte Carlo methods were reviewed. Investigations of newer techniques such as polynomial chaos and stochastic finite element analyses were collected. Existing methods in molecular modeling were reviewed. Literature on methods of harmonic analysis and describing functions in control and dynamical systems were reviewed. A study of existing software products that purport capabilities in uncertainty propagation was done. Most such

United Technologies Research Center

products are in the area of reliability analysis and/or probabilistic optimization. A repository of all identified documents is being maintained and all documents are available to all members of the technical and programmatic team.

3.2 Uncertainty Propagation

Uncertainty analysis is a research topic that has received much attention in recent years. Increased use of physics-based models in the study of dynamical systems, in a wide range of applications, calls for model prediction analyses and quantification in terms of uncertainties in descriptions and operating environments. In this section we focus on several advanced methods for propagating and evaluating the effects of uncertainty in complex dynamical model parameters and their initial conditions.

Polynomial Chaos (PC) (i.e. Stochastic Finite Elements) is an analytical approach based on expansions of uncertain quantities in terms of prescribed random basis functions. This methodology has received significant attention during recent years and has been applied to uncertainty propagation in complex dynamical systems, which are described by partial differential equation models. It has been demonstrated that for a certain class of problems arising in fluid mechanics, finite elements and/or chemical systems, PC can be considerably (up to several orders of magnitude) faster than Monte Carlo (MC) or similar methods. Furthermore, the analytical representation in the PC method can be of great benefit in system analysis.

3.2.1 Monte Carlo Methods

In the framework we proposed for uncertainty analysis of large nonlinear systems, the most important objects are invariant measures. These can always be computed using Monte Carlo methods, usually at a high cost. We studied application of Monte-Carlo methods in a set of dynamical systems with known asymptotic dynamics. Uncertain inputs and/or parameters were randomly sampled against some predetermined probability density functions and the model was run many times. A wide variety of sampling techniques were investigated, including pure random selection, randomized quasi-Monte Carlo techniques, and Latin hypercube methods. Approximately ten different probability density functions were identified to sample from in order to allow for a generalized technique. Additionally, the importance sampling methods were investigated, as well as Markov chain Monte Carlo methods.

It is well known that Monte Carlo methods, while guaranteed to work over the long run, are poorly suited to high dimensions (large numbers of uncertain inputs and/or parameters). Additionally, since numerous evaluations of the overall model are required, these methods suffer large penalties if the model evaluation is costly, either in time or in dollars. Finally, there is no appropriate way to allow the inherent structure induced on the problem by the physical nature of the problem to be useful in reducing the computational complexity. Monte Carlo techniques are the epitome of "black box" methods, were no

United Technologies Research Center

understanding of the model is used. Monte Carlo methods can be considered for lower dimensional base-line analyses, to measure improvements over other candidate approaches. Additionally, the method can be used in the cases when polynomial chaos expansion fails due to the compact nature of the asymptotic dynamics, to provide a simulation tool for measure propagation in localized dynamics.

3.2.2 Polynomial Chaos

In 1938, Wiener[1] investigated an approach he called "homogeneous chaos". This work was expanded by Ghanem and Spanos[2]. The idea is to project the variables of the problem onto a "stochastic space", spanned by a set of complete orthogonal polynomials that are functions of the random variables. The goal is to eliminate the large sample requirments of Monte Carlo methods, thereby dramatically reducing the computational requirement in the study of uncertainty propagation.

In Wiener's original work, his random variables were assumed normally distributed, and he used the Hermite polynomials as his basis functions. Xiu and Karniadakis[3] investigated alternative pairs of random variables and orthogonal polynomial basis functions, such as gamma distributed random variables with Laguerre polynomials.

Our efforts focused on developing an analytical understanding of these methods and identifying the class of problems where they may show promise and classes of problems where polynomial chaos methods are not suitable for uncertainty propagation. We have studied a hierarchy of models starting from simple linear models with parametric uncertainty, to limit cycling models with additive noise.

For a large class of smooth dynamical systems, these polynomial chaos methods are effective in markedly reducing the computational burden inherent in the Monte Carlo methods mentioned above. In our experience we have found two to three orders of magnitude reductions in computational effort. However, we have also found limitations. It was discovered, following earlier work by Karniadakis, that polynomial chaos expansions can break down if the asymptotic dynamics resides on a compact attractor for all (compactly supported) uncertain parameter values. A solution to this is proposed to be the development of spectral element methods tuned to the asymptotic dynamics of the nonlinear system under study. In addition, multiscale spectral element methods could be used to provide multiscale uncertainty propagation methods. This way, the substantial speed-up achieved by polynomial chaos methods can be preserved for asymptotically compact uncertain attractors. In addition, the above described utilization of the graph structure of the problem is used to render polynomial chaos methods useful for a class of large networked systems, where a brute-force expansion might fail due to a large number of uncertain parameters.

The truncated polynomial chaos expansion has a structure of an N-dimensional

United Technologies Research Center

dynamical system, where N is mxn, m is the dimension of the phase-space for the dynamical system under study and n is the order of truncation. We have proven some properties of the resulting dynamical system for the cases discussed above. In particular, it can be shown that for a compact uncertain attractor, the polynomial chaos expansion asymptotically diverges due to the fact that the output measure has its density in a "bad space".

References for this section: (Note: Each section has its own references, renumbered, starting at 1.)

[1] Wiener, N., "The homogeneous chaos", *Amer. J. Math.*, 60, pp. 897-936, 1938

[2] Ghanem, R., and Spanos, P., *Stochastic Finite Elements: A Spectral Approach*, Springer-Verlag, New York, 1991.

[3] Xiu, D. and Karniadakis, G.E., "The Wiener-Askey Polynomial Chaos for Stochastic Differential Equations", *SIAM J. Sci. Comp.*, Vol. 24, No. 2, pp. 619-644, 2002.

3.2.3 Density Mapping

Enhancing engineering performance and productivity through systematic and integrated designs that account for the effects of uncertainty is a key economic priority[1]. A unified paradigm, referred to as "Analytical Systems Engineering", recently formulated at the United Technologies Research Center, has identified uncertainty propagation through networks of nonlinear components as an essential component. This view is also echoed in [2] or in [3] (at the end of this secton), where large-scale, interconnected systems are designed using model-based techniques that employ uncertainty descriptions explicitly. Since all system models have varying levels of uncertainty [4], designers often use large safety margins, which result in more complex and expensive systems [5]. As a result, a natural path in modern systems design is to make decisions on the best system structure from the perspective of greater robustness to uncertainty.

Before moving towards design, addressing uncertainty analysis in a model-based complex engineering systems framework is important. This has traditionally been addressed by Monte Carlo (MC) like methods. This classic approach (see [6]) employs a large number of simulations with a random selection of variables from their prescribed distribution (parametric or empirical).

Unfortunately, uncertainty propagation techniques using MC methods, even in their advanced forms, do not scale well with system size. The natural choice in such cases is to break the large system into pieces. More precisely, the physics-based models, which are often converted to monolithic systems of uncertain nonlinear differential/algebraic equations, are to be decomposed using graph decomposition methods into subsystems evolving on different time scales, as mentioned in [7].

We find that the time scale separation can be exploited to increase computational efficiency when propagating input uncertainty in a subsystem-by-subsystem manner. This approach has been also advocated in [8], where arbitrary interconnections of multivariable systems (represented either in a continuous or discrete form) with nonlinear or linear dynamics (nonlinear time varying, distributed linear time invariant or lumped linear time invariant) are decomposed into aggregate, strongly connected subsystems. Following this procedure each subsystem is addressed using "the minimum set technique" and transformed into a typical feedback interconnection.

Alternatively, in [9], a Recursive Projection Method (RPM) is developed to solve nonlinear parameter problems for which the convergence is achieved for certain parameter values. The correction applied for divergent domains involves Newton's integration method. RPM provides reliable results, when the number of divergent modes is small comparative to the system's dimension. The algorithm has been successfully demonstrated on folds, bifurcations and unstable system branches. This approach is believed by its authors to greatly accelerate iteration convergence.

Similarly, extensions from the backward Euler formula, conventionally used to obtain a system of nonlinear algebraic equations from an original system of nonlinear algebraic differential equations, can be grouped under the waveform relaxation (WR) method. This technique has been successfully employed in [10] to address large scale systems, such as integrated circuits. The iterative WR method decomposes the system in several dynamical subsystems, which are independently analyzed for the entire time interval. This method comes with sufficient convergence guarantees, also revealed in [10].

In [11] graph theory is also used in the context of autocatalytic networks/sets to classify the uncertainty of the network and predict its influence over short and medium time-scales. Therefore, looking at how networks evolve with time, more precisely looking at their dynamics, it can be beneficial from a computation speed perspective. It is essential, when dealing with irreducible (i.e. strongly connected) graphs (e.g. dynamical subsystems), to perform related computations in corresponding time scales [12].

Finding a subset of the state space of a dynamical system where typical trajectories stay longer before entering different regions, conventionally called almost invariant sets [13], entitles a macroscopic behavior analysis of dynamical systems networks. In effect this separation permits individual sub-system uncertainty propagation studies. Algorithms for containment of such almost invariant sets are presented in [13].

To address slow convergence rate and clustering issues associated with Monte Carlo methods, new methods such as: polynomial chaos [14] (i.e. stochastic finite elements), stochastic surface response methods [15] and probabilistic collocation methods [16] were used with significant success. Complementing these approaches, the propagation of uncertainty in the distribution of initial conditions for a network of dynamical systems can be studied in an exact manner using Liouville's equation as in [17].

A bottleneck in the application of uncertainty propagation methods in a subsystem-by-subsystem way is associated with the existence of correlated signals due to typical parallel or feedback connections found in conventional subsystems. To address this issue, the propagation of uncertain inputs through interconnections of dynamical systems, with simple asymptotic behavior, was studied. The method of choice is a discrete density mapping, analogous to the input-output Perron-Frobenius operator.

The advocated method assumes that a large system is broken into components, which evolve on different timescales or have simple attractor structure. Then, uncertainty propagation methods are used to map the input distribution through components and arrive at a stationary density for the states/outputs of interest. In a chain topology only the need for a transfer operator is observed. This is in contrast with the parallel connection, which adds complexity through the necessity of summing correlated signals. In the case of feedback structures this complexity is further augmented by the requirement for convergence of the iterations.

An electronic version of this work in its full depth is included here. The same paper can be found in the appendix of the printed report and is entitled: *Propagation of Uncertain Inputs Through Networks of Nonlinear Components.*

References for this section:

[1] Helton, J.C., "Treatment of uncertainty in performance assessment for complex systems", *Risk Analysis*, vol. 14, no. 4, pp. 483-511, 1994.
[2] Wojtkiewicz, S.F., Eldred, M.S., Field, R.V., et al., "Uncertainty quantification in large computational engineering models", *AIAA-2001-1455*
[3] Axelsson, J., "Model based systems engineering using a continuous-time extension of the unified modeling language (UML)", *Systems Engineering*, vol. 5, no. 3, pp. 165-179, 2002.
[4] Carlson, J.M., and Doyle, J.C., "Highly optimized tolerance: Robustness and design in complex systems", *Physics Review Letters*, vol. 84, no. 11, pp. 2529-2532, 2000.
[5] Sage, A.P., "Systems engineering: Purpose, function, and structure", *The Journal of the International Council On Systems Engineering*, vol. 1, no. 1, pp. 1, 1998.
[6] Friedel, I., and Keller, A., "Fast generation of randomized low discrepancy point sets:, in *Monte Carlo and Quasi-Monte Carlo Methods 2000*, H. Niederreiter, K. Fang, and F. Hickernell, eds., Springer, pp. 257-273, 2000.
[7] Strogatz, S.H., "Exploring complex networks", *Nature*, vol. 410, pp. 268-276, 2001
[8] Callier, F.W., Chan, W.S., and Desoer, C.A., "Input-output stability of interconnected systems using decompositions: An improved formulation", *IEEE Transactions on Automatic Control*, vol. 23, no. 2, pp. 150-163, 1978.
[9] Shroff, G., and Keller, H.B., "Stabilization of unstable procedures: The recursive projection method", *SIAM J. Numer. Anal.*, vol. 30, no. 4, pp. 1099-1120, 1993.
[10] Lelarasmee, E., Ruehli, A.E., and Sangiovanni-Vincentelli, A.L., "The waveform relaxation method for time domain analysis of large scale integrated circuits", *IEEE Trans. On CAD of IC and Syst.*, vol. 1, pp. 131-145, 1982.
[11] Jain, S., and Krishna, S., *Graph Theory and the Evolution of Autocatalytic Networks*, chap. 16, Wiley – VCH, 2002.

United Technologies Research Center

[12] Vidyasagar, M., *Input-Output Analysis of Large-Scale Interconnected Systems: Decomposition, Well-Posedness & Stability*, Springer-Verlag, 1981.

[13] Froyland, G. and Dellnitz, M., "Detecting and locating near-optimal almost-invariant sets and cycles", *Society for Industrial and Applied Mathematics*, vol. 24, no. 6, pp. 1839-1863, 2003.

[14] Ghanem, R., and Spanos, P., *Stochastic Finite Elements: A Spectral Approach*, Springer, New York, 1991.

[15] Isukapalli, S.S., *Uncertainty Analysis of Transport-Transportation Models*, Ph.D. thesis, Rutgers University, 1999.

[16] Tatang, M.A., *Direct Incorporation of Uncertainty in Chemical and Environmental Engineering Systems*, Ph.D. thesis, Massachusetts Institute of Technology, 1995.

[17] Ehrendorfer, M., "The Liouville equation in atmospheric predictability", *Proceedings ECMWF Seminar on Predictability of Weather and Climate*, pp. 47-81, 2003.

3.3 Graph Decomposition

Complex physical systems often possess an inherent structure from which they derive the robustness of their behavior. For example, the DNA molecule has a strong backbone structure that allows global modes [1] and gene regulatory networks have a hierarchical structure that allows complex gene expressions [2]. Similarly, in complex engineering systems such as coordinated group of vehicles, sensor and communication networks are designed by interconnecting subsystems in a systematic manner. There is significant interest in robust design methods for complex, interconnected dynamical systems. The design of such systems can be significantly accelerated by using models for robustness assessment and redesign. This requires understanding how uncertainty in various parameters and the system model itself affects the model outputs. Computational methods such as Monte-Carlo, polynomial chaos and various modifications of these can be used to propagate probabilistic information from the inputs/parameters to the outputs of a static or dynamical system. Unfortunately, the computational effort for these methods scales poorly with system complexity and there is a strong need for efficient alternatives. A promising direction is the decomposition of a complex system using graph theoretic methods followed by block-by-block propagation with iterations when necessary.

Graph theoretic methods are used widely in control theory [3], computer science, and network systems. More recently, graph theoretic techniques have been employed in conjunction with set oriented numerical methods for computing the almost invariant sets of dynamical systems [4]. There is a close connection between Markov chain theory and graph theory [5]. We refer the reader to standard text books and/or review papers such as [6], [7] for basic notions from algebraic graph theory and graph algorithms such as spanning and induced subgraphs, cycles, connectedness of undirected graphs, strongly connectedness and topological sorting of directed graphs, adjacency, incidence and Laplacian matrices, the significance of the eigenvalues of these matrices, reducibility and irreducibility of the adjacency matrix, depth first search and breadth first search.

The aim of this effort was to introduce graph theoretic methods for decomposing a complex dynamical system into hierarchically and/or weakly connected subsystems for

United Technologies Research Center

the purpose of uncertainty propagation in systems. The structure resulting from graph decomposition with series, parallel or feedback connections among subsystems can be exploited for efficient methods for computation of uncertainty propagation [8]. In the paper included here (electronic version, and in the appendix in the print version of this report), entitled: *Graph Decomposition Methods for Uncertainty Propagation in Complex, Nonlinear Interconnected Dynamical Systems,* we briefly review a structural decomposition algorithm [3], [9] which employs the so-called equation graph of a dynamical system and identifies the subsystems and the associated hierarchy.

References for this section:

[1] Mezic, I., "DNA clues for design of robust, flexible networks", UCSB preprint, 2004.
[2] Stark, J., Callard, R., and Hobank, M., "From the top down: Towards a predictive biology of signaling networks," *Trends in biotechnology,* vol. 21, pp. 290–293, 2003.
[3] Callier, F.M., Chan, W.S., and Desoer, C.A., "Input-output stability theory of interconnected systems using decomposition techniques," *IEEE Transactions on Circuits and Systems,* vol. 23, no. 12, pp. 714–729, 1976.
[4] Dellnitz, M., and Preis, R., *Symbolic and Numerical Scientific Computation,* ser. Lecture Notes in Computer Science, 2630. Springer, 2003, ch. Congestion and almost invariant sets in dynamical systems, pp. 183–209. [Online]. Available: http://mathwww.upb.de/ agdellnitz/papers/congestion.ps.gz
[5] Jarvis, J.P., and Shier, D.R., *Applied Mathematical Modeling: A Multidisciplinary Approach.* CRC Press, 1999, ch. 17. Graph-Theoretic Analysis of Finite Markov Chains, pp. 271–289.
[6] Godsil, C., and Royle, G., *Algebraic Graph Theory.* Springer, 2001.
[7] Merris, R., "Laplacian matrices of graphs: A survey," *Linear Algebra and Its Applications,* vol. 197–198, pp. 143–176, 1994.
[8] Huzmezan, M., and Kalmar-Nagy, T., "Propagation of uncertain inputs through networks of nonlinear components," in *Proc. of the IEEE CDC,* Bahamas, December 2004, (submitted).
[9] Mezic, I., "Coupled nonlinear dynamical systems: Asymptotic behavior and uncertainty propagation," 2004, submitted to CDC 2004.

3.4 Spectral Balance

Many industrial flows involve complex interactions of acoustic waves, vorticity, fuel transport, and chemical reactions. The control objective often is to create beneficial non-equilibrium dynamics with control. Examples include control of flow separation and mixing enhancement. Our effort here focused on a frequency domain framework for analysis and non-equilibrium control design for a large class of models of physical phenomena involving multiple oscillatory modes coupled through nonlinear terms and/or transport delay, that are driven by broad-band disturbances. While motivated by specific problems arising in military aeroengines, the methods developed are applicable to a large class of distributed dynamical systems involving oscillatory dynamics with nonlinear cross-coupling, saturated nonlinearities, transport delay, and broad-band disturbances. The *spectral balance* framework that we developed generalizes the standard harmonic balance and Gaussian signal balance in feedback systems [1], [2]. The framework was

United Technologies Research Center

introduced and illustrated in an example of a nonlinear system that exhibits noise-induced transitions between two stable equilibria. The example presented was a scalar model with cubic nonlinearity after a pitchfork bifurcation driven by a broad-band disturbance. An approximate and iterative spectral balance of the constant and broad-band signals (including determination of equilibria) was solved. The solution of this approximate spectral balance was used to reformulate the original model using a loop transformation so that an iterative procedure for finding the spectrum of the output converges to the true spectrum.

An electronic version of this work in its full depth is included here. The same paper can be found in the appendix of the printed report and is entitled: *Spectral balance: A frequency domain framework for analysis of nonlinear dynamical systems.*

References for this section:

[1] Mees, A.I., "Describing functions: Ten years on", *IMA J. Applied Mathematics*, vol. 32, pp. 221-233, 1984
[2] Gelb, A., and Vender Velde, W.E., *Multiple-Input Describing Functions and Nonlinear Systems Design*, McGraw-Hill, 1968.

3.5 Convergence

Robust design of complex, interconnected systems requires efficient computational methods for uncertainty propagation. Knowledge of the probability distribution function (pdf) of key output variables derived from the knowledge of input variables enables better decision making during design. Existing methods for propagation of uncertainty such as Monte-Carlo, polynomial chaos and stochastic surface response methods scale poorly with problem size and are computationally very demanding for complex systems [1].

In order to overcome the barrier of computational effort, a new approach based on decomposition of complex systems has been emerging as a promising direction. In this approach, a complex system is first decomposed using graph theoretic methods into subsystems connected in series, parallel or feedback [2]. Then, a block-by-block propagation is performed accounting for the dependencies among variables [3]. Such a method exploits the underlying hierarchical structure of a complex system and provides the flexibility to use different methods for different subsystems of the original system.

Feedback loops at the system level, or encompassing a large number of subsystems, pose a significant risk to the block-by-block framework since the structural decomposition methods described in [2] identify the feedback loops as a single subsystem. The

decomposition method based on the Jacobian value and the associated graph Laplacian, also described in [2], can identify weak feedback connections only. However, moderate to strong feedback *due to a controller* is common in many engineering systems. The ability to propagate uncertainty through such feedback loops block-by-block without having to solve the closed loop system in entirety is very attractive. Thus, there is a need for alternative approaches to speeding up the computation for uncertainty propagation in feedback systems.

In this work, we developed an iterative method to compute the probability density function of the output of a feedback loop from the probability density function of the input. We derived the problem setup and formulated the iteration equations by abstracting a computational scheme conceived and implemented by Huzmezan and Kalmar-Nagy [3]. We proved the point-wise convergence of the iteration to the true closed loop probability density function under the assumption that the loop operator was contractive.

Additionally, we considered the case where there is additional parametric uncertainty in the loop operator. We showed that the problem could be cast as a system of iterated random functions. Based on the results in [4,5], we claim that the iteration converges to the solution of the closed loop probability density function under the assumption that the loop operator is contractive on an average. The proof of this claim and extension to dynamic systems will be considered in future work.

An electronic version of this work in its full depth is included here. The same paper can be found in the appendix of the printed report and is entitled: *An Iterative Method for Propagation of Probability Distributions in Feedback Systems.*

References for this section:

[1] Runolfsson, T., Mezic, I., and Myers, M., "Uncertainty analysis of dynamical systems," in *Proc. of the SIAM Conf. on Application of Dynamical Systems*, 2003.

[2] Varigonda, S., Kalmar-Nagy, T., LaBarre, B., and Mezic, I., "Graph decomposition methods for complex, interconnected dynamical systems," in *Proc. of the IEEE CDC*, Bahamas, 2004, (submitted).

[3] Huzmezan, M., and Kalmar-Nagy, T., "Propagation of uncertain inputs through networks of nonlinear components," in *Proc. of the IEEE CDC*, Bahamas, December 2004, (submitted).

[4] Diaconis, P., and Freedman, D., "Iterated random functions," *SIAM Review*, vol. 41, pp. 45–76, 1999.

[5] Jarner, S.F., and Tweedie, R., "Locally contracting iterated functions and stability of markov chains," *J. Appl. Prob.*, vol. 38, pp. 494–507, 2001. [Online]. Available: http://www.maths.lancs.ac.uk/ jarner

United Technologies Research Center

3.6 Conservative Systems

This work studied the effect of uncertainty, using random perturbations, on area preserving maps of $\mathbf{R}^n$ to itself. The focus was on the standard map and a discrete Duffing oscillator in $\mathbf{R}^2$ as specific examples. We related the level of uncertainty to the large-scale features in the dynamics in a precise way. We also studied the effect of such perturbations on bifurcations in such maps. The main tools used for these investigations was a study of the eigenfunction and eigenvalue structure of the associated Perron-Frobenius operator along with set oriented methods for the numerical computations.

Uncertainty is obviously of central importance for dynamic and control systems both from a theoretical and a practical point of view. While this topic has received much attention in the control community, there is still much to learn about the effect of random perturbations on such systems. This work focused our attention on perturbations of conservative system as a first step towards studying mechanical systems (including molecular systems) in the presence of uncertainty. An important aspect of our approach was to try to extract the key dynamical features that survive in a noisy environment. One can make the case that such features are the most important ones to compute.

An electronic version of this work in its full depth is included here. The same paper can be found in the appendix of the printed report and is entitled: *Uncertainty in the Dynamics of Conservative Maps.*

This work showed that one could effectively use the theory and computation associated with the Perron-Frobenius operator to study the effect of uncertainty on area preserving maps and illustrated the methods on the standard map and the discrete Duffing oscillator. The level of uncertainty was related in a quantitative way to the large-scale features, often ones that are the most important to compute. This work also studied the way in which uncertainty affects the bifurcation of such maps.

3.7 Applications

3.7.1 DNA

We investigated the dynamics of DNA molecules using a coarse-grained model presented in [1]. In particular we analyzed the robustness of the beneficial DNA dynamics with respect to uncertainty in the model parameters and the initial conditions. It

was found that the DNA model shows a remarkable robustness of the beneficial dynamics to uncertainty in model parameters and the initial conditions. The beneficial behavior enables coding of the genetic material and involves a synchronous behavior of the molecules.

Reference for this section:

[1] Yakushevich, L.V., Savin, A.V., and Manevitch, L.I., "Nonlinear dynamics of topological solitons in DNA," *Physical Review E 66, 016614*, 2002.

3.7.2 Molecular Models

We summarize the efforts made in the following three areas of molecular modeling in the context of uncertainty analysis:

(a) We have identified systems in molecular mechanics for conformational analysis by classical molecular dynamics. The globally optimum configuration is subject to uncertainty in the inter-atomic potential. We propose to test polynomial chaos on classical molecular dynamics calculations on the nitrogen molecule and the more complicated trimer molecule CS_2.

(b) We have been studying the quantification of uncertainty in classical and quantum molecular dynamics theories in relation to property predictions in molecular systems. These theories involve the simulation of dynamical systems in time that may cover such processes as bond-breaking, bond-formation, chemical reaction, and diffusion. These theories are general but our ultimate application targets are in such areas as proton diffusion in PEM fuel cell membranes and hydrogen absorption in metal-hydride materials for hydrogen storage. A fundamental issue is uncertainty propagation in these dynamical systems. The uncertainty arises in parameters pertaining to the semi-empirical force-fields if classical molecular dynamics are used; this can affect the accuracy of transport properties, such as diffusivity, estimated by molecular dynamics. We have identified this issue as a first problem to be rigorously analyzed by polynomial chaos methods. We plan to compute the errors in the diffusivity obtained from classical molecular dynamics calculations subject to random errors in the parameters comprising the functional form of the inter-atomic potential. We plan to start with a simple Lennard-Jones system with uncertainty in the collision diameters and the well- depths and propose to extend the study to cover more sophisticated potentials for metal-ceramics of interest to UTC and solid-oxide fuel cells within the context of polynomial chaos.

(c) When molecular modeling calculations are done at a more fundamental level (e.g., Hohenberg-Kohn density functional theory at the electronic level) there is the uncertainty in the form of the exchange- correlation functional. Despite forty years of density functional theory, the local density approximation and the generalized gradient approximations are the only parameterizations available for the exchange correlation functional. We know that these are not satisfactory for instance in the

United Technologies Research Center

accurate calculations of cohesive energies, reaction barrier heights etc. The application of polynomial chaos to study uncertainty propagation due to the exchange correlation functional is an excellent idea. But, it cannot be done without an understanding of the uncertainty in the density functional. We propose to consider using the semi-empirical density functionals that the chemists have constructed by fitting a guessed at form with parameters to the results of configuration-interaction computations for small molecular systems. This can be taken as a standard for comparisons. Then the various physically motivated functionals would deviate from that standard, and one could study the propagation of those deviations through the Car-Parrinello quantum dynamics computation. This area is of interest to UTC as Car-Parrinello calculations are used in hydrogen storage calculations and in the calculation of chromia ion migration in the cathodes of solid oxide fuel cells.

An electronic version of this work in its full depth is included here. The same paper can be found in the appendix of the printed report and is entitled: *Dynamics in Molecular Modelling and the Scope for Uncertainty Analysis by Dellnitz-Preis and Polynomial Chaos Methods.*

3.7.3 Aeroacoustics

For this application we studied a thermo-acoustic model on a cylindrical or annular geometry, capable of modeling instabilities of tangential acoustic modes. The model accounts for nonuniform density, damping, rotational flow, and heat-release coupling. It is shown that deliberately introducing spatial variations in some quantities has a similar effect to adding damping to the system. The effects of these symmetry-breaking concepts are evaluated on the model through linear analysis and the net amount of additional damping is computed. We show how various symmetry-breaking concepts are robust with respect to the uncertainty in the model parameters and we examine propagation of uncertainty with respect to a recently defined measure of uncertainty.

Thermo-acoustic instabilities in gas turbine and rocket engines develop when acoustic waves in combustors couple with an unsteady heat-release field in a positive feedback loop. For a summary of active control of thermo-acoustic instabilities see [3]. Thermo-acoustic modeling and control is well-studied for axially extended combustion chambers, as in [5], [7], [14], [10], where the acoustic to heat release coupling is dominated by longitudinal acoustic modes. However, comparably less attention has focused on thermo-acoustic modeling in combustion chambers with annular or cylindrical geometries. Our efforts for the aeroacoustic application focused on the development a low-order thermo-acoustic model on a circular geometry, similar to that of [1].

Often thermo-acoustic instabilities are dominated by a few natural acoustic modes, which can accurately be modeled with a low-dimensional model. Accurate heat-release models are difficult and time-consuming to implement. A low-order thermo-acoustic model, properly calibrated with acoustic data, can provide insight into the possibly deleterious acoustic-heat-release coupling and may provide a platform for fast evaluation of preliminary design concepts.

We began be defining *symmetry-breaking* as the deliberate introduction of spatial variations in the system parameters in order to change the stability properties. Recent work has focused on analysis of heterogeneous distributed systems [6],[9],[11]. Symmetry-breaking is commonly referred to as mistuning in the literature regarding the dynamics of arrays of turbine blades on a disk. Studies of stability properties of turbine blade flutter through the introduction of spatial nonuniformities has appeared in [2], [16]. Optimal mistuning in arrays of bladed disks has appeared in [15], [17]. A study of the effects of asymmetry on compressor stall inception has appeared in [8].

As in the case of mistuning in arrays of bladed disks in turbines, this form of passive control is often more feasible than implementing an active control scheme. This may also be true for the case in combustion chambers, where high temperatures prohibit adequate sensing and may damage the actuators required for active control. Furthermore, We have found that symmetry-breaking can be a more cost-effective means of stability enhancement.

An electronic version of this work in its full depth is included here. The same paper can be found in the appendix of the printed report and is entitled: *Symmetry-Breaking and Uncertainty Propagation in a Reduced Order Thermo-acoustic Model.*

References for this section:

[1] Banaszuk, A., Hagen, G., Mehta, P., and Oppelstrup, J., "A linear model for control of thermoacoustic instabilities on an annular domain", *Proceedings of the IEEE Conference on Decision and Control*, 2003.
[2] Bendiksen, O.O., "Localization phenomena in structural dynamics", *Chaos, Solitons, and Fractals*, vol. 11, pp. 1621-1660, 2000.
[3] Candel, S.M., "Combustion instabilities coupled by pressure waves and their active control", *Fourth International Symposium on Combustion, The Combustion Institute*, pp. 1277-1296, 1992.
[4] Culick, F.E., "Nonlinear behavior of acoustic waves in combustion chambers", Parts I and II. *Acta Astronautica*, vol. 3, pp. 715-757, 1976.
[5] Dowling, A.P., "Nonlinear self-excited oscillations of a ducted flame", *Journal of Fluid Mechanics*, vol. 346, pp. 271-290, 1997.
[6] Dullerud, G. and D'Andrea, R., "Distributed control of inhomogeneous systems with boundary conditions", *Proceedings of the 38th IEEE Control Conference on Decision and Control*, pp. 186-190, 1999.
[7] Fleifl, M., Annaswamy, A.M., Ghoneim, Z.A., and Ghoniem, A.F., "Response of a laminar premixed flame to flow oscillations: A kinematic modal and thermoacoustic instability results", *Combustion and Flame*, vol. 106, pp. 487-510, 1996.

[8] Graf, M.B., Wong, T.S., Greitzer, E.M., Marble, F.E., Tan, C.S., Shin,H.W., and Wisler, D.C., "Effects of nonaxisymmetric tip clearance on axial compressor performance and stability", *Transactions ASME Journal of Turbomachinery*, 1998.

[9] Hagen, G., "Absolute stability of a heterogeneous semilinear dissipative parabolic pde", *Submitted to the 43rd IEEE Conference on Decision and Control*, 2004.

[10] Jacobson, C.A., Khibnik, A.I., Banaszuk, A., Cohen, J., and Proscia, W., "Active control of combustion instabilities in gas turbine engines for low emissions, Part 1: Physics-based and experimentally identified models of combustion instability", *AVI*, 2000.

[11] Jovanovic, M.R., Bamieh, B., and Grebeck, M., "Parametric resonance in spatially distributed systems", *Proceedings of the 2003 American Control Conference, Denver, CO.*, pp. 119-124, 2003.

[12] Mezic, I., and Runolfsson, T., "Uncertainty analysis of complex dynamical systems", *To appear in Proceedings of the 2004 American Control Conference*, 2004.

[13] Morse, P.M., and Ingard, K.U., *Theoretical Acoustics*. Princeton University Press, 1968.

[14] Peracchio, A., and Proscia, W., "Nonlinear heat release/acoustic model for thermo-acoustic instability in lean premixed combustors", *ASME paper 98-GT-269*, 1998.

[15] Petrov, E.P., Vitali,R., and Haftka, R.T., "Optimization of mistuned bladed discs using gradient-based response surface approximations", *AIAA-2000-1522*, 2000.

[16] Rivas-Guerra, A.J., and Mignolet, M.P., "Local/global effects of mistuning on the forced response of bladed disks", *Journal of Engineering for Gas Turbines and Power*, vol. 125, pp. 1-11, 2003.

[17] Shapiro, B., "A symmetry approach to extension of flutter boundaries via mistuning",. *Journal of Propulsion and Power*, vol. 14, no. 3, pp. 354-366, 1998.

4.0 Personnel Supported

UTRC Personnel:

Dr. Andrzej Banaszuk, Principal Engineer & Project Manager
Dr. Robert LaBarre, Principal Mathematician
Dr. Tamas Kalmar-Nagy, Research Engineer
Dr. Mihai Huzmezan, Senior Research Engineer
Dr. Subbarao Varigonda, Research Engineer
Dr. Prahant Mehta, Research Engineer
Dr. Gregory Hagen, Research Engineer
Dr. Mark Myers, Fellow
Dr. Hubertus Tummerscheit, Research Engineer
Dr. Prasana Venkatesh, Research Engineer
Dr. Igor Fedichenia, Research Engineer
Dr. Mihai Dorobantu, Project Leader

External Personnel:

Dr. Jerrold Marsden, Professor, California Institute of Technology
Dr. Igor Mezic, Professor, University of California – Santa Barbara
Dr. Michael Dellnitz, University of Paderborn & djs^2 GmbH
Mr. Mirko Hessel, University of Paderborn & djs^2 GmbH

Additional interactions with:

Dr. Yannis Kevrekedis, Princeton University (Myers)
Dr. Roger Ghanem, Johns Hopkins University (Mezic)
Dr. Oliver Junge, University of Paderborn (Marsden, Mezic, Tummerscheit)

5.0 Publications

[1] Banaszuk, A., Mezic, I., and Mehta, P., "Spectral Balance: Frequency Domain Framework for Analysis of Nonlinear Dynamical Systems with Noise", Submitted to the *43rd IEEE Conference on Decision and Control*, December 2004.

[2] Hagen, G., and Banaszuk, A., "Symmetry-Breaking and Uncertainty Propagation in Reduced Order Thermo-acoustic Model", Submitted to the *43rd IEEE Conference on Decision and Control*, December 2004.

[3] Huzmezan, M., and Kalmar-Nagy, T., "Propagation of Uncertain Inputs Through Networks of Nonlinear Components", Submitted to the *43rd IEEE Conference on Decision and Control*, December 2004.

[4] Junge, O., Marsden, J.E., and Mezic, I., "Uncertainty in Dynamics of Conservative Maps", Submitted to the *43rd IEEE Conference on Decision and Control*, December 2004.

[5] Mezic, I., "Coupled Nonlinear Dynamical Systems: Asymptotic Behavior and Uncertainty Propagation", Submitted to the *43rd IEEE Conference on Decision and Control*, December 2004.

[6] Varigonda, S., "An Iterative Method for Propagation of Probability Distributions in Feedback Systems", Submitted to the *43rd IEEE Conference on Decision and Control*, December 2004.

[7] Varigonda, S., Kalmar-Nagy, T., LaBarre, R., and Mezic, I., "Graph Decomposition Methods for Uncertainty Propagation in Complex, Nonlinear Interconnected Dynamical Systems", Submitted to the *43rd IEEE Conference on Decision and Control*, December 2004.

[8] Venkatesh, P., "Dynamics in Molecular Modelling and the Scope for Uncertainty Analysis by Dellnitz-Preis and Polynomial Chaos", Internal UTRC Report, August 2003.

6.0 Interactions / Transitions

(a) Meetings / Conferences

1. SIAM meeting on Mathematics in Industry, Toronto, Canada – October 2003, Minisymposium on *Uncertainty Analysis in Dynamical Systems*

2. Center for Multiscale Modeling and Simulation (CIMMS), Caltech – October 2003. *Uncertainty Analysis in the Design of Dynamical Systems*

3. *Design of Dynamical Systems Robust to Uncertainty*, DARPA/UTRC Workshop, January 2004

    Electronic version of the program is included here. The program is also included in the appendix of the printed report.

    9

4. 43rd IEEE Conference on Decision and Control, December 2004.

(b) Advisory Functions

    None

(c) Transitions

    The symmetry breaking concepts to reduce sensitivity of dynamical systems to uncertainty developed under this contract were applied in two internally funded projects to investigate design of aeroengine combustors robust to thermoacoustic instabilities.

    Using advanced mathematical concepts developed for uncertainty propagation through dynamical systems UTRC and PW are currently looking at validation and verification (V&V) of model based controllers for life extension of hybrid systems such as gas turbines.

7.0 Appendix

Propagation of Uncertain Inputs Through Networks of Nonlinear Components

Mihai Huzmezan, *Senior Member, IEEE,* and Tamás Kalmár-Nagy, *Member, IEEE*

(Invited Paper)

Abstract—Physics based models are often converted to monolithic systems of uncertain nonlinear differential/algebraic equations. Graph decomposition methods can be used to decompose such system into subsystems evolving on different time scales. This time scale separation can be exploited to increase computational efficiency when propagating input uncertainty in a subsystem-by-subsystem manner. In this paper the propagation of uncertain inputs through series, parallel and feedback interconnections of dynamical systems with simple asymptotic behavior is studied by employing discrete density mapping (analogous to the input-output Perron-Frobenius operator). A process control example is used to illustrate the method.

Index Terms—Perron-Frobenius, Density Mapping, Uncertainty Propagation, Networks of Dynamical Components

I. INTRODUCTION

Enhancing engineering performance and productivity through systematic and integrated designs that account for the effects of uncertainty is a key economic priority [1]. A unified paradigm, the "analytical systems engineering", recently formulated at the United Technologies Research Center, has identified uncertainty propagation through networks of nonlinear components as an essential component. This view is also echoed in [2] or in [3], where large-scale, interconnected systems are designed using model-based techniques that employ uncertainty descriptions explicitly. Since all system models have varying levels of uncertainty [4], designers often use large safety margins, which result in more complex and expensive systems [5]. As a result, a natural path in modern systems design is to make decisions on the best system structure from the perspective of greater robustness to uncertainty.

Before moving towards design addressing uncertainty analysis in a model-based complex engineering systems framework is important. This has been traditionally been addressed by Monte Carlo (MC) like methods. This classic approach (see [6]) employs a large number of simulations with a random selection of variables from their prescribed distribution (parametric or empirical).

Unfortunately, uncertainty propagation techniques using MC methods, even in their advanced forms, do not scale well with system size. The natural choice in such cases is to break the large system into pieces. More precisely, the physics based models, which are often converted to mono-

United Technologies Research Center
411 Silver Lane, East Hartford, CT -06108, USA
Phone: +1 860 610-7620, email: huzmezm@utrc.utc.com
United Technologies Research Center
411 Silver Lane, East Hartford, CT -06108, USA
Phone: +1 860 610-2189, email: kalmart@utrc.utc.com

lithic systems of uncertain nonlinear differential/algebraic equations, are to be decomposed using graph decomposition methods into subsystems evolving on different time scales, as mentioned in [7].

In the authors' view the time scale separation can be exploited to increase computational efficiency when propagating input uncertainty in a subsystem-by-subsystem manner. This approach has been also advocated in [8], where arbitrary interconnections of multivariable systems (represented either in a continuous or discrete form) with nonlinear or linear dynamics (nonlinear time varying, distributed linear time invariant or lumped linear time invariant) are decomposed into aggregate, strongly connected subsystems. Following this procedure each subsystem is addressed using "the minimum set technique" and transformed into a typical feedback interconnection.

Alternatively, in [9], a Recursive Projection Method (RPM) is developed to solve nonlinear parameter problems for which the convergence is achieved for certain parameter values. The correction applied for divergent domains involves Newton's integration method. RPM provides reliable results, when the number of divergent modes is small comparative to the system's dimension. The algorithm has been successfully demonstrated on folds, bifurcations and unstable system branches. This approach is believed by its authors to greatly accelerate iteration convergence.

Along the same thinking path, extensions from the backward Euler formula, conventionally used to obtain a system of nonlinear algebraic equations from an original system of nonlinear algebraic differential equations, can be grouped under the waveform relaxation (WR) method. This technique has been successfully employed in [10] to address large scale systems, such as integrated circuits. The iterative WR method decomposes the system in several dynamical subsystems, which are independently analyzed for the entire time interval. This method comes with sufficient convergence guarantees, also revealed in [10].

In [11] graph theory is also used in the context of autocatalytic networks/sets to classify the uncertainty of the network and predict its influence over short and medium time-scales. Therefore, looking at how networks evolve with time, more precisely looking at their dynamics, it can be beneficial from a computation speed perspective. It is essential, when dealing with irreducible (i.e. strongly connected) graphs (e.g. dynamical subsystems), to perform related computations in corresponding time scales [12].

Finding a subset of the state space of a dynamical system where typical trajectories stay longer before entering different regions, conventionally called almost invariant sets [13],

entitles a macroscopic behavior analysis of dynamical systems networks. In effect this separation permits individual sub-system uncertainty propagation studies. Algorithms for containment of such almost invariant sets are presented in [13].

To address slow convergence rate and clustering issues associated with Monte Carlo methods, new methods such as: polynomial chaos [14] (i.e. stochastic finite elements), stochastic surface response methods [15] and probabilistic collocation methods [16] were used with significant success. Complementing these approaches, the propagation of uncertainty in the distribution of initial conditions for a network of dynamical systems can be studied in an exact manner using the Liouville's equation as in [17].

A bottle neck in the application of uncertainty propagation methods in a subsystem-by-subsystem way is associated with the existence of correlated signals due to typical parallel or feedback connections found in conventional sub-systems. To address this issue, in this paper, the propagation of uncertain inputs through interconnections of dynamical systems, with simple asymptotic behavior, is studied. The method of choice is a discrete density mapping, analogous to the input-output Perron-Frobenius operator.

The advocated method assumes that a large system is broken into components, which evolve on different timescales or have simple attractor structure. Then, uncertainty propagation methods are used to map input distribution through components and arrive to a stationary density for the states/outputs of interest. In a chain topology only the need for a transfer operator is observed. This is in contrast with the parallel connection, which adds complexity through the necessity of summing correlated signals. In the case of feedback structures this complexity is further augmented by the requirement for converge of the iterations.

Following the introduction, Section II makes reference to chains, parallel and feedback connections which are approached with the density mapping method described in Section III. In Section III B convergence guarantees are addressed. To illustrate the method an industrial process control example abstraction is offered in Section IV. The conclusions are stated in Section V.

II. SIGNAL FLOW DECOMPOSITION: CHAINS, PARALLEL AND FEEDBACK CONNECTIONS

The starting assumption for the uncertainty propagation method application is that a nonlinear system under investigation is broken into interconnected components.

In this case the simplest topology that can arise is a chain, as shown in Figure 1. In this case the output of a block serves as input to the following block. If the input-output maps f_1, f_2, ... are known for all blocks, then the output of the chain can simply be calculated as the composition of these maps $f_1 \circ f_2 \circ ...$ acting on the input of the first block. To consider uncertain inputs, it is necessary to extend the notion of single input-output mapping to probability densities. The resulting formalism, analogous to the Perron-Frobenius operator is discussed below.

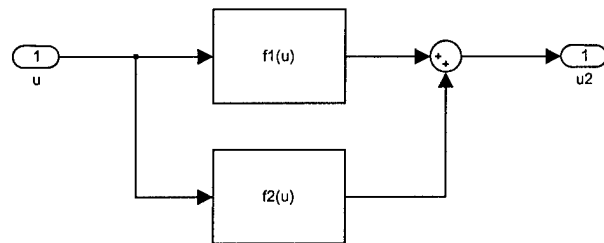Fig. 1. Density propagation through chains

Fig. 2. Parallel summation

The computational advantage of propagating input densities in a block-by-block manner, which corresponds to the composition of maps, becomes clear when the dynamics of different blocks include completely different timescales. Complications arise when considering a parallel connection, see Figure 2. In this case, the resulting probability densities (output uncertainties) have to be summed. For densities of independent random variables, this operation would be a simple convolution. However, when these densities are dependent, correlation information should be used to sum them correctly, fact also discussed in the next section.
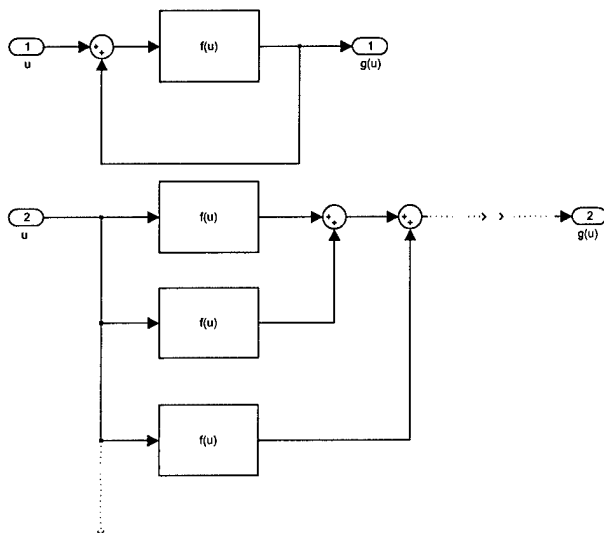

Fig. 3. Feedback loop with loop operator G

Finally, the feedback connection, shown in Figure 3, can be thought of as infinite series of parallel connections for which the convergence aspects are discussed in Subsection B.

III. THE DENSITY MAPPING METHOD

The paper proposes a simple algorithm that can be used to propagate input uncertainty through nonlinear compo-

nents. While this algorithm can be thought of as a simple implementation of the Perron-Frobenius operator [18], it has been extended to account for the mapping of the distribution support (akin to cell-to-cell mapping [19]). This extension was necessary to enable operations with correlated densities (e.g. parallel or feedback loop connections).

To understand the proposed technique first we review the Perron-Frobenius operator of a scalar map in the context of the proposed input-output uncertainty mapping. The one-dimensional map:

$$u_{n+1} = f(u_n) \qquad (1)$$

corresponds to the action of a block upon u_n, the system input. This action results by applying on u_n the mapping corresponding to the asymptotic dynamics of the system f and has as result u_{n+1}, the output. The uncertainty of u_n will be represented by its probability density G. Therefore the map has a corresponding Perron-Frobenius operator U acting on G:

$$G_{n+1} = UG_n = \int \delta(u - f(x)) G_n(x) dx =$$

$$= \sum_\alpha \frac{G_n(f_\alpha^{-1}(u))}{|f'(f_\alpha^{-1}(u))|} \qquad (2)$$

where the summation should be taken over all inverse branches $f_\alpha^{-1}(u)$.

g(u)
G(U)
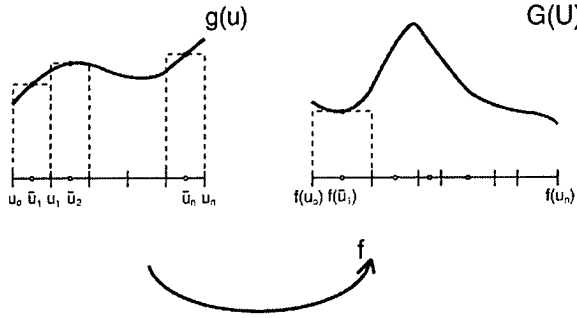
Fig. 4. Density mapping

In the following a straightforward numerical implementation of this mapping is described. Taking a cell-based approximation of the input probability density (histogram) $\{(\tau_i, \tau_{i+1}), G_i\}$ with cell-width w a collection of rectangles (bins) is produced. Consecutively the mapping f is applied to the corner points of all rectangles. Their resulting heights are derived from the density conservation condition. This procedure yields a new set

$$\{(f(\tau_i), f(\tau_{i+1})), h_i\} \qquad h_i = \frac{G_i w}{|f(\tau_i) - f(\tau_{i+1})|} \qquad (3)$$

If the map f is many-to-one, this collection will contain overlapping rectangles.

The overall output density can be produced by 're-binning', a procedure which involves finding the total area

over a bin on the support of the resulting distribution $[\min f(\tau_i), \max f(\tau_i)]$. This corresponds to summing over the inverse branches of the map. Re-binning is useful when propagating densities in a system with chain topology. On the other hand, re-binning destroys information about the mapping of the original support into the support of the output in the same fashion as polynomial chaos methods. This information is crucial when dealing with densities mapped through parallel or feedback connections.

A. Summing Correlated Probability Densities

Consider the parallel connection shown in Figure 2. At the summing junction we have two lists $\{(f_1(x_i), f_1(x_{i+1})), h_i\}$, $\{(f_2(x_i), f_2(x_{i+1})), h_i\}$ produced from the same input density G. Note that the lists contain the same h_i's, because of the density conservation. Consequently, to produce the parallel structure output density, the sum of these lists are then taken as

$$\{(f_1(x_i), f_1(x_{i+1})), h_i\} \oplus \{(f_2(x_i), f_2(x_{i+1})), h_i\} =$$
$$= \{(f_1(x_i) + f_2(x_i), f_1(x_{i+1}) + f_2(x_{i+1})), h_i\} \quad (4)$$

This represents the list produced by the simple application of the operator $f_1 + f_2$ to the original density.

B. Feedback Loop: Convergence Issues

As discussed the feedback connection represents a natural extension of dealing with the summation of correlated signal density functions. Obtaining the feedback signals involves a summation of a set-point, generally, with a processed feedback signal that has been generated as a result of that set point. Propagating densities instead of signals through the loop is facilitated by keeping track of the uncertainty propagation in terms of density lists. For computation purposes a finite number of iterations is expected before convergence is realized. To minimize the computational load management of the bin size for the original distribution is required. Under such conditions the savings obtained are significant, i.e. two orders of magnitude smaller versus traditional methods such as Monte Carlo.

A rigorous proof for the convergence of the iterative scheme proposed is offered in [20]. For completeness a sketch of the proof is presented here for feedback systems falling under the class presented in Figure 3 for which u is the input, x the internal signal and $y = fx$, where f is an operator, the output.

The above signals have associated corresponding probability density functions (pdf) (i.e. for u the pdf is G_u). Applying the Perron-Frobenius theorem on the closed loop relation $x = (I - f)^{-1}u$, the pdf of x, G_x, can be written as:

$$G_x = G_u((I - f)x)|I - df| \qquad (5)$$

where df is the derivative of f and $|\cdot|$ denotes the absolute value of the determinant. The proof developed in [20] shows that a sequence iteration for G_x converges to the closed loop expression in Eq 5, which is the correct closed loop solution.
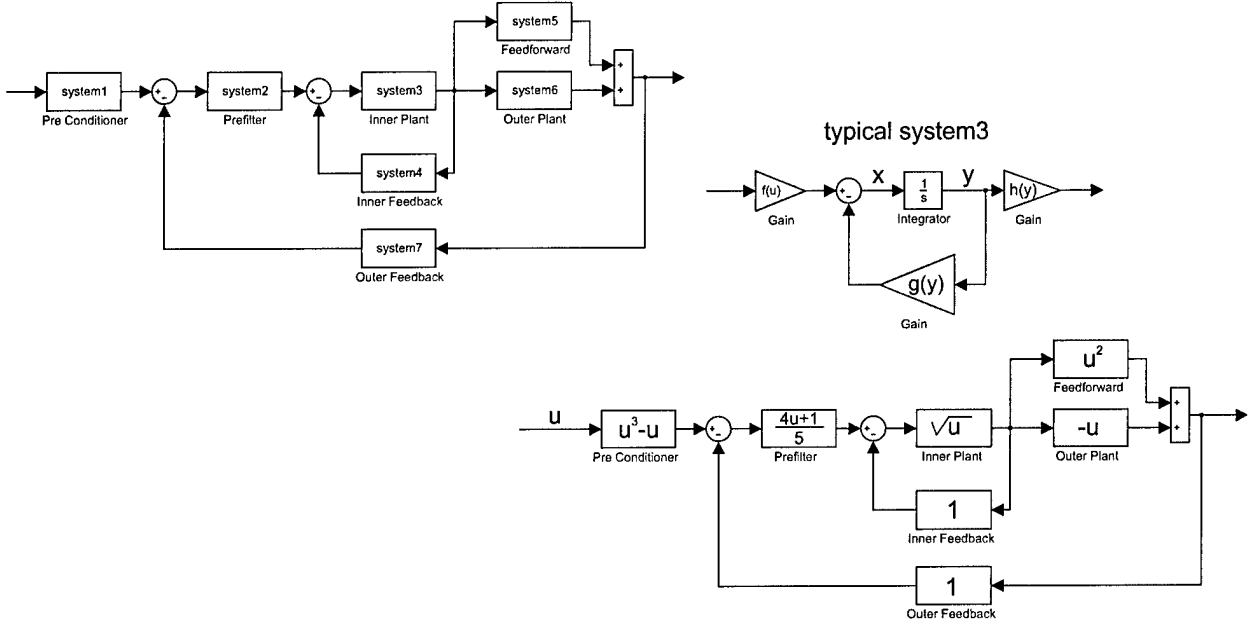
Fig. 5. Typical process control structure and its corresponding asymptotic map

Note that the operator f can be nonlinear. Also note that, as presented in [20], the multidimensional generalization of this computational method is possible.

C. Benefits of a Block-by-block Propagation in a Multi Time Scale System

Another benefit of using the proposed approach is revealed in a multi time scale system. For such n-equation system a simple calculation can quantify the computational benefits.

Assuming that to compute the solution of one equation requires (in average) k operations and assuming that the step-size required to resolve the fastest timescale is dt_{fast} it results that to integrate the system to t_{final} requires approximately $n \times k \times \frac{t_{final}}{dt_{fast}}$ steps. Further, assuming an overall system decomposition into 10 subsystems, with fastest timescale dt_{fast} separated. The number of operations required to integrate this system is approximately $\frac{1}{10} \times n \times k \times \frac{t_{final}}{dt_{fast}}$, which represents an order of magnitude computation speed up.

IV. PROCESS CONTROL EXAMPLE

Well acclaimed techniques steaming from robust control theory such as H_∞ loop-shaping or μ analysis and synthesis are considering, in general, worst case scenarios and do not use, most of the time, existent additional information (i.e. probabilistic knowledge) about uncertainty. As shown in this paper, a direct characterization of uncertainty is a possible and useful alternative. Using this approach, for a control systems framework, is a useful exercise, which can be further generalized to complex networks of dynamical components. The example for uncertainty propagation has been generated through the abstraction of a typical indus-

trial controls closed loop. This process control structure, see Figure 5, involves: inner control loops, feedforwards and outer control loops.

Using the developed tools to understand how input uncertainty propagates through this network of dynamical components requires each component's nonlinear map. These maps can be extracted from the asymptotic behavior of the individual nonlinear dynamic subsystem.

Therefore, the network structure, also displayed in Figure 5, is captured through steady state models displaying series, parallel and feedback interconnections of nonlinear components.

Recall that the density mapping method operates in terms of density lists, which once mapped through a block are constructing other lists. This procedure replaces traditional signal propagation through blocks. The interconnections of the overall system, first decomposed in standard building blocks, are represented with in a similar fashion as in the Matlab Control Systems Toolbox.

The evolution of an initial uncertain input distribution (solid thick line), presented in Figure 6, localized at outer loop set point level is mapped in a successive manner through the network components. The result showing the successive convergence to the known closed loop solution (also solid thick line), known in this simulation example, is displayed in Figure 6 (dotted lines). Note that to produce this plot the density lists were 're-binned' as presented in Section III, based on the same support and bin size as for the original distribution.

V. CONCLUSIONS

The propagation of uncertain inputs through series, parallel and feedback interconnections of dynamical systems
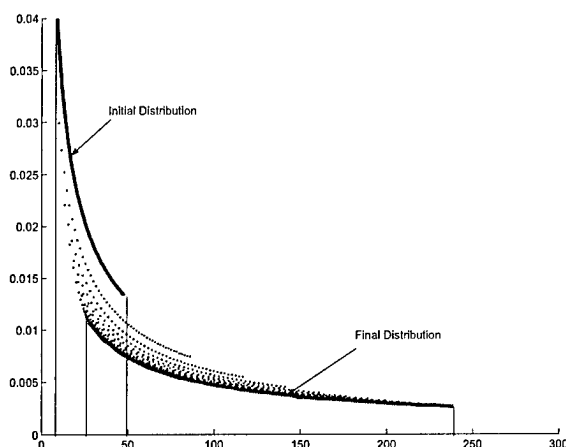
Fig. 6. Density mapping iterations convergence

with simple asymptotic behavior has been studied by employing the discrete density mapping method. Convergence guarantees further explored in [20] reflect the practical observations made when developing the code.

The proposed method achieves at least an order of magnitude computational gains versus Monte Carlo methods. Understanding the role of density lists in dealing with correlated signal density functions provides a framework for an extension of current work to integrate PC methods. The basic idea of this future approach is to decompose the distribution of an uncertain input into small pieces of uniform distributions and propagate these distributions based on the PC methods. In this way the correlation information is preserved for later operation on dependent densities. Given the uniform distribution characteristic of every cell the PC expansion will be performed on an orthonormal Legendre basis. This extension opens the road for the propagation of uncertain inputs through interconnections of uncertain dynamical systems with uncertain initial conditions.

Extensions of the current method to multivariable nonlinear dynamical systems are possible. Considering a single multivariable nonlinear block note that the uncertainty propagation method presented generalizes to volumes instead of areas since the underlaying principle is the conservation of probability. Also dealing with products is achieved by using a logarithmic conversion followed by the application of knowledge acquired in the case of summing correlated signal density functions.

REFERENCES

[1] J.C. Helton, "Treatment of uncertainty in performance assessments for complex systems," *Risk Analysis*, vol. 14, no. 4, pp. 483–511, 1994.
[2] S.F. Wojtkiewicz, M.S. Eldred, R.V. Field, and et al., "Uncertainty quantification in large computational engineering models," .
[3] Jakob Axelsson, "Model based systems engineering using a continuous-time extension of the unified modeling language (UML)," *Systems Engineering*, vol. 5, no. 3, pp. 165–179, 2002.
[4] J. M. Carlson and J. C. Doyle, "Highly optimized tolerance: Robustness and design in complex systems," *Physics Review Letters*, vol. 84, no. 11, pp. 2529–2532, 2000.
[5] Andrew P. Sage, "Systems engineering: Purpose, function, and structure," *The Journal Of The Iinternational Council On Systems Engineering*, vol. 1, no. 1, pp. 1, 1998.
[6] I. Friedel and A. Keller, "Fast generation of randomized low discrepancy point sets," in *Monte Carlo and Quasi-Monte Carlo Methods 2000*, H. Niederreiter, K. Fang, and F. Hickernell, Eds. 2000, pp. 257–273, Springer.
[7] S.H. Strogatz, "Exploring complex networks," *Nature*, vol. 410, pp. 268–276, 2001.
[8] F. M. Callier, W. S. Chan, and C. A. Desoer, "Input-output stability of interconnected systems using decompositions: An improved formulation," *IEEE Transactions on Automatic Control*, vol. 23, no. 2, pp. 150–163, 1978.
[9] G. Shroff and H. B. Keller, "Stabilization of unstable procedures: The recursive projection method," *SIAM J. Numer. Anal.*, vol. 30, no. 4, pp. 1099–1120, 1993.
[10] E. Lelarasmee, A. E. Ruehli, and A. L. Sangiovanni-Vincentelli, "The waveform relaxation method for time-domain analysis of large scale integrated circuits," *IEEE Trans. on CAD of IC and Syst.*, vol. 1, pp. 131–145, 1982.
[11] S. Jain and S. Krishna, *Graph Theory and the Evolution of Autocatalytic Networks*, chapter 16, Wiley - VCH, 2002.
[12] M. Vidyasagar, *Input-Output Analysis of Large-Scale Interconnected Systems: Decomposition, Well-Posedness & Stability*, Springer-Verlag, 1981.
[13] G. Froyland and M Dellnitz, "Detecting and locating near-optimal almost-invariant sets and cycles," *Society for Industrial and Applied Mathematics*, vol. 24, no. 6, pp. 1839–1863, 2003.
[14] Ghanem R. and Spanos P., *Stochastic Finite Elements: A Spectral Approach*, Springer, New York, 1991.
[15] S.S Isukapalli, *Uncertainty Analysis of Transport-Transformation Models*, Ph.D. thesis, Rutgers, The State University of New Jersey, 1999.
[16] M. A. Tatang, *Direct Incorporation of Uncertainty in Chemical and Environmental Engineering Systems*, Ph.D. thesis, Massachusetts Institute of Technology, 1995.
[17] M. Ehrendorfer, "The liouville equation in atmospheric predictability," in *Proceedings ECMWF Seminar on Predictability of Weather and Climate*, 2003, pp. 47–81.
[18] J. L. McCauley, *Chaos, Dynamics, and Fractals*, vol. 2 of *Nonlinear Science*, Cambridge University Press, 1993.
[19] C. Hsu, *Cell-to-Cell Mapping*, Springer-Verlag, New York, 1987.
[20] S. Varigonda, "Iterative method for uncertainty propagation in feedback systems," in *Control and Decision Conference*, Bahamas, 2004.

Graph Decomposition Methods for Uncertainty Propagation in Complex, Nonlinear Interconnected Dynamical Systems

Subbarao Varigonda, Tamas Kalmár-Nágy, Bob LaBarre, Igor Mezić

Abstract—Uncertainty propagation in complex, interconnected dynamical systems systems can be performed more efficiently by decomposing the network based on the hierarchy and/or the strength of coupling. In this paper, we first present a structural decomposition method that identifies the hierarchy of subsystems. We briefly review the notion of horizontal–vertical decomposition (HVD) or strongly connected components (SCC) decomposition of a dynamical system and describe algorithms based on Markov chain theory and graph theory to obtain the HVD from the equation graph of the system. We also present a non-structural decomposition method to identify the weakly connected subsystems of a system based on the Laplacian of a graph derived from the Jacobian. While most of prior efforts in this direction concentrated on stability, robustness and concrete results were limited to linear systems, we use it for uncertainty propagation and study of asymptotic behavior of nonlinear interconnected systems. We illustrate the two methods using a fuel cell system example. These two methods provide a framework for efficient propagation of uncertainty in complex nonlinear systems.

I. INTRODUCTION

Complex physical systems often possess an inherent structure from which they derive the robustness of their behavior. For example, the DNA molecule has a strong backbone structure that allows global modes [1] and gene regulatory networks have a hierarchical structure that allows complex gene expressions [2]. Similarly, complex engineering systems such as coordinated group of vehicles, sensor and communication networks are designed by interconnecting subsystems in a systematic manner.

There is significant interest in robust design methods for complex, interconnected dynamical systems. The design of such systems can be significantly accelerated by using models for robustness assessment and redesign. This requires understanding how uncertainty in various parameters and the system model itself affects the model outputs. Computational methods such as Monte-Carlo, polynomial chaos and various modifications of these can be used to propagate probabilistic information from the inputs/parameters to the outputs of a static or dynamical system. Unfortunately, the computational effort for these methods scales poorly with system complexity and there is a strong need for efficient alternatives. A promising direction is the decomposition of a complex system using graph theoretic methods followed by block-by-block propagation with iterations when necessary.

Graph theoretic methods are used widely in control theory [3] computer science and network systems. More recently, graph theoretic techniques have been employed in conjunction with set oriented numerical methods for computing the almost invariant sets of dynamical systems [4]. There is a close connection between Markov chain theory and graph theory [5]. We refer the reader to standard text books and/or review papers such as [6], [7] for basic notions from algebraic graph theory and graph algorithms such as spanning and induced subgraphs, cycles, connectedness of undirected graphs, strongly connectedness and topological sorting of directed graphs, adjacency, incidence and Laplacian matrices, the significance of the eigenvalues of these matrices, reducibility and irreducibility of the adjacency matrix, depth first search and breadth first search.

The aim of this paper is to introduce graph theoretic methods for decomposing a complex dynamical system into hierarchically and/or weakly connected subsystems for the purpose of uncertainty propagation in systems. The structure resulting from graph decomposition with series, parallel or feedback connections among subsystems can be exploited for efficient methods for computation of uncertainty propagation [8]. We briefly review a structural decomposition algorithm [3], [9] that employs the so-called equation graph of a dynamical system in and identifies the subsystems and the associated hierarchy in Section II. The notion of horizontal–vertical decomposition (HVD) of a dynamical system is introduced and two algorithms for generating the HVD are presented.

The structural decomposition method presented in Section II considers only the directionality of influence among variables (*i.e.*, whether a variable influences another variable) but not the strength of interaction. A limitation of this method, as described in Section II-A, is that it does not yield any useful structure for a system or subsystem whose equation graph is strongly connected. However, this limitation can be overcome using another graph theoretic method described in Section III. The latter method accounts for the strength of coupling between variables and identifies any weakly connected subsystems using a graph partitioning technique. The two methods can be applied in conjunction to achieve a fine decomposition of a complex system. We demonstrate the methodology using a reduced order fuel cell system model in Section IV.

II. STRUCTURAL DECOMPOSITION METHODS FOR DYNAMICAL SYSTEMS

Let (X, μ, T^t, P) be a dynamical system and $\mathcal{N} = 1, ..., N \subset \mathbb{Z}$ where $X = \bigotimes_{i \in \mathcal{N}} X_i$, each X_i a compact subset

of $\mathbb{R}$. Let $\Pi_i : X \to X_i$ be the usual projection to the $i - th$ component.

In addition, $\mu = \bigotimes_{i \in \mathcal{N}} \mu_i$ where μ_i is a probabilistic measure on X_i and $T^t(x,p) : X \times P \to X$ is either a discrete-time family induced by a map (in which case $t \in \mathbb{Z}$) or a flow of a system of first-order autonomous system of ordinary differential equations. The parameters p are defined on $P = \bigotimes_{i \in \mathcal{M}} P_i$, where each P_i a compact subset of $\mathbb{R}$. The change in x_i is given by a function $f_i(x)$, where $x \in X$. This, of course is the $i - th$ component of either the vector field $f(x) = d/dt|_{t=0}(T^t(x,p))$ or $T^1(x,p) - x$, in the case $t \in \mathbb{Z}$. The Jacobian matrix is defined as

$$J(x,p) = Df(x,p),$$

or, in components,

$$J_{ji}(x,p) = \frac{\partial f_i}{\partial x_j}(x,p),$$

where j represents the column and i the row of the matrix.

We define the following matrix $M(x,p)$ from $J(x,p)$:

$$M_{ji}(x,p) = \frac{1}{l_i} \text{ if } |J_{ji}(x,p)| \neq 0,$$
$$M_{ji}(x,p) = 0 \text{ otherwise.} \qquad (1)$$

where l_i is the number of non-zero entries in row i (i.e. the number of components for which component i influences the change of state). Note that an arbitrary state-dependent matrix $A(x)$ could be transformed to a stochastic matrix this way. From the matrix M we can decompose the system to its horizontal-vertical decomposition (HVD) [9]. The decomposition is obtained by spectral analysis of M. This is the same as the one used in [3] except that the decomposition itself is related to Markov chain theory and different vertical levels are identified as left eigenvectors of M. For completeness and to set the decomposition in reader's mind we show here a figure from [9] in which the decomposition is graphically depicted. The graph theoretic decomposition - equivalent to the one described by [3] is provided in the next section. These decompositions split the system into vertical levels, with components on each level affecting change only in the ones above them. This is very significant for uncertainty propagation. Assume there is parametric uncertainty in parameter p that only affects a state at the lowest level. Since dynamics at the lowest level is not affected by the dynamics at the levels above, the asymptotic probability density at the lowest level can be used as the input for the states above. In this way, the computational effort for probability density propagation is substantially reduced.

A. Decomposition based on graph theory

We now present an alternative method to obtain the HVD of a dynamical system using graph theory. The key observation is that the recurrent states obtained recursively using the Markov chain theory for the HVD correspond to the strongly connected components (SCC) of the equation graph. Note that
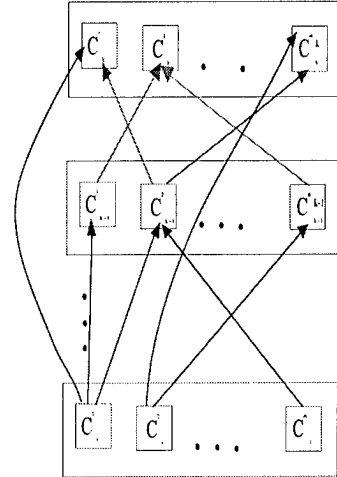

Fig. 1. Decomposition described in the theorem

any digraph can be uniquely decomposed into its SCC [5], [10].

Each SCC of the equation graph can be identified as a subsystem (a supernode) and the *condensed graph* representing the interactions between the supernodes is an acyclic digraph (ADG) [5]. The HVD can be obtained in a straight forward manner from this condensed graph. The subsystems corresponding to vertices with out-degree zero belong to level 1 of the HVD. These vertices can be deleted and the process repeated to successively identify the subsystems in the next level.

The SCC of a digraph can be identified efficiently using the depth first search (DFS) algorithm [5], [10]. In particular, the following graph algorithm generates the SCC: i) form a DFS forest of the given digraph and post-order the vertices, ii) form a DFS forest of the reverse graph of the original graph (*i.e.*, with all the edges reversed in direction) using the ordering obtained in step i). The SCC are given by the DFS forest in step ii). The DFS of a graph can be carried out using efficient algorithms and the computational effort is of the order $n + e$ where n is the number of vertices and e, the number of edges [5].

III. DECOMPOSITION BASED ON THE JACOBIAN VALUE

In this section we investigate the use of the Jacobian matrix to decompose a system of equations into a collection of weakly coupled systems, each of which consists of strongly coupled equations. We note that the Jacobian matrix is generally state-dependent, hence varies with time as the states evolve. This variation may reflect the fact that in different regions of state space the strength of the couplings between variables change.

Our method is along the lines of [4] where transitions between regions in state space for a dynamical system are described by a Markov chain whose underlying graph was employed to identify the number of *almost invariant sets*. A symmetrized adjacency matrix is formed from the stochastic

matrix of the Markov chain and from this the graph Laplacian is constructed. The eigenvalues of the graph Laplacian are used to determine the number and location of the almost invariant sets in state space.

Here we propose the use of a normalized numerical Jacobian matrix to replace the Markov chain probability transition matrix. Then we proceed analogously to build an *equation graph*. Eigenvalues of the associated graph Laplacian are used to identify the number of weakly coupled subsystems.

Given an n dimensional system, $\dot{x} = f(x)$, we form the matrix W (transpose of the Jacobian) with entries evaluated at a given point in state space

$$w_{i,j} = \left| \frac{\partial f_j(x)}{\partial x_i} \right|.$$

The entries of the ith row are normalized by their row sums

$$S_i = \sum_{j=1}^{n} \left| \frac{\partial f_j(x)}{\partial x_i} \right|.$$

Normalizing the entries by their row sums, we get

$$S_i = \sum_{j=1}^{n} \left| \frac{\partial f_j(x)}{\partial x_i} \right|.$$

Let the normalized matrix be P. Clearly, P is a stochastic matrix, and as such can be thought of as the probability transition matrix for a Markov chain. In our method, the x_i act as labels for the graph vertices. The P matrix measures the 'effect' that x_i has on each x_j. Next we form the diagonal matrix $M = diag\{\mu_i\}$, where μ_i is the ith component of the stationary probability vector for P. Finally, we form the symmetric matrix

$$A = \frac{1}{2}\left(MP + (MP)^T \right)$$

and use it as a weighted adjacency matrix for our equation graph, with vertices labeled by the states x_i. This symmetrization corresponds to converting a directed graph into an undirected graph, or equivalently, to reversibilizing a Markov chain.

In order to determine the number of subsystems the system should be decomposed into, we form a generalized Laplacian matrix (see [6]) associated with the graph determined by the weighted adjacency matrix, A. To form the generalized Laplacian, we first compute the degree of each vertex in the graph determined by A as

$$\deg(v_i) = \sum_{j=1}^{n} A_{i,j}$$

where each vertex v_i corresponds to one of the state variables x_i. Finally we form the generalized Laplacian matrix

$$L = D^{-\frac{1}{2}}(D - A)D^{-\frac{1}{2}}.$$

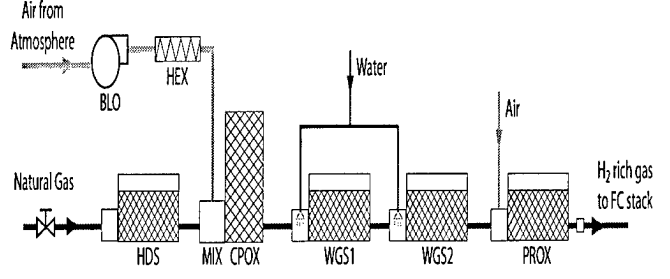where $D = diag\{\deg(v_i)\}$ is the degree matrix.

Fig. 2. Schematic of the fuel processing system of a fuel cell power plant showing various reaction stages

Note that L is symmetric, positive semidefinite, and so has no negative eigenvalues. The multiplicity of the zero eigenvalue gives (see [6]) the number of connected components of the graph determined from A. Numerically, while we will always find one zero eigenvalue, there may be others that are close to zero. In [4], the multiplicity of the zero (and near-zero) eigenvalues is used as an indicator of the number of almost invariant sets in the phase space. In our case, the connected components of the graph map to subsystems of equations. Consequently we use the multiplicity of the zero (and near-zero) eigenvalues to determine the number of weakly coupled subsystems into which our original system decomposes. An example is shown in the next section.

As mentioned previously, with the evolution of the dynamical system, the state variables change and so does the evaluated Jacobian matrix. This means that the decomposition may be different in different regions of state space. The current approach is to mimic the modified Newton approach to nonlinear equation solvers, where a new Jacobian is evaluated when certain convergence criteria are not met.

IV. APPLICATION TO A FUEL CELL SYSTEM MODEL

In this section, we demonstrate the two decomposition algorithms discussed in Sections II and III using a fuel cell system model. The fuel cell system consists of a fuel processor that combines natural gas fuel with air and reforms it into hydrogen rich gas using a series of reactors. A schematic of the fuel processor (without the fuel cell itself) is shown in Figure 2.

The hydrogen rich gas feeds into the anode channel of a PEM (polymer electrolyte membrane) fuel cell which combines hydrogen from the anode with air from the cathode to produce electricity, heat and water. The model we consider has highly simplified physics and was developed for control studies [11], [12]. The model has 10 states and two control inputs. Figure 3 shows the lumped volumes in the model and the respective state variables in the volumes.

The pressures and partial pressures in the volumes are denoted by p. The superscripts *hex,hds,wrox,an* refer to the volume (component) name and the subscripts H_2, CH_4 and *air* refer to the species. The temperature of the CPOX reactor is denoted by T_{cpox} and the speed of the blower by ω_{blo}. The states of the system are ordered as $x =$
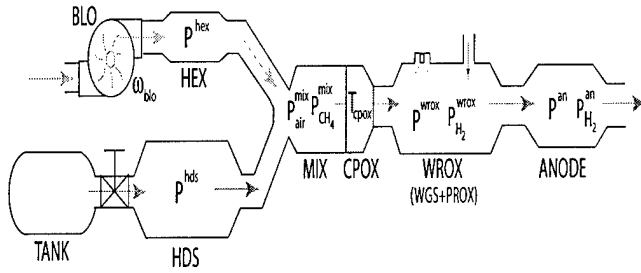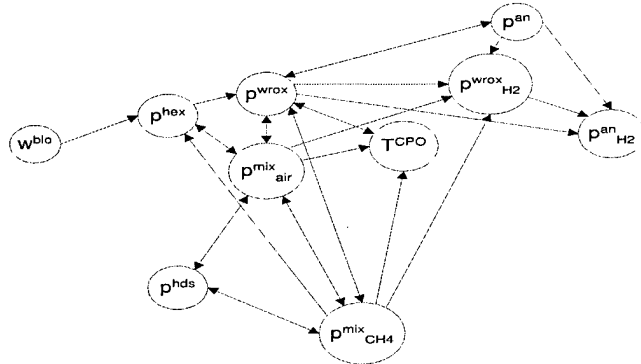
Fig. 3. Lumped volume model of the fuel cell power plant

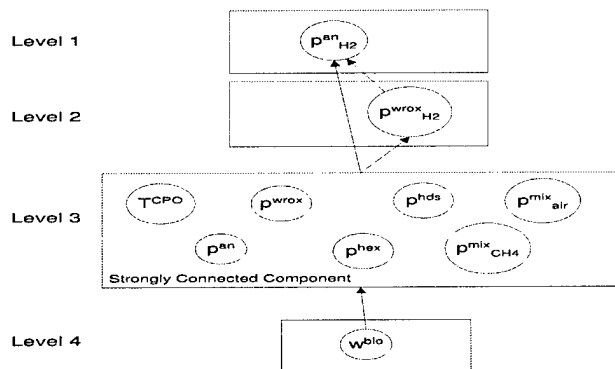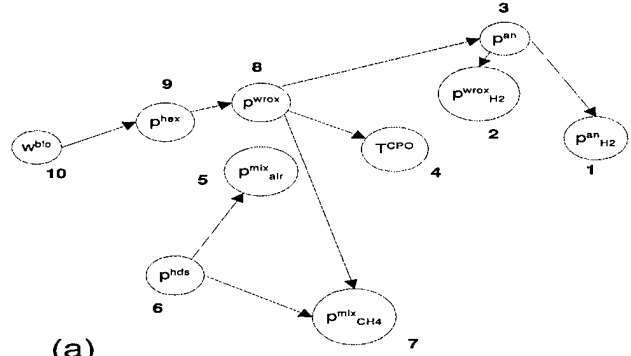

Fig. 4. Equation graph of the fuel cell system model

(a)

(b)

Fig. 6. (a) DFS tree of the equation graph for the fuel cell system with post-ordering of the vertices. (b) The DFS forest of the reversed graph showing the strongly connected components of the original graph

$[T_{cpox}, p^{an}_{H_2}, p^{an}, p^{hex}, \omega_{blo}, p^{hds}, p^{mix}_{CH_4}, p^{mix}_{air}, p^{wrox}_{H_2}, p^{wrox}]'$.

The equation graph of the system showing the who-affects-who relation is shown in Figure 4. The Jacobian of the system at an operating point of interest is given in Eq 2

Applying the Markov chain decomposition method of Section ??, we obtain the HVD as shown in Figure 5. At levels 1, 2 and 4, we have subsystems with a single state whereas at level 3, we have a subsystem with 7 states.

Using the graph theoretic algorithm described in Section II-A, a DFS tree for the equation graph can be constructed with post-ordering of the vertices as shown in Figure 6(a). The DFS forest for the reverse graph using the ordering from the previous step is shown in Figure 6(b). This yields the
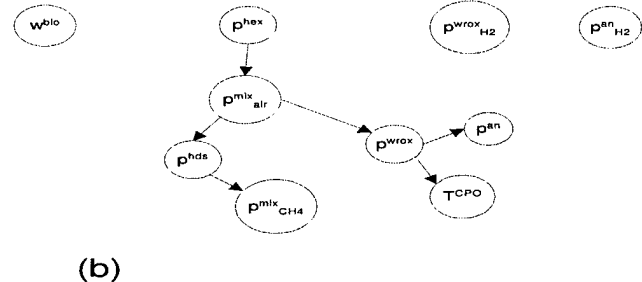

Fig. 5. Horizontal-vertical decomposition of the fuel cell system model

strongly connected components of the original equation graph. Notice that the strongly connected components are precisely the same as the subsystems at various levels in Figure 5 from the Markov chain method.

The subsystem at level 3 in Figure 5 contains 7 states and is a strongly connected component. The Jacobian value method described in Section III can be applied to further decompose this subsystem into weakly connected subsystems. We construct the stochastic matrix and the Laplacian of the associated graph. The eigenvalues of the Laplacian are

$$[\ 0\quad 0.0296\quad 0.1958\quad 0.6518\quad 0.8769\quad 0.9912\quad 1.1089\ ]$$

and shown in Figure 7. It can be observed that the second eigenvalue is relatively closer to zero than the rest of the eigenvalues. This indicates that the 7 state system can be decomposed into two weakly coupled subsystems. The two subsystems can be identified as $\{T_{cpox}, p^{an}, p^{WROX}\}$ and $\{p^{hex}, p^{hds}, p^{mix}_{CH_4}, p^{mix}_{air}\}$ based on the sign of the components of the second eigenvector. Physically, this decomposition relates to the downstream and upstream dynamics of the CPOX reactor.

V. CONCLUSION/SUMMARY

Promise of graph decomposition methods for enabling efficient uncertainty propagation in complex, networks of dynamical systems.

$$J = \begin{bmatrix} -0.074 & 0 & 0 & 0 & 0 & 0 & -3.53 & 1.0748 & 0 & 1e-6 \\ 0 & -1.468 & -25.3 & 0 & 0 & 0 & 0 & 0 & 2.5582 & 13.911 \\ 0 & 0 & -156 & 0 & 0 & 0 & 0 & 0 & 0 & 33.586 \\ 0 & 0 & 0 & -124.5 & 212.63 & 0 & 112.69 & 112.69 & 0 & 0 \\ 0 & 0 & 0 & 0 & -3.333 & 0 & 0 & 0 & 0 & 0 \\ 0 & 0 & 0 & 0 & 0 & -32.43 & 32.304 & 32.304 & 0 & 0 \\ 0 & 0 & 0 & 0 & 0 & 331.8 & -344 & -341 & 0 & 9.9042 \\ 0 & 0 & 0 & 221.97 & 0 & 0 & -253.2 & -254.9 & 0 & 32.526 \\ 0 & 0 & 2.0354 & 0 & 0 & 0 & 1.8309 & 1.214 & -0.358 & -3.304 \\ 0.0188 & 0 & 8.1642 & 0 & 0 & 0 & 5.6043 & 5.3994 & 0 & -13.61 \end{bmatrix} \quad (2)$$
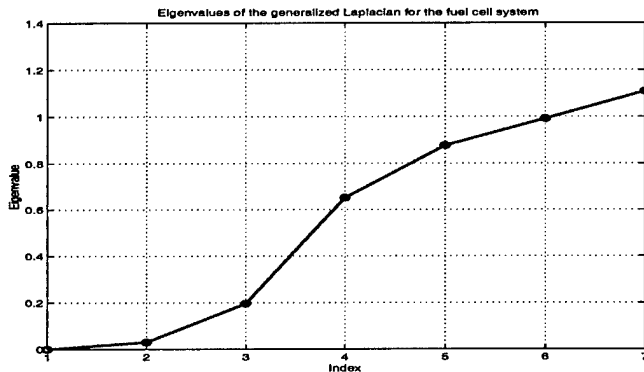
Fig. 7. Eigenvalues of the Laplacian for the level 3 subsystem in Figure 5

REFERENCES

[1] I. Mezić, "Dna clues for design of robust, flexible networks," 2004, uCSB Preprint.

[2] J. Stark, R. Callard, and M. Hobank, "From the top down: towards a predictive biology of signalling networks," *Trends in biotechnology*, vol. 21, pp. 290–293, 2003.

[3] F. M. Callier, W. S. Chan, and C. A. Desoer, "Input-output stability theory of interconnected systems using decomposition techniques," *IEEE Transactions on Circuits and Systems*, vol. 23, no. 12, pp. 714–729, 1976.

[4] M. Dellnitz and R. Preis, *Symbolic and Numerical Scientific Computation*, ser. Lecture Notes in Computer Science, 2630. Springer, 2003, ch. Congestion and almost invariant sets in dynamical systems, pp. 183–209. [Online]. Available: http://math-www.upb.de/ agdellnitz/papers/congestion.ps.gz

[5] J. P. Jarvis and D. R. Shier, *Applied Mathematical Modeling: A Multidisciplinary Approach.* CRC Press, 1999, ch. 17. Graph-Theoretic Analysis of Finite Markov Chains, pp. 271–289.

[6] C. Godsil and G. Royle, *Algebraic Graph Theory.* Springer, 2001.

[7] R. Merris, "Laplacian matrices of graphs: A survey," *Linear Algebra and Its Applications*, vol. 197–198, pp. 143–176, 1994.

[8] M. Huzmezan and T. Kalmár-Nágy, "Propagation of uncertain inputs through networks of nonlinear components," in *Proc. of the IEEE CDC*, Bahamas, December 2004, (submitted).

[9] I. Mezić, "Coupled nonlinear dynamical systems: Asymptotic behavior and uncertainty propagation," 2004, submitted to CDC 2004.

[10] U. Lorch, "An introduction to graph algorithms," Lecture Notes, Department of Computer Science, University of Auckland, New Zealand, March 2000. [Online]. Available: http://www.cs.auckland.ac.nz/ ute/220ft/

[11] J. T. Pukrushpan, A. Stefanopoulou, and S. Varigonda, "Control oriented model of an integrated fuel cell stack and fuel processor system," in *Proc. of the First IFAC Symposium on Advances in Automotive Control*, Univ. of Salermo, Italy, 2004 (to appear).

[12] J. T. Pukrushpan, A. Stefanopoulou, H. Peng, S. Varigonda, L. M. Pedersen, and S. Ghosh, "Control of natural gas catalytic partial oxidation for hydrogen generation in fuel cell applications," *IEEE Trans. Contr. Syst. Tech*, (to appear).

Spectral balance: a frequency domain framework for analysis of nonlinear dynamical systems

Andrzej Banaszuk   Prashant G. Mehta

Abstract—A frequency-domain framework for analysis, computations, and uncertainty propagation in nonlinear systems driven by broad-band disturbances is introduced and illustrated in a simple example of a nonlinear system that exhibits noise-induced transitions between two stable equilibria. The spectral balance framework generalizes the standard harmonic and Gaussian signal balance in feedback systems. The application example presented is a scalar model with cubic nonlinearity after pitchfork bifurcation driven by a broad-band disturbance. An approximate and iterative spectral balance (including determination of equilibria) is solved. The solution of the approximate spectral balance is used to reformulate the original model using a loop transformation so that an iterative procedure for finding the spectrum of the output converges to the true spectrum of the solution.

I. INTRODUCTION

Many industrial flows involve complex interactions of acoustic waves, vorticity, fuel transport, and chemical reactions. The control objective often is to create beneficial non-equilibrium dynamics with control. Examples include control of flow separation and mixing enhancement. In this paper we introduce a frequency domain framework for analysis and non-equilibrium control design for a large class of models of physical phenomena involving multiple oscillatory modes coupled through nonlinear terms, transport delay, and driven by broad-band disturbances. While motivated by specific problems arising in military aeroengines, the methods will be applicable to large class of distributed dynamical systems involving oscillatory dynamics with nonlinear cross-coupling, saturated nonlinearities, transport delay, and broad-band disturbances.

The *spectral balance* framework that we propose generalizes the standard harmonic balance and Gaussian signal balance in feedback systems [4], [2]. The framework is introduced and illustrated in an example of a nonlinear system that exhibits noise-induced transitions between two stable equilibria. The example presented is a scalar model with cubic nonlinearity after pitchfork bifurcation driven by a broad-band disturbance. An approximate and iterative spectral balance of the constant and broad-band signals (including determination of equilibria) is solved. The solution of this approximate spectral balance is used to reformulate the original model using a loop transformation so that an iterative procedure for finding the spectrum of the output converges to the true spectrum.

United Technologies Research Center, 411 Silver Lane, East Hartford, CT. 06108. Email: BanaszA@utrc.utc.com
    Email: MehtaPG@utrc.utc.com

II. SPECTRAL BALANCE

Consider a model of a lightly damped stable linear system with transfer function $G_0(j\omega)$, in a feedback loop with a static nonlinearity $f(\cdot)$, subject to a driving disturbance $n(t)$ with the Fourier transform $N(j\omega)$. An uncertainty in the model is represented by an (in general nonlinear) operator $\Delta(\cdot)$ in a feedback loop around the nominal model The
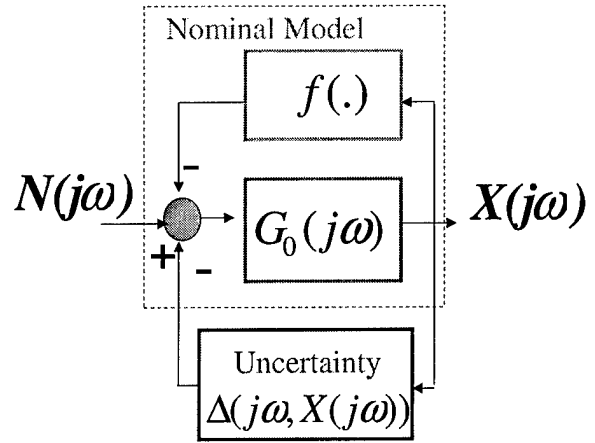

Fig. 1.   The model structure

model equations are

$$X(j\omega) = G_0(j\omega)(N(j\omega) - \Delta(j\omega, X(j\omega)) - Y(j\omega)) \quad (1)$$

$$y(t) = f(x(t)) \quad (2)$$

where, $X(\cdot) = \mathcal{F}x(\cdot)$, $Y(\cdot) = \mathcal{F}y(\cdot)$, and $N(\cdot) = \mathcal{F}n(\cdot)$, are the Fourier transforms of the corresponding temporal signals. We assume that nonlinear mapping $f(\cdot)$ is Lipshitz on each bounded set. The equation (2) can be represented in the frequency domain as

$$Y(j\omega) = \hat{f}(X(j\omega)) := \mathcal{F}f(\mathcal{F}^{-1}X(j\omega)). \quad (3)$$

Now, the feedback system (1)–(2) can be represented as

$$X(j\omega) = G_0(j\omega)(N(j\omega) - \hat{f}(X(j\omega) - \Delta(j\omega)X(j\omega))). \quad (4)$$

Note that for the linear case $f(x) = 0$, $\Delta(j\omega, X(j\omega)) = \Delta(j\omega)X(j\omega)$ the mapping of the uncertainty $\Delta(j\omega)$ to the output of the system is given by the formula

$$X(j\omega) = (I + G_0(j\omega)\Delta(j\omega))^{-1}G_0(j\omega)N(j\omega). \quad (5)$$

involving the sensitivity function $(I + G_0(j\omega)\Delta(j\omega))^{-1}$. Note that the frequency domain representation greatly

simplifies the uncertainty propagation analysis.

1. Uncertainty propagation. The sensitivity function $(I + G_0(j\omega)\Delta(j\omega))^{-1}$ allows to explicitly map the probability distribution of the uncertain parameters contributing to $\Delta(j\omega)$ to the probability distribution of the output $Y(j\omega)$.

2. The frequency domain representation greatly accelerates computation of this mapping. Note that only the algebraic calculations need to be performed in evaluating the formula (5). In contrast, a time domain counterpart of the (5) would require evaluation of the convolution integrals over long period of time. Moreover, in the time domain formulation one needs to wait for transients to subside, which is the issue when dealing with lightly damped dynamics. There are additional benefits of the frequency domain representation in the case when $G_0(j\omega)$ contains time delays.

3. Tools from the robust linear control theory allow to handle dynamic uncertainty in case when only the bounds on the uncertain operator are known [1].

Appart from application to the uncertainty propagation, the frequency domain formulation allows to study fundamental limitations of achievable control performance using methods of the complex analysis.

The *spectral balance* approach is a frequency domain framework for the uncertainty analysis of nonlinear systems that includes the case of non-equlibrium bounded dynamics that retains the advantages of the linear sensitivity function framework: explicit formulas mapping uncertainty to the output and the speed of computation. We will begin with the particular case of system in Figure 1 using the fixed point formulation (4). To introduce the spectral balance framework we will consider the case without uncertainty shown in Figure 2 with the corresponding fixed point
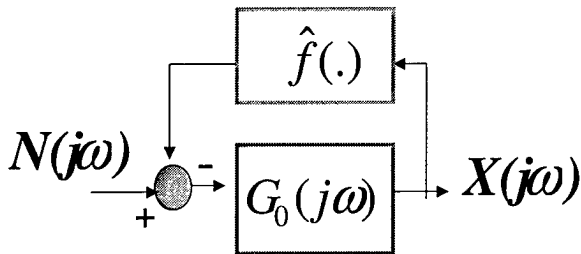

Fig. 2. The model structure

formulation of the spectral balance equation given by (6)

$$X(j\omega) = G_0(j\omega)(N(j\omega) - \hat{f}(X(j\omega)). \tag{6}$$

Note that the spectral balance framework generalizes the standard harmonic balance (where the input signal $n(\cdot)$ is periodic, or when the dynamics has limit cycles) and Gaussian signal balance (where the input signal $n(\cdot)$ is a Gaussian broad band signal) in feedback systems [4], [2].

We assume that the dynamics of (2) is globally bounded and that there is an attractor. Eventually we intend to introduce a spectral balance framework for the class of *bounded power* signals on an infinite time interval. In this paper we restrict the attention to the space of L_2 signals on the interval $[0, T]$, where T is *large* relative to the slowest time scale in the system. The induced operator norms are the H_∞ norms.

A sufficient condition for existence of a *unique* solution of the spectral balance equation (6) is

$$||G_0(j\omega)(\hat{f}(X_2(j\omega)) - \hat{f}(X_1(j\omega)))|| < ||X_2(j\omega) - X_1(j\omega)||. \tag{7}$$

For all $X_i(j\omega)$ in $L_2[0, T]$. Note that in this case a unique solution to (6) exists (by applying the Banach Contraction Mapping Theorem [3]). Moreover, the approximate solution of the spectral balance equation can be obtained by successive approximations using the formula

$$X_{i+1}(j\omega) = G_0(j\omega)(N(j\omega) - \hat{f}(X_i(j\omega)). \tag{8}$$

with an arbitrary initial condition.

Note that if the condition (7) is satisfied for all $X_i(j\omega)$ in a closed set B in $L_2[0, T]$ that is invariant for the mapping $G_0(j\omega)(N(j\omega) - \hat{f}(\cdot))$, one can approach a solution of the spectral balance equation (6) in B using (8) with $X_0(j\omega) \in B$.

III. LOOP TRANSFORMATION

A sufficient condition for (7) is the small gain condition for the feedback loop in (2). However, even if the condition (7) is not satisfied, which would be the case if the loop gain is large, one can attempt to enforce the condition (7) for an *equivalent* feedback system to (2) by a *loop transformation*. An example of a *linear* loop transformation is shown in Figure 3. Here $H(j\omega)$ is an arbitrary stable linear operator,

$$G_1(j\omega) := (I + H(j\omega)G_0(j\omega))^{-1}G_0(j\omega). \tag{9}$$

and

$$\hat{f}_1(X(j\omega)) := \hat{f}(X(j\omega)) - H(j\omega)X(j\omega). \tag{10}$$

The spectral balance condition for the system in Figure 3 is

$$X(j\omega) = G_1(j\omega)(N(j\omega) - \hat{f}_1(X(j\omega)). \tag{11}$$

Note that a sufficient condition for the contraction condition for the *transformed* spectral balance (11) is

$$||G_1(j\omega)(\hat{f}_1(X_2(j\omega)) - \hat{f}_1(X_1(j\omega)))|| < ||X_2(j\omega) - X_1(j\omega)||. \tag{12}$$

If the nonlinear part of the loop in Figure 2 has a stabilizing effect, the role of the operator $H(j\omega)$ is to reduce the H_∞ gain of the nonlinear part of the loop and increase the
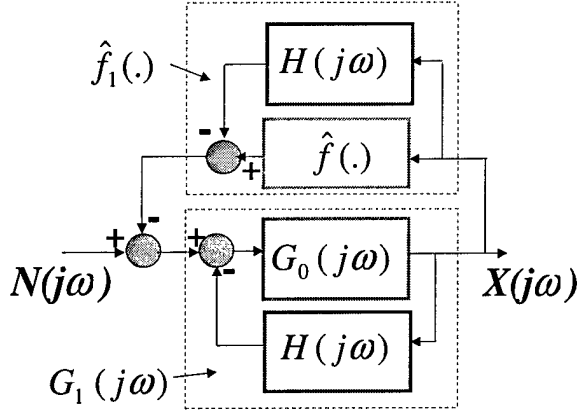
Fig. 3. The loop transformation to enforce loop contractivity

contractivity of the linear part of the loop. More precisely, the gain of the nonlinear operator $\hat{f}(X(j\omega))$ is reduced by subtraction of a *linear* approximation of $\hat{f}(X(j\omega))$ and the approximate linear operator is incorporated in the linear part of the modified loop. Thus, a good choice of $H(j\omega)$ is the one that minimizes $||\hat{f}_1(X(j\omega))||$ for $X(j\omega)$ representing the solution of the spectral balance equation (11).

Of course, the minimization of $||\hat{f}_1(X(j\omega))||$ requires knowledge of $X(j\omega)$ itself, which is exactly the solution of the spectral balance equation that we seek. Note that we are interested in the case of system (2) having non-equilibrium attractors or subject to a large driving disturbance, so that an approximation of nonlinear operator $\hat{f}(X(j\omega))$ by its linearization at $(X(j\omega) = 0$ is not suitable.

The key idea introduced in this paper is to proceed in the following three steps:

1. Find an *approximate* solution $X_{appr}(j\omega)$ close to $X(j\omega)$. For this, the describing function techniques, both for harmonic and random Gaussian signals, can be utilized. In fact, as we will show in the next section, it may be not necessary to find an approximate solution $X_{appr}(j\omega)$, but only few parameters describing such a solution, like its time average and the average power.

2. Utilize the knowledge of $X_{appr}(j\omega)$ (or the parameters describing it) to find a linear transformation $H(j\omega)$ that minimizes (or at least reduces) $||\hat{f}_1(X_{appr}(j\omega))|| = ||\hat{f}(X_{appr}(j\omega)) - H(j\omega)X_{appr}(j\omega)||$.

3. Use $H(j\omega)$ to define the loop transformation (9)–(10). If the contraction condition (12) is satisfied on a closed set B in $L_2[0,T]$ that is invariant for the mapping $G_1(j\omega)(N(j\omega) - \hat{f}_1(\cdot))$, one can approach a solution of the spectral balance equation (6) in B using the iterative

process defined by

$$X_{i+1}(j\omega) = G_1(j\omega)(N(j\omega) - \hat{f}_1(X_i(j\omega))) \quad (13)$$

starting with an arbitrary $X_0(j\omega) \in B$.

At present it is not clear under what general conditions the procedure described above will result in finding solutions to the spectral balance equations. In the next section we will show one example of a system with nontrivial dynamics, for which that the procedure yields the desired result.

IV. EXAMPLE

Consider the equation

$$\dot{x}(t) + ax(t) + bx^3(t) = n(t). \quad (14)$$

Here we assume that $a < 0$, $b > 0$, and the input signal $n(\cdot)$ has zero mean and flat spectrum $|N(j\omega)| = \sigma_i$ for all ω. In the sequel we will refer to the input signal $n(\cdot)$ as *noise*, even though we emphasize that in this paper we only consider the deterministic case. Note that for $a = 0$ the system (14) undergoes a *pitchfork bifurcation* and the equilibrium $x = 0$ becomes unstable for all $a > 0$. Two locally stable equilibria occur at $x = \sqrt{-\frac{a}{b}}$ and $x = -\sqrt{-\frac{a}{b}}$. Note that for a small value of σ_i^2 the solution $x(t)$ will be close to one of the stable equilibria. For some higher value of σ_i^2 the solution $x(t)$ will be transitioning from a neighborhood of the one of the stable equilibria to the other, as shown in Figure 4. Note that the spectral
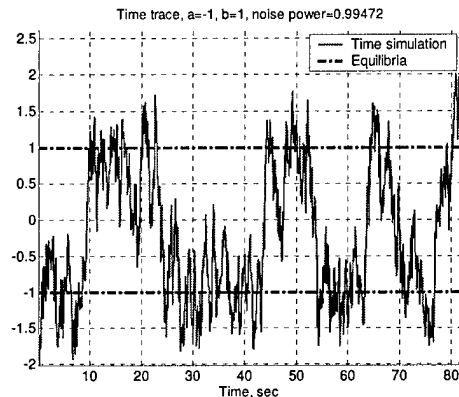
Typical solution

Fig. 4. Typical solution of system (14): noise-induced transitions between two stable equilibria

balance equation for (14) is

$$X(j\omega) = \frac{1}{j\omega + a}(N(j\omega) - \hat{f}(X(j\omega))), \quad (15)$$

where $f(x) := bx^3$. Note that, since $a < 0$, the linear operator $\frac{1}{j\omega+a}$ is unstable, and the contraction condition (7) is not satisfied. However, the nonlinear operator $f(x)$ has a stabilizing effect, so that we can attempt to transform the loop to an equivalent one, for which the contraction condition is satisfied, as described in Section III.

Let $\bar{x} := \frac{1}{T}\int_0^T x(t)dt$ denote the time average of $x(t)$ and let $x'(t) := x(t) - \bar{x}$ denote the deviation of $x(t)$ from its average value. Let $\sigma_x^2 := \frac{1}{T}\int_0^T x'(t)^2 dt$ denote the mean power of $x'(t)$. In what follows we will compute *approximate* value of $\bar{x}$ and σ_x^2 by solving *approximate spectral balance* equations. By taking the time average of (16) and using the fact that the average of $(\bar{x} + x'(t))^3$ is $\bar{x}^3 + 3b\sigma_x^2$ we obtain

$$\bar{x}(a + 3b\sigma_x^2 + b\bar{x}^2) = \bar{n} = 0. \tag{16}$$

Subtracting (16) from (14) and re-arranging terms yields

$$\dot{x}'(t) + (a+h)x'(t) + f_1(x'(t)) = n(t), \tag{17}$$

where

$$h := b\sigma_x^2 + 3b\bar{x}^2 \tag{18}$$

$$f_1(x'(t)) := b(x'^2 - \sigma_x^2)(x' + 3\bar{x}). \tag{19}$$

To find approximate values of $\bar{x}$ and σ_x^2 we will neglect the term $h(\bar{x}, \sigma_x, x'(t))$ in (17) and solve the equation

$$\dot{x}'(t) + (a + b\sigma_x^2 + 3b\bar{x}^2)x'(t) = n(t). \tag{20}$$

Note that for fixed values of $\bar{x}$ and σ_x^2 (20) is a linear equation that can be solved in the frequency domain as

$$X'(j\omega) = \frac{N(j\omega)}{j\omega + a + b\sigma_x^2 + 3b\bar{x}^2}. \tag{21}$$

For a moment we assume that the values of $\bar{x}$ and σ_x^2 are such that $a + b\sigma_x^2 + 3b\bar{x}^2 > 0$, so that the transfer function $\frac{1}{j\omega+a+b\sigma_x^2+3b\bar{x}^2}$ us stable. This assumption will be verified after $\bar{x}$ and σ_x^2 are calculated.

Now we obtain the closure equation for σ_x^2 by integrating the absolute values of both sides of (21) over all frequencies

$$\sigma_x^2 = \frac{1}{2\pi}\int_{-\infty}^{\infty} |\frac{\sigma_i}{j\omega + a + b\sigma_x^2 + 3b\bar{x}^2}|^2 d\omega. \tag{22}$$

The equations (16) and (22) form an *approximate spectral balance* for the system (14. The integral in (22) can be analytically evaluated so that we can write the following equation

$$\sigma_x^2 = \frac{\sigma_i^2}{2(a + b\sigma_x^2 + 3b\bar{x}^2)}. \tag{23}$$

Now, solving (16) and (23) we obtain

$$\sigma_i^2 < \frac{a^2}{4b} \Rightarrow \tag{24}$$

$$\sigma_x^2 = \frac{|a|}{8b}(1 - \sqrt{1 - \frac{4b\sigma_i^2}{a^2}}), \tag{25}$$

$$\bar{x}^2 = -\frac{a}{b} - 3\sigma_x^2 \tag{26}$$

$$\sigma_i^2 > \frac{a^2}{4b} \Rightarrow \tag{27}$$

$$\sigma_x^2 = \frac{|a|}{2b}(1 + \sqrt{1 + \frac{2b\sigma_i^2}{a^2}}), \tag{28}$$

$$\bar{x} = 0. \tag{29}$$

Figure 5 graphically represents the solution to the approximate spectral balance equations as function of the input power σ_i for $a = -1$, $b = 1$. The solutions for $\bar{x}$ and
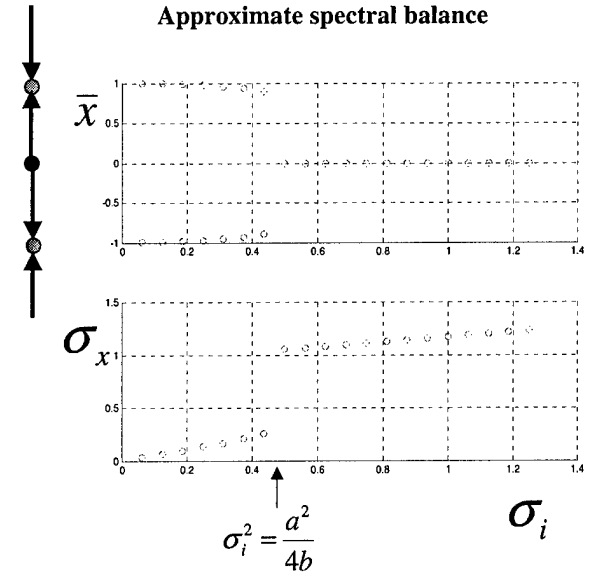
Approximate spectral balance

Fig. 5. Solutions to approximate spectral balance equations as function of the input power

σ_x^2 have a natural intepretation. For $\sigma_i < \frac{a^2}{4b}$ there are two values of the time average $\bar{x}$ close to the no-noise equilibria that can be attained. The value of σ_x (that could be interpreted as standard deviation of $x(t)$) is small, so that the solution $x(t)$ stays close to an equilibrium solution and does not transition to the neighborhood of the other equilibrium. Above the critical value of the input power $\sigma_i = \frac{a^2}{4b}$ the solutions $x(t)$ deviate from the stable equilibria far enough to transition between the neighborhoods of the both equilibria. Since the transitions back and forth can occur, $\bar{x} = 0$ becomes the mean and the standard deviation σ_x is close to the distance from the new mean $\bar{x} = 0$ to the value where the solution $x(t)$ spends most of the time: close to the no-noise equilibria of (14).

We will now use the values of $\bar{x}$ and σ_x^2 given by (5) to perform a loop transformation as described in Section III.

More precisely, we will solve the perturbation equation (17) in the frequency domain using the fixed point formulation

$$X'(j\omega) = \frac{1}{j\omega + a + h}(N(j\omega) - \hat{f}_1(X'(j\omega))). \quad (30)$$

It can be easily verified that $a+h > 0$ for $\bar{x}$ and σ_x^2 given by (29). Analytic verification of the contraction condition for the operator $\frac{1}{j\omega+a+h}(N(j\omega) - \hat{f}_1(\cdot))$ is difficult. Therefore we will assume that the contraction condition is satisfied and proceed with an iterative solution to (30) using

$$X'_{i+1}(j\omega) = \frac{1}{j\omega + a + h}(N(j\omega) - \hat{f}_1(X'_i(j\omega))) \quad (31)$$

with $X'_0(j\omega) = 0$ and verify the contraction condition numerically. To illustrate and verify this procedure, a numerical solution of (14) for $a = -1$, $b = 1$, and $\sigma_i > \frac{a^2}{4b}$ was obtained. The spectrum $N(j\omega)$ of the noise from the time domain simulation was saved and used in the formula (31). Figure 6 shows an excellent agreement of the spectrum $X'(j\omega)$ from the time domain simulation and the spectrum $X'_{10}(j\omega)$ from the iterative procedure (31) after 10 iterations. Figure 7 shows comparison of the

Simulation and approximation after 10 iterations: spectra (fft)
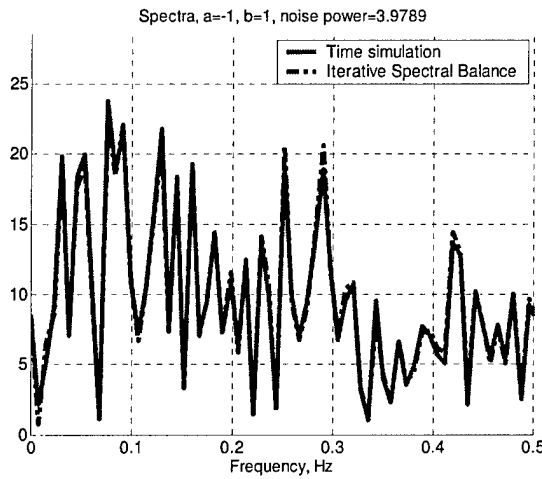

Fig. 6. Solution to iterative spectral balance equations: spectra

time traces of the solutions of (14) obtained by the time domain simulation and by the iterative spectral balance and the inverse Fourier transform. Figure 8 shows decay of the power of the approximation error $X'(j\omega) - X'_i(j\omega)$ normalized by the power of $X'(j\omega)$ as a function of iteration step i. Finally, Figure 9 shows the contraction rate $\frac{\|X'_{i+2}(j\omega) - X'_{i+1}(j\omega)\|}{\|X'_{i+1}(j\omega) - X'_i(j\omega)\|}$ as a function of iteration step i. This verifies the contraction at the rate of about 0.8 was indeed achieved by the loop transofrmation involving solution of the approximate spectral balance.

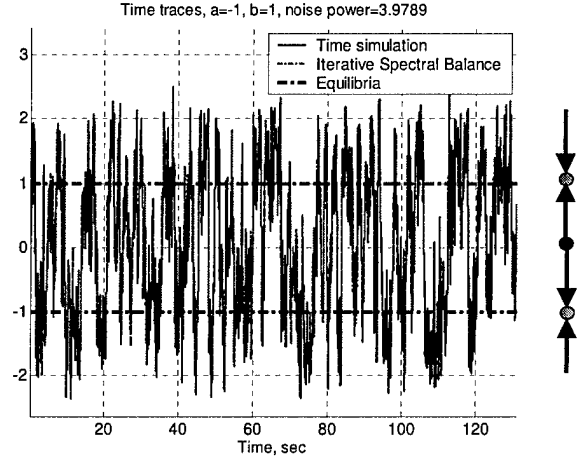## Simulation and approximation after 10 iterations: time traces

Fig. 7. Solution to iterative spectral balance equations: time traces
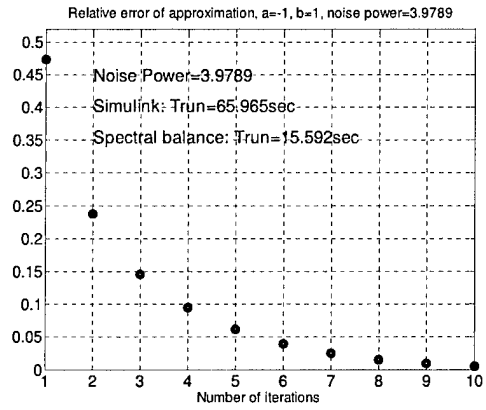
2^{10} FFT points

Fig. 8. Solution to iterative spectral balance equations: relative approximation error for 2^{10} FFT points

In the case that were examined obtaining an approximate solution of (14) using the formula (31) was orders of magnitude faster that the time domain simulations using Simulink.

V. CONCLUSION

A frequency-domain framework for analysis, computations, and uncertainty propagation in nonlinear systems driven by broad-band disturbances was introduced and illustrated in a simple example of a nonlinear system that exhibits noise-induced transitions between two stable equilibria. The spectral balance framework generalizes the standard harmonic and Gaussian signal balance in feedback
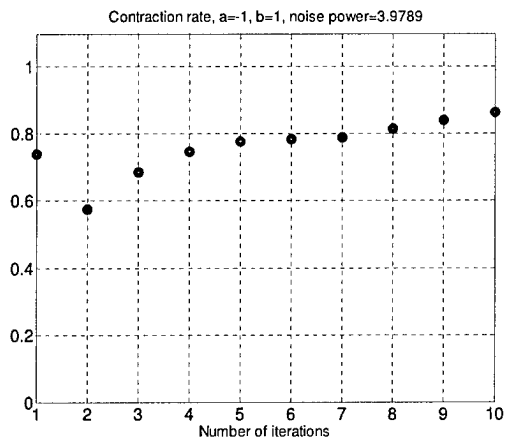
Fig. 9. Solution to iterative spectral balance equations: contraction rate

systems. The application example presented is a scalar model with cubic nonlinearity after pitchfork bifurcation driven by a broad-band disturbance. An approximate and iterative spectral balance (including determination of equilibria) is solved. The solution of the approximate spectral balance is used to reformulate the original model using a loop transformation so that an iterative procedure for finding the spectrum of the output converges to the true spectrum of the solution. The future work will involve more carefull study of the function spaces suitable for the spectral balance formulation and obtaining some analytic sufficient conditions for the contraction.

REFERENCES

[1] J. Doyle, B.A. Francis, and A. Tannenbaum. *Feedback Control Theory.* MacMillan, New York, 1992.
[2] A. Gelb and W.E. Vender Velde. *Multiple–Input Describing Functions and Nonlinear System Design.* McGraw–Hill, 1968.
[3] H. K. Khalil. *Nonlinear Systems.* Macmillan, New York, 1996.
[4] A.I. Mees. Describing functions: Ten years on. *IMA J. Applied Mathematics,* 32:221–233, 1984.

An Iterative Method for Propagation of Probability Distributions in Feedback Systems

Subbarao Varigonda

United Technologies Research Center, East Hartford, CT 06108, USA.

Abstract—Efficient propagation of probability distributions in feedback systems is central to a decomposition based approach for uncertainty propagation in complex, interconnected systems. In this note, we propose an iterative method for static feedback systems to obtain the probability density of the output from that of the input. We prove the convergence of the proposed method under the assumption that the loop operator is contractive. The method is illustrated with an example. It is shown, based on the results from the theory iterated random functions, that the method extends to the case when additional parametric uncertainty is present within the loop.

Fig. 1. Feedback loop with loop operator G

I. INTRODUCTION

Robust design of complex, interconnected systems requires efficient computational methods for uncertainty propagation. Knowledge of the probability distribution function (pdf) of key output variables derived from the knowledge of input variables enables better decision making during design. Existing methods for propagation of uncertainty such as Monte-Carlo, polynomial chaos and stochastic surface response methods have scale poorly with problem size and are computationally very demanding for complex systems [1].

In order to overcome the barrier of computational effort, a new approach based on decomposition of complex systems has been emerging as a promising direction. In this approach, a complex system is first decomposed using graph theoretic methods into subsystems connected in series, parallel or feedback [2]. Then, a block-by-block propagation is performed accounting for the dependencies among variables [3]. Such a method exploits the underlying hierarchical structure of a complex system and provides the flexibility to use different methods for different subsystems of the original system.

Feedback loops at the system level, or encompassing a large number of subsystems pose a significant risk to the block-by-block framework since the structural decomposition method described in [2] identify the feedback loops as a single subsystem. The decomposition method based on the Jacobian value and the associated graph Laplacian, also described in [2], can identify weak feedback connections only. However, moderate to strong feedback (*e.g.*, due to a controller) is common in many engineering systems. The ability to propagate uncertainty through such feedback loops block-by-block without having to solve the closed loop system in entirety is very attractive. Thus, there is a need for alternative approaches
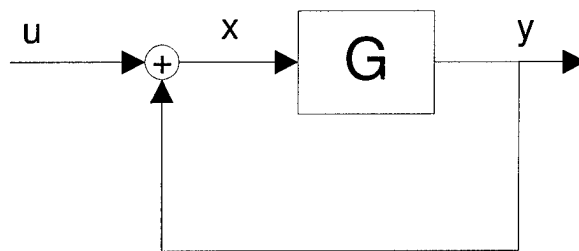
to speeding up the computation for uncertainty propagation in feedback systems.

In this note, we seek an iterative method to compute the pdf of the output of a feedback loop from the pdf of the input. The feedback system under consideration is shown in Figure 1. The loop has input u, the internal signal x and output $y = Gx$ where G is the loop operator (possibly nonlinear). In Section II, we present the problem setup and formulate the iteration equations by abstracting a computational scheme conceived and implemented by Kalmár-Nágy and Huzmezan [3]. We prove the point-wise convergence of the iteration to the true closed loop pdf under the assumption that the loop operator is contractive.

In Section V, we consider the case when there is additional parametric uncertainty in the loop operator. We show that the problem can be cast as a system of iterated random functions. Based on the results in [4], [5], we claim that the iteration converges to the solution of the closed loop pdf under the assumption that the loop operator is contractive on an average. The proof of this claim and extension to dynamic systems will be considered in future work.

II. PROBLEM FORMULATION AND ITERATION SCHEME

Consider the feedback system shown in Figure 1. The input u belongs to a Banach space X (*e.g.*, $\mathbb{R}^n$) and is randomly distributed with probability measure μ_u. The assumption of a normed linear space is made to simplify the notions of derivative and contraction of the loop operator, but it may be possible to relax it to a metric space.

Assuming μ_u is absolutely continuous with respect to the Lebesgue measure, a probability density function (pdf), $p_u(u)$ can be defined for u. The loop operator G is possibly nonlinear and maps X to itself. Furthermore, we assume that G is contractive in the sense that G shrinks distances in the

associated norm. We also assume that G is one-to-one and the derivative of G, dG exists and satisfies $\|dG\| < 1$ which implies that G is uniformly Lipschitz with Lipschitz constant $L < 1$. Notice that the assumption of a single loop operator G is not restrictive since G can be thought of as a composition of several operators.

The problem is to compute the pdf, $p_y(y)$ of the output y in an iterative fashion, without directly employing the closed loop solution $y = G(I - G)^{-1}u$. For practical reasons, we restrict our treatment to finite approximations of the pdf's (i.e., discretized versions). This allows a gridding (box covering) of the space X and a finite matrix representation for dG. Recently, efficient computational methods using such box coverings, known as set-oriented numerical methods, have been developed and extensively applied for exploring the almost-invariant sets and invariant measures of dynamical systems [6], [7].

We formulate the iterative scheme for obtaining $p_x(x)$. Since $y = G(x)$, $p_y(y)$ can be readily obtained from the pdf of x, $p_x(x)$ using the Perron-Frobenius theorem [8, chapter 17]:

$$p_y(y) = \frac{p_x(G^{-1}y)}{|dG|_{x=G^{-1}y}}.$$

Here the subscript on dG indicates where the derivative is to be evaluated and $|\cdot|$ denotes the absolute value of the determinant. Note that due to the one-to-one assumption on G, there is only one pre-image for y. Otherwise, the right hand side would involve the sum over all pre-images [8].

Using the Perron-Frobenius theorem on the closed loop relation $x = (I - G)^{-1}u$, the pdf of x is given by

$$p_x^{cl}(x) = p_u((I - G)x)|I - dG| \qquad (1)$$

We define below a sequence iteration for $p_x(x)$ that converges to the closed loop expression in Eq 1. The proof of convergence is given in Section III.

We first describe the iterative scheme proposed by Kalmár-Nágy and Huzmezan for a simple scenario [3] . Assume that u, x, y are scalars and G is a static, one-to-one map. The proposed iteration scheme grids u into intervals, say of length δu, which leads to a discretization of the pdf as a histogram. The first iterate, $p_x^0(x)$ is taken as $p_u(x)$, with $\delta x^0 = \delta u$. Then, $p_y(y)$ is given by $\frac{p_x^0(G^{-1}y)}{|dG|}$ with $\delta y^0 = |dG|\delta x^0$. The second iterate, $p_x^1(x)$ is obtained by making use of the fact that the area under the curve is conserved, ie, $p_u(u)\delta u = p_x^1(x)\delta x^1$. The interval δx^1 is taken as the sum $\delta u + \delta y^0$. The process is repeated until $p_x(x)$ converges. The iterations are described by

$$x^{k+1} = u + Gx^k \qquad (2)$$
$$\delta x^{k+1} = \delta u + \delta y^k \qquad (3)$$
$$\delta y^k = |dG|\delta x^k \qquad (4)$$
$$p_x^{k+1}(x) = \frac{p_u(u)\delta u}{\delta x^{k+1}}. \qquad (5)$$

When G is not one-to-one, the "overlaps of measure" in the x space should be taken care by adding them properly.

We now present a generalization of the above iteration scheme and prove its convergence under the assumption that G is contractive and one-to-one. Let dG denote the derivative of G, $M = dx/du$ and $|\cdot|$ denote the absolute value of the determinant.

The main idea of the iterative method is to define a discrete dynamical system from the given static feedback system such that the stationary distribution of the Perron-Frobenius equation for the discrete dynamical system is the same as the desired closed loop distribution for the static feedback system. The key steps of method are as follows:

1) Partition the u space into a collection of boxes B_i with center points u_i
2) Assign the measure p_i to the box B_i from the pdf of u, i.e., $p_i = \mu_u(B_i)$
3) Compute the image of each B_i iteratively under the assumption that the image set can be characterized by x and $M = dx/du$. This holds for sufficiently small B_i.
4) Assign the measure p_i to the (converged) image set in x space.

The underlying assumption is that if the size of B_i is sufficiently small, the image set of B_i is also a box completely characterized by its center point, x and the linear operator, $M = dx/du$ that captures the volume mapping from the u space to the x space. The probability density is assumed to be uniform with in each box for all variables.

The following two maps are employed for the iteration:

$$x^{k+1} = u + Gx^k \qquad (6)$$
$$M^{k+1} = I + (dG)M^k. \qquad (7)$$

The initial conditions are $x^0 = u$ and $M^0 = I$. The iteration of the center points of the boxes is captured by Eq 6 and the expansion of volume elements is captured by Eq 7 which is the iteration for $M = dx/du$.

The pdf of x is successively approximated as

$$p_x(x^k) = \frac{p_u(u)}{|M^k|}.$$

The output is given by $y^k = Gx^k$ and the output pdf is given by $p(y^k) = \frac{p_x^k(G^{-1}y^k)}{|dG|}$.

III. Proof of Convergence

Notice that

$$x^k = (\sum_{i=0}^{k} G^i)u = (I + G + G^2 + \ldots + G^k)u.$$

If G is linear, i.e., if dG is independent of x, a similar expression can be obtained for M^k:

$$M^k = \sum_{i=0}^{k} dG^i = I + dG + dG^2 + \ldots + dG^k.$$

However, we do not assume linearity of G.

Since G is contractive, by the contraction mapping theorem, the map in Eq 6 converges to $x^* = (I - G)^{-1}u$. Since dG is

where f_θ is a random map selected according to a given probability measure μ_θ, under the assumption that f_θ are all Lipschitz and contractive in an average sense, the existence of a stationary measure and the convergence are described in [4]. The meaning of *contraction on an average* has also been quantified in terms of the Lipschitz constants of f_θ. In [5], the contraction on average assumption is relaxed and the results are extended to more general random maps.

VI. CONCLUSION

Iterative methods for uncertainty propagation in feedback systems, together with graph decomposition methods and block-by-block propagation can lead to efficient computational methods for complex systems. We present here an iterative scheme to compute the pdf of the output from the pdf of the input for a nonlinear feedback loop. The convergence of the proposed scheme is shown under the assumption that the loop operator is a contraction. Possible extension to the case when there is additional parametric uncertainty in the loop operator is described. Future work will focus on a more rigorous development of the iterative method and include dynamical systems, parametric and initial condition uncertainty as well as integration with graph decomposition techniques and block-by-block propagation methods.

REFERENCES

[1] T. Runolfsson, I. Mezic, and M. Myers, "Uncertainty analysis of dynamical systems," in *Proc. of the SIAM Conf. on Application of Dynamical Systems*, 2003.

[2] S. Varigonda, T. Kalmár-Nágy, B. LaBarre, and I. Mezic, "Graph decomposition methods for complex, interconnected dynamical systems," in *Proc. of the IEEE CDC*, Bahamas, 2004, (submitted).

[3] M. Huzmezan and T. Kalmár-Nágy, "Propagation of uncertain inputs through networks of nonlinear components," in *Proc. of the IEEE CDC*, Bahamas, December 2004, (submitted).

[4] P. Diaconis and D. Freedman, "Iterated random functions," *SIAM Review*, vol. 41, pp. 45–76, 1999.

[5] S. F. Jarner and R. Tweedie, "Locally contracting iterated functions and stability of markov chains," *J. Appl. Prob.*, vol. 38, pp. 494–507, 2001. [Online]. Available: http://www.maths.lancs.ac.uk/ jarner

[6] M. Dellnitz and O. Junge, *Handbook of Dynamical Systems II: Towards Applications.* World Scientific, 2002, ch. Set Oriented Numerical Methods for Dynamical Systems, pp. 221–264. [Online]. Available: http://math-www.upb.de/ agdellnitz/papers/handbook.pdf

[7] M. Dellnitz and R. Preis, *Symbolic and Numerical Scientific Computation*, ser. Lecture Notes in Computer Science, 2630. Springer, 2003, ch. Congestion and almost invariant sets in dynamical systems, pp. 183–209. [Online]. Available: http://math-www.upb.de/ agdellnitz/papers/congestion.ps.gz

[8] C. Beck *et al.*, *Thermodynamics of Chaotic Systems.* Cambridge University Press, 1995.

[9] T.-Y. Li, "Finite approximation of the Frobenius-Perron operator. a solution to Ulam's conjecture," *J. Approx. Theory*, vol. 17, pp. 177–86, 1976.

Fig. 2. Convergence of the iterates of pdf of x for the feedback loop with $\sqrt{x}$

also a contraction, the map in Eq 7 converges to $M^* = (I - dG)^{-1}$ with dG evaluated at x^*. Thus the pdf of x converges to

$$p_x(x^*) = \frac{p_u(u)}{|(I - dG)^{-1}|} = p_u((I - G)x)|I - dG|$$

which is the correct closed loop solution given in Eq 1.

Thus, we have shown point-wise convergence of the estimated pdf of x to the closed loop pdf, $p_x^{cl}(x)$ at selected grid points. A well-known result due to Li (see [9] and [8, chapter 17]) guarantees the convergence of finite approximations of pdf's to the continuous ones as the grid size becomes sufficiently small.

Remark 1: The multidimensional generalization of the computational method proposed by Kalmár-Nágy and Huzmezan involves tracking the corner points of the boxes. The corner point information gives the edge length. The addition rule in Eq 3 is employed for each linear dimension which in turn gives, $|M^{k+1}|$, the volume of the box in $(k+1)^{\text{th}}$ step around x^{k+1} in proportion to the volume of the box around u. Employing Eq 7 in the iteration eliminates the need to keep track of the corner points since the expansion of infinitesimal volumes under the map can be computed as the determinant of M^{k+1}.

IV. EXAMPLE

We now illustrate the method with a simple example. Consider the feedback system with $G(x) = \sqrt{x}$. The pdf of u is given by .... Figure 2 shows the closed loop pdf of x and the iterates of the pdf converging to the closed loop solution.

V. PARAMETRIC UNCERTAINTY IN THE LOOP OPERATOR

We now consider the case when additional uncertainty may be present in the loop operator G. Suppose that G depends on a parameter θ whose pdf is given by $p_\theta(\theta)$. The measure on θ induces a measure on G, μ_G. As in Section II, we can again define an iteration on x^k and M^k with the difference being that G is drawn randomly at each iteration step. Let G^k denote the sample of G drawn at iteration step k according to μ_G. Let dG^k denote the derivative of G^k. The iteration for x^k takes the form

$$x^{k+1} = u + G^k x^k. \tag{8}$$

This system belongs to the class of iterated random functions described in [4], [5]. For the system $x^{k+1} = f_\theta(x^k)$

Uncertainty in the Dynamics of Conservative Maps

Oliver Junge
Institute for Mathematics
University of Paderborn
Warburger Str. 100
D-33098 Paderborn
Germany

Jerrold E. Marsden
Control and Dynamical Systems
California Institute of Technology, MC 107-81
Pasadena, CA 91125
USA

Igor Mezic
Department of Mechanical
and Environmental Engineering
UCSB
Santa Barbara, CA 93106
USA

Abstract—This paper studies the effect of uncertainty, using random perturbations, on area preserving maps of $\mathbb{R}^n$ to itself. We focus on the standard map and a discrete Duffing oscillator in $\mathbb{R}^2$ as specific examples. We relate the level of uncertainty to the large scale features in the dynamics in a precise way. We also study the effect of such perturbations on bifurcations in such maps. The main tools used for these investigations is a study of the eigenfunction and eigenvalue structure of the associated Perron-Frobenius operator along with set oriented methods for the numerical computations.

I. INTRODUCTION

Uncertainty is obviously of central importance for dynamic and control systems both from a theoretical and a practical point of view. While this topic has received much attention in the control community, there is still much to learn about the effect of random perturbations on such systems. In this paper we focus our attention on perturbations of conservative system as a first step towards studying mechanical systems (including molecular systems) in the presence of uncertainty. An important aspect of our approach is to try to extract the key dynamical features that survive in a noisy environment. One can make the case that such features are the most important ones to compute.

The specific context we work in is as follows. Let $f : X \to X$ be an area preserving map of a compact subset X of $\mathbb{R}^2$ to itself. Let $\mathcal{B}$ be the Borel-σ-algebra on X and μ the standard volume measure on X. We model a perturbed version of the map f by a stochastic process which maps a point $x \in X$ near the image point $f(x)$ with high probability. Formally, for a given perturbation size $\delta > 0$, we consider a *stochastic transition function* $p_\delta : X \times \mathcal{B} \to [0, 1]$ corresponding to a *small random perturbation* of f in the sense of [1], i.e., we require

1) $x \mapsto p_\delta(x, B)$ to be measurable for each $B \in \mathcal{B}$;
2) $p_\delta(x, \cdot)$ to be a probability measure for each $x \in X$;
3) for all continuous functions $g : X \to \mathbb{R}$

$$\lim_{\delta \to 0} \sup_{x \in X} \left| \int g(y) \, p_\delta(x, dy) - g(f(x)) \right| = 0. \quad (1)$$

A typical small random perturbation of f is given by letting $p_\delta(x, \cdot)$ be the uniform distribution on a δ-ball around $f(x)$.

Throughout the paper, we focus on two example systems,
1) the *standard map*

$$\begin{pmatrix} x_1 \\ y_1 \end{pmatrix} = \begin{pmatrix} x + \varepsilon y + \varepsilon^2 \mu \sin(2\pi x), \\ y + \varepsilon \mu \sin(2\pi x) \end{pmatrix} \quad (2)$$

on the two-torus, as resulting from a symplectic time discretization of the ordinary differential equation for the pendulum. We fix the step size $\varepsilon = 1$ and view μ as a bifurcation parameter;

2) and the *Duffing map*,

$$\begin{pmatrix} x_1 \\ y_1 \end{pmatrix} = \begin{pmatrix} x + \varepsilon y + \frac{\varepsilon^2}{2}(\mu x - x^3), \\ y + \frac{\varepsilon}{2}(\mu x - x^3 + \mu x_1 - x_1^3) \end{pmatrix} \quad (3)$$

on $\mathbb{R}^2$, as resulting from applying the Newmark scheme to the Duffing equations (see, e.g., [10]). Here ε is a fixed parameter (corresponding to the stepsize in the Newmark scheme) and $\mu \in \mathbb{R}$ is a bifurcation parameter.

A. Stochastic transition functions

A measure μ on $\mathcal{B}$ is called *invariant* for a stochastic transition function p, if

$$\int p(x, A) \, \mu(dx) = \mu(A) \quad (4)$$

for all $A \in \mathcal{B}$. A transition function $p : X \times \mathcal{B} \to [0, 1]$ is called *reversible* w.r.t an invariant probability measure μ, if

$$\int_A p(x, B) \, \mu(dx) = \int_B p(x, A) \, \mu(dx). \quad (5)$$

The value

$$p(A, B) := \frac{1}{\mu(A)} \int_A p(x, B) \, \mu(dx) \quad (6)$$

is the probability to map from set A into set B in one step. The corresponding probability for the time reversed system is given by

$$\hat{p}(A, B) = \frac{\mu(B)p(B, A)}{\mu(A)}. \quad (7)$$

A stochastic transition function with invariant measure μ is called *uniformly ergodic*, if there are constants $q < 1$ and $M > 0$, such that

$$\|p^n(x, \cdot) - \mu\| \leq M q^n, \quad n = 0, 1, 2, \ldots, \quad (8)$$

for all $x \in X$.

A typical small random perturbation of f is given by letting $p_\delta(x, \cdot)$ be the uniform distribution on a δ-ball around $f(x)$. This is an example of an *absolutely continuous transition function*, which generally is of the form

$$p_\delta(x, B) = \int_B k_\delta(f(x), y) \, d\mu(y),$$

where $k : X \times X \to [0, \infty)$ is some suitable kernel. In this case, the transition function of the time reversed system is explicitly given by

$$\hat{p}_\delta(x, A) = \int_A k_\delta(f(y), x) \, d\mu(y). \tag{9}$$

B. Macroscopic dynamics

It is instructive to consider the situation when there is no noise, for an area-preserving mapping T (both of the maps introduced earlier fall into this category). In this case, the Perron-Frobenius operator, say acting on functions in L^2 is given by $Pf(x) = f \circ T^{-1}$ and its adjoint, Koopman operator by $Uf = f \circ T$. These are both examples of the so-called "transfer operators" ([9]). The spectral properties of these can be related to phase-space structure of conservative maps. In particular, invariant sets of T can be obtained as level sets of functions in eigenspace at 1 of U (see e.g. [11]). In addition, invariant densities of T are functions in eigenspace at 1 of P. The operators P and U are unitary and thus their spectrum is confined to the unit circle in the complex plane. Their spectrum can be analyzed via study of a simpler, symmetrized operator $(U + P)/2$. Since P is normal, any eigenfunction f of P at eigenvalue λ is an eigenfunction of U at eigenvalue $\bar{\lambda}$, the complex conjugate of λ. In that case, we have

$$\frac{1}{2}(U + P)f = \frac{(\lambda + \bar{\lambda})}{2} f = \text{Re}(\lambda)f,$$

and thus f is an eigenvalue of the *symmetrized operator* $(U + P)/2$ associated with the eigenvalue $\text{Re}(\lambda)$. In the case when T is ergodic (and the eigenspace at 1 is one-dimensional), all of the other eigenspaces are at most two-dimensional. However, typical area-preserving maps have a more complicated structure where regular regions of periodic and quasi-periodic motion coexist with chaotic areas. An example of this is shown in Figure 1, for the standard map. In this case, the eigenspace at 1 can be obtained using the projection operator $P_T f = (1/n)\sum_{j=0}^{n-1} f \circ T^j f$. An example of such computation is given in figure 2.

In the presence of noise the decomposition of the state space of an area-preserving map into invariant sets with "regular" resp. "chaotic" dynamics, as described above, (cf. Figure 1) is no longer possible.

Due to the noise, the evolution may become transitive on the state space. However, for certain types of perturbations and if the perturbation is sufficiently small, certain invariant sets of the unperturbed map can still be recovered as *almost invariant* subsets. In fact, this is the more likely thing one
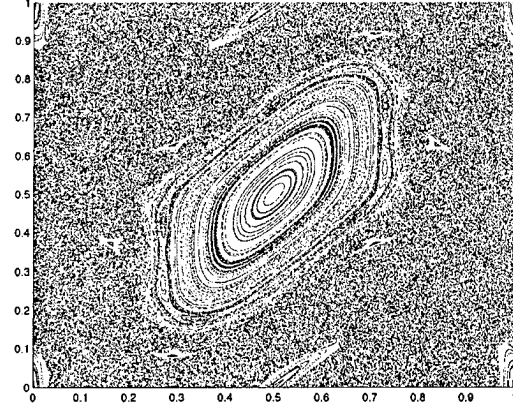

Fig. 1. Standard map: 500 iterates of 500 different initial conditions, chosen at random according to a uniform distribution, $\mu = 0.3$.
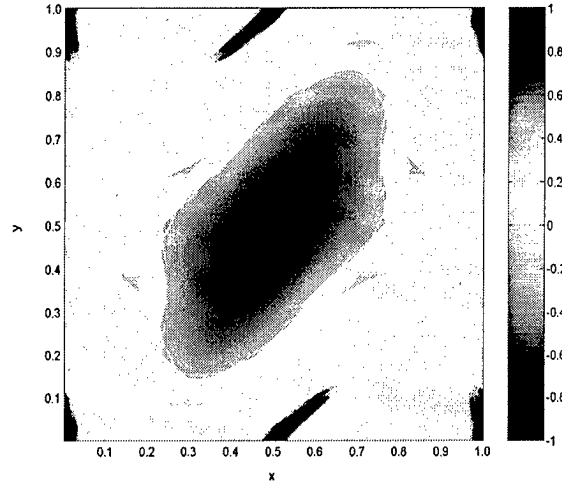

Fig. 2. Standard map: Invariant sets obtained from $P_T f$, for $f = \cos(2\pi y), \mu = 0.3$.

will see in a more realistic noisy and uncertain model of a system. Intuitively, a set $A \subset X$ is *almost invariant*, if the *invariance ratio* of A,

$$p_\delta(A, A), \tag{10}$$

is close to 1, i.e. if the probability to stay within the set A under the evolution is high. We refer to [2] for a more formal definition. For the perturbed system, it is therefore natural to ask for a decomposition of the state space into almost invariant sets when one is interested in a more macroscopic and robust description of the dynamical behavior. Thus, we aim at finding sets A for which (10) is as large as possible. This question has actually been treated in [3], [4] in detail. It is a trivial (but important) observation, that

$$p_\delta(A, A) = \hat{p}_\delta(A, A) = \frac{1}{2}(p_\delta(A, A) + \hat{p}_\delta(A, A)), \tag{11}$$

i.e. when looking for sets that maximize $p_\delta(A, A)$, we might as well consider the transition function

$$r_\delta(x, A) = \frac{1}{2}(p_\delta(x, A) + \hat{p}_\delta(x, A)), \qquad (12)$$

which is reversible.

C. Transfer operators

As mentioned before, spectral properties of transfer operators can be used to explore transport in phase space. One possibility to identify sets with a large almost invariance ratio is via a spectral analysis of a transfer operator associated to the evolution law under consideration, see e.g. [2]. For a given ("pointwise") evolution law, an associated transfer operator describes the evolution of probability measures or densities on the state space. For a deterministic map f, the *Perron-Frobenius* operator $P : \mathcal{M} \to \mathcal{M}$,

$$P\mu(A) = \mu(f^{-1}(A)), \quad A \in \mathcal{B}, \qquad (13)$$

where, instead of $L^2(M)$ here P is defined on $\mathcal{M}$, the space of probability measures on $(X, \mathcal{B})$. The corresponding transfer operator of a stochastic transition function p_δ is given by $P_\delta : \mathcal{M} \to \mathcal{M}$,

$$P_\delta\mu(A) = \int p_\delta(x, A) \, d\mu(x). \qquad (14)$$

In the case that p_δ is absolutely continuous, we can equivalently consider P_δ as an operator on $L^2(X)$, and $P_\delta : L^2 \to L^2$ is given by

$$(P_\delta h)(y) = \int k_\delta(f(x), y) \, h(x) \, dm(x).$$

Note that for the standard inner product on L^2, the adjoint of P_δ is given by

$$(P_\delta^T g)(x) = \int k_\delta(f(x), y) \, g(y) \, dm(y).$$

We first study an example of the Perron-Frobenius operator for a stochastic perturbation of a conservative map on a circle; specifically, we discuss the spectral properties of the Perron-Frobenius operator associated with rotations on the circle. In this example, spectral properties can be analytically computed and as a result are simple to understand. Let $T : S^1 \to S^1; \theta' = \theta + \omega$, be a rotation on the circle, where ω is a constant. Note that this map preserves the Haar measure on the circle. The Perron-Frobenius operator associated with it is given by $Pf(\theta) = f(\theta - \omega)$. The eigenfunctions of P associated with eigenvalue $\exp(-i2\pi n\omega)$, $n \in \mathbb{N}$ are easily computed to be $\exp(i2\pi n\theta)$. These eigenfunctions span $L^2(S^1)$. Consider the following stochastic perturbation of this conservative system: $T_\xi : \theta' = \theta + \omega + \xi$, where ξ is a random variable uniformly distributed on $[-\delta/2, \delta/2]$, where δ is a constant. The Perron-Frobenius operator associated with

T_ξ is $P_\xi f(\theta) = \frac{1}{\delta} \int_{-\delta/2}^{\delta/2} f(\theta - \omega - \xi)d\xi$. If we set $f(\theta) = \exp(i2\pi n\theta)$, we obtain

$$
\begin{aligned}
Pf(\theta) &= \frac{1}{\delta} \int_{-\delta/2}^{\delta/2} \exp(i2\pi n(\theta - \omega - \xi))d\xi \\
&= \frac{1}{\delta} \exp(-i2\pi n\omega) \exp(i2\pi n\theta) \\
&\quad \int_{-\delta/2}^{\delta/2} \exp(-i2\pi n\xi)d\xi \\
&= \frac{\sin(n\pi\delta)}{n\pi\delta} \exp(-i2\pi n\omega) \exp(i2\pi n\theta)
\end{aligned}
$$

$$(15)$$

Therefore, $\exp(i2\pi n\theta)$ are eigenfunctions of P_ξ associated with eigenvalue $\lambda_n = \frac{\sin(n\pi\delta)}{n\pi\delta} \exp(-i2\pi n\omega)$. For fixed n, if $\delta \to 0$, $\lambda_n \to 1$. In figure 3 we show eigenvalues of P_ξ for $\omega = \pi/320, \delta = 0.01$. For large n the eigenvalues tend to zero. The eigenvalue with the largest modulus smaller than 1 is $\lambda_1 = \frac{\sin(\pi\delta)}{\pi\delta} \exp(-i2\pi\omega)$, with the associated eigenfunction $\exp(i2\pi\theta)$. The adjoint operator of P_ξ is the
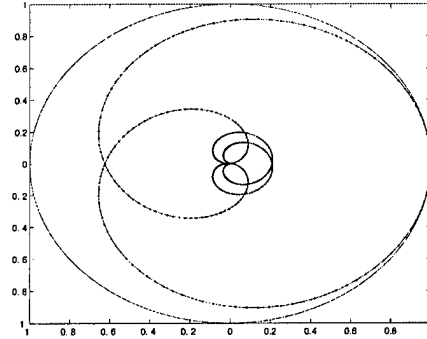

Fig. 3. Eigenvalues of P_ξ for $\omega = \pi/320, \delta = 0.01$ shown as full solid circles inside the unit circle

Koopman operator $U_\xi f(\theta) = \frac{1}{\delta} \int_{-\delta/2}^{\delta/2} f(\theta + \omega + \xi)d\xi$. In this case the Perron-Frobenius and Koopman operators are *normal* and thus the *symmetrized operator* $(P_\xi + U_\xi)/2$ has eigenvalues $(\sin(n\pi\delta)/(n\pi\delta) \cos(2\pi n\omega))$ and the same eigenfunctions as P_ξ. For small ω the second largest eigenvalue is obtained for $n = 1$. The associated eigenfunctions are given by $c_1 \sin(2\pi\theta) + c_2 \cos(2\pi\theta)$. Clearly any two arcs that split the circle in two are almost invariant sets.

For a reversible and uniformly ergodic stochastic transition function p, the essential spectral radius of the corresponding transfer operator $P : L^2 \to L^2$ is bounded away from one, i.e. $\sigma(P) \subset [\ell, r] \cup \{1\}$ with $r < 1$; see [6]. By combining Theorem 3.1 and Corollary 4.33 of [6], we obtain:

Proposition 1 *Let the stochastic transition function p be reversible and uniformly ergodic. Assume that*

$$\sigma(P) \subset [\ell, r] \cup \{\lambda_2, 1\}, \qquad (16)$$

with $r < \lambda_2$ and λ_2 a simple eigenvalue of P. Then for any set $A \in \mathcal{A}$

$$1 - \lambda_2 \le p(A, A^C) + p(A^C, A) \le 1 - \kappa\lambda_2, \qquad (17)$$

where $0 < \kappa \le 1$.

In fact, one has (see [6])

$$\kappa = \sqrt{\frac{\mu(A^C)}{\mu(A)}} \int_A v_2 \, d\mu - \sqrt{\frac{\mu(A)}{\mu(A^C)}} \int_{A^C} v_2 \, d\mu,$$

where v_2 is the eigenvector of P corresponding to the eigenvalue λ, i.e. κ is measuring the "L^2-deviation" of v_2 from $\sqrt{\frac{\mu(A^C)}{\mu(A)}} \chi_A - \sqrt{\frac{\mu(A)}{\mu(A^C)}} \chi_{A^C}$. So, roughly speaking, the maximal almost invariance ratio of any set A is given by $(\lambda_2 + 1)/2$.

Also, the form of κ suggests a strategy for the identification of A, given v_2: the quantity will be maximized, if the set A is defined to be the subset of X, on which v_2 is positive. This strategy of identifying almost invariant subsets of phase space has successfully been applied to the identification of conformations of molecules, see [5], [12].

In Figure 4 we show six eigenvectors of the reversibilized discretized transfer operator (of the unperturbed system). Clearly the almost invariant sets defined by the positive resp. negative components of these modes are in very good agreement with invariant sets of the unperturbed system (c.f. Figure 1) for the eigenvectors $v_2, \ldots, v_6$. The eigenvector v_7 decomposes the "chaotic sea" itself.

D. Discretization

Numerically, we need to work with a finite dimensional subspace L_d of L^2 and a corresponding approximation of P on L_d. A common ansatz is to let L_d be the subspace of step-functions that are piecewise constant on the elements of a partition of X. More precisely, let $\mathcal{P} = \{B_1, \ldots, B_d\}$ be a finite subset of $\mathcal{B}$ such that $\mu(B_i \cap B_j) = 0$ for $B_i, B_j \in \mathcal{P}, B_i \ne B_j$ and $\bigcup_{i=1}^d B_i = X$. Let $L_d = \text{span}\{\chi_{B_1}, \ldots, \chi_{B_d}\}$ and let $Q_d : L^2 \to L_d$ be the orthogonal projection onto L_d. The discretized transfer operator P_d is defined as

$$P_d = Q_d P_\delta. \qquad (18)$$

It is easy to see (see e.g. [2]) that in this case the discretized operator can be represented by a stochastic matrix with entries

$$p_{ij} = \frac{m(f^{-1}(B_i) \cap B_j)}{m(B_j)}, \quad i, j = 1, \ldots, d. \qquad (19)$$

For bounded perturbations of the underlying map f, i.e. if $p(x, \cdot)$ has sufficiently small support, then this *transition matrix* is sparse and even if the number d of partition elements is quite large, a couple of eigenvalues and corresponding eigenvectors can efficiently be computed by Arnoldi methods as e.g. implemented in ARPACK [8] (which is available as the `eigs` command in MATLAB).
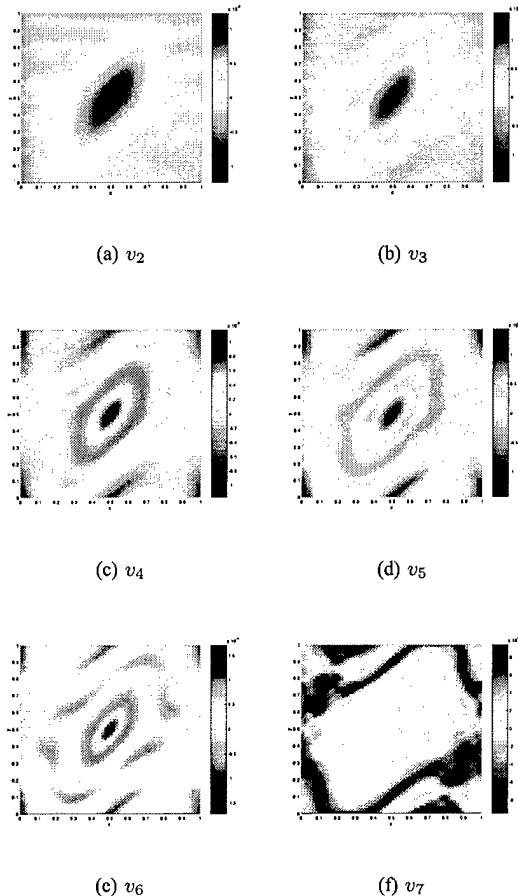

(a) v_2 (b) v_3

(c) v_4 (d) v_5

(e) v_6 (f) v_7

Fig. 4. Standard map: eigenvectors $v_2, \ldots, v_7$ to the six largest eigenvalues (except 1) $\lambda_2 < \cdots < \lambda_7$ of the reversibilized discretized transfer operator of the unperturbed system on a partition of 2^{12} boxes, $\mu = 0.3$.

As an example, again we have a look at the standard map. We consider the reversibilized discretized transfer operator, which in this case is given by the matrix $R_d = (P_d + P_d^T)/2$ and the decomposition of the state space given by the sign structure of the eigenvector corresponding to the second largest eigenvalue. In Figure 5 we show this eigenvector, computed on four different partitions of the phase space. Note that the overall shape of the decomposition is already quite well resolved on a partition with only 256 boxes.

II. Spectral Properties of the Transfer Operator

A. The dependence of the spectrum on the perturbation size

Let us focus on a particular perturbation of the given map f: We consider

$$k_\delta(f(x), y) = \frac{1}{\mu(B_\delta(0))} \chi_{B_\delta(f(x))}(y) \qquad (20)$$

In [7] we prove:

(a) 2^6 boxes   (b) 2^8 boxes

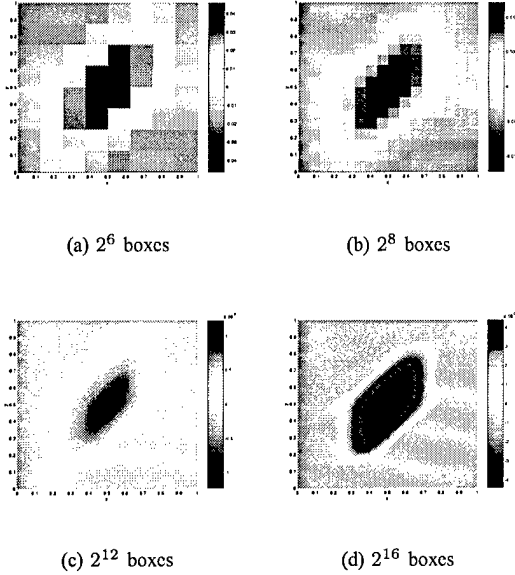(c) 2^{12} boxes   (d) 2^{16} boxes

Fig. 5. Standard map: eigenvector to the second largest eigenvalue of the reversibilized discretized transfer operator of the unperturbed system for different partitions, $\mu = 0.3$.

Proposition 2 *If A is an invariant set of the unperturbed system, then the probability $p_\delta(A, A^C)$ to map from A into its complement A^C under the perturbed system can be estimated as*

$$p_\delta(A, A^C) \leq \frac{\text{length}(\partial A)}{\mu(A)} \delta + \mathcal{O}(\delta^2) \qquad (21)$$

as $\delta \to 0$.

Combining this estimate with Proposition 1, we obtain

Theorem 1 *Let A be an invariant set of the unperturbed map f. Assume that the reversibilized small random perturbation $r_\delta = \frac{1}{2}(p_\delta + \hat{p}_\delta)$ of f is uniformly ergodic. Then*

$$1 - \lambda_2 \leq \frac{\text{length}(\partial A)}{\mu(A)\mu(A^C)} \delta + \mathcal{O}(\delta^2), \qquad (22)$$

Proof: Note that $\mu(A) + \mu(A^C) = 1$ and $\text{length}(\partial A) = \text{length}(\partial A^C)$. ∎

Note that the constant in c_2 relates the length of the boundary of A to its volume. In particular this means that a larger eigenvalue corresponds to an almost invariant set of larger volume. So in this sense larger eigenvalues detect "more important" almost invariant sets.

In Figure II-A we show how the four largest real eigenvalues of the discretized transfer operator (14 subdivisions, 2^{14} boxes) for the standard map depend on the perturbation size δ. For the computation of the transition matrix we used 16 test points in a regular grid in each box of the covering and 256 points on a regular grid in each δ-neighborhood of the corresponding image points in order to sample $p_\delta(x, \cdot)$.

Note that this numerical result is in very good agreement with Theorem 1.
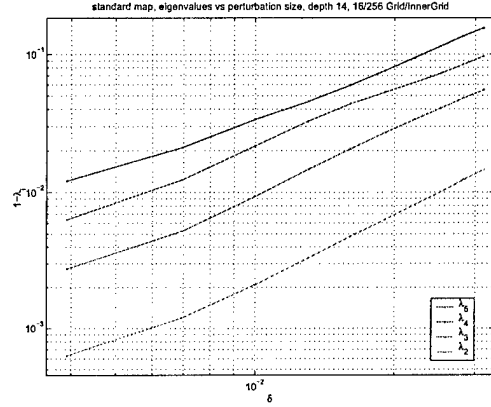

Fig. 6. Standard map: the four largest real eigenvalues (except 1) in dependence of the perturbation size.

B. Spectrum for a fixed value of the bifurcation parameter

Suppose that we are given a symmetry transformation $\kappa : X \to X$, such that $\kappa^2 = id$ and the map f satisfies the equivariance condition

$$\kappa \circ f = f^{-1} \circ \kappa. \qquad (23)$$

Define the action of $\kappa : L^2 \to L^2$ by

$$\kappa h = h \circ \kappa.$$

Proposition 3 *Suppose that the kernel k satisfies*

$$k_\delta(f(x), y) = k_\delta(\kappa \circ f^{-1}(y), \kappa(x)), \qquad (24)$$

then

$$\kappa P_\delta = P_\delta^T \kappa. \qquad (25)$$

Proof: We compute

$$P_\delta^T \kappa h(x) = \int k_\delta(f(x), y) \, h \circ \kappa(y) \, d\mu(y) \qquad (26)$$

$$= \int k_\delta(\kappa \circ f^{-1}(y), \kappa(x)) \, h \circ \kappa(y) \, d\mu(y) \qquad (27)$$

$$= \int k_\delta(\kappa(y'), \kappa(x)) \, h \circ \kappa \circ f(y') \, d\mu(y'), \qquad (28)$$

where the latter equality follows from the change of variables $y' = f^{-1}(y)$ and the fact that f is area preserving. Using the equivariance condition (23) we continue

$$= \int k_\delta(\kappa(y'), \kappa(x)) \, h \circ f^{-1} \circ \kappa(y') \, d\mu(y') \qquad (29)$$

$$= \int k_\delta(\tilde{y}, \kappa(x)) \, h \circ f^{-1}(\tilde{y}) \, d\mu(\tilde{y}) \qquad (30)$$

$$= \int k_\delta(f(\hat{y}), \kappa(x)) \, h(\hat{y}) \, d\mu(\hat{y}) \qquad (31)$$

$$= P_\delta h \circ \kappa(x) = \kappa P_\delta h(x), \qquad (32)$$

where, again, we performed two changes of variables, exploiting the area preservation property of κ. ∎

Corollary 1 *Let $h \in L^2$ be an eigenfunction of P_δ to the eigenvalue λ, then κh is an eigenfunction of P_δ^T to the eigenvalue λ.*

Numerical support for this Corollary is shown in Figure 7. We computed the transition matrix on a covering of 2^{12} boxes, using 100 points on a regular grid—without any perturbation (i.e., $\delta = 0$), and for $\varepsilon = 0.1$ and $\mu = -0.2$. The figure shows $e^{i\pi}\kappa h$ in the left column, where h is the eigenvector of P_δ and the eigenvector of P_δ^T in the right column, both for the same eigenvalue $\lambda = 0.9902 + i\,0.0647$.
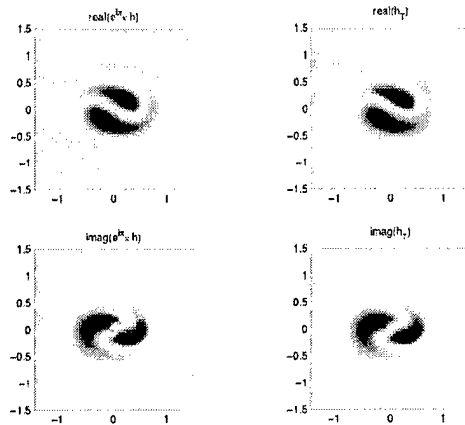

Fig. 7. Duffing map: Comparison of $e^{i\pi}\kappa h$ (left column), where h is the eigenvector of P_δ, and the corresponding eigenvector of P_δ^T (right column).

C. Spectrum in dependence of the bifurcation parameter

As a bifurcation parameter of the map under consideration is varied, it is natural to expect the spectrum of the (discretized) transfer operator to change. In particular, we expect the corresponding eigenmodes to reflect changes in the global dynamical behavior of the system. As an example situation we consider the dynamics of the Duffing map as the parameter μ is varied. It is well known that at $\mu = 0$ the origin undergoes a pitchfork bifurcation, leading to two stable equilibria for $\mu > 0$. In Figure 8 we show how part of the spectrum of the reversibilized discretized transfer operator depends on $\mu \in [-0.35, 0.7]$.

One particular eigenfunction (associated to the eigenvalue represented by the red curve in Figure 8) appears to become the dominant one as μ changes from -0.35 to 0.7. For positive μ, this positive resp. negative components of this eigenfunction are associated to neighborhoods of the two equilibria which are created in the pitchfork bifurcation, bounded by the homoclinic orbits of the origin. For negative μ however, this geometric situation is not present, but still the sign structure of this eigenmode defines a qualitatively similar decomposition of the state space into two almost invariant sets.

III. CONCLUSIONS.

In this paper we have shown that one can effectively use the theory and computation associated with the Perron-Frobenius operator to study the effect of uncertainty on area preserving maps and illustrated the methods with the standard map and a discrete Duffing oscillator. The level of uncertainty is related in a quantitative way to the large scale features, often the ones that are the most important to first compute. It was also shown the way in which uncertainty affects the bifurcations of such maps.

REFERENCES

[1] Y. Kifer, *Random Perturbations of Dynamical Systems.* Birkhäuser, 1988.
[2] M. Dellnitz and O. Junge, "On the approximation of complicated dynamical behavior," *SIAM J. Numer. Anal.*, vol. 36, no. 2, pp. 491–515, 1999.
[3] G. Froyland and M. Dellnitz, "Detecting and Locating Near-Optimal Almost-Invariant Sets and Cycles", *SIAM Journal on Scientific Computing*, vol. 24, no. 6, pp. 1839-1863, 2003.
[4] G. Froyland and M. Dellnitz, "μ Almost-invariant sets and Adaptive Boundary Refinement", *Preprint*.
[5] P. Deuflhard and M. Dellnitz and O. Junge and Ch. Schütte, "Computation of Essential Molecular Dynamics by Subdivision Techniques I: Basic Concept", in *P. Deuflhard,J. Hermans, B. Leimkuhler and A.E. Mark, S. Reich and R.D. Skeel (eds.) "Computational Molecular Dynamics: Challenges, Methods, Ideas"*, Lecture Notes in Computational Science and Engineering, vol. 4, pp. 98–115, Springer, 1998.
[6] W. Huisinga, "Metastability of markovian systems: A transfer operator approach in application to molecular dynamics," Ph.D. dissertation, Free University Berlin, 2001.
[7] O. Junge, J. E. Marsden and I. Mezic, "Random Perturbations of Conservative Maps," *in preparation*.
[8] R. B. Lehoucq and D. C. Sorensen, "Deflation techniques for an implicitly restarted Arnoldi iteration", *SIAM J. Matrix Analysis and Applications*, vol. 17, no. 4, pp. 789-821, 1996.
[9] A. Lasota and M. C. Mackey, *Chaos, Fractals and Noise*. Springer-Verlag, 1994.
[10] J. E. Marsden and M. West, "Discrete mechanics and variational integrators", *Acta Numerica* vol. 10, pp. 357–514, 2001.
[11] I. Mezić and A. Banaszuk "Comparison of complex systems", *Physica D* (submitted), 2004.
[12] Ch. Schütte and W. Huisinga and P. Deuflhard, "Transfer Operator Approach to Conformational Dynamics in Biomolecular Systems", in *B. Fiedler (ed.): Ergodic Theory, Analysis, and Efficient Simulation of Dynamical Systems*, Springer-Verlag, pp. 191-223, 2001.
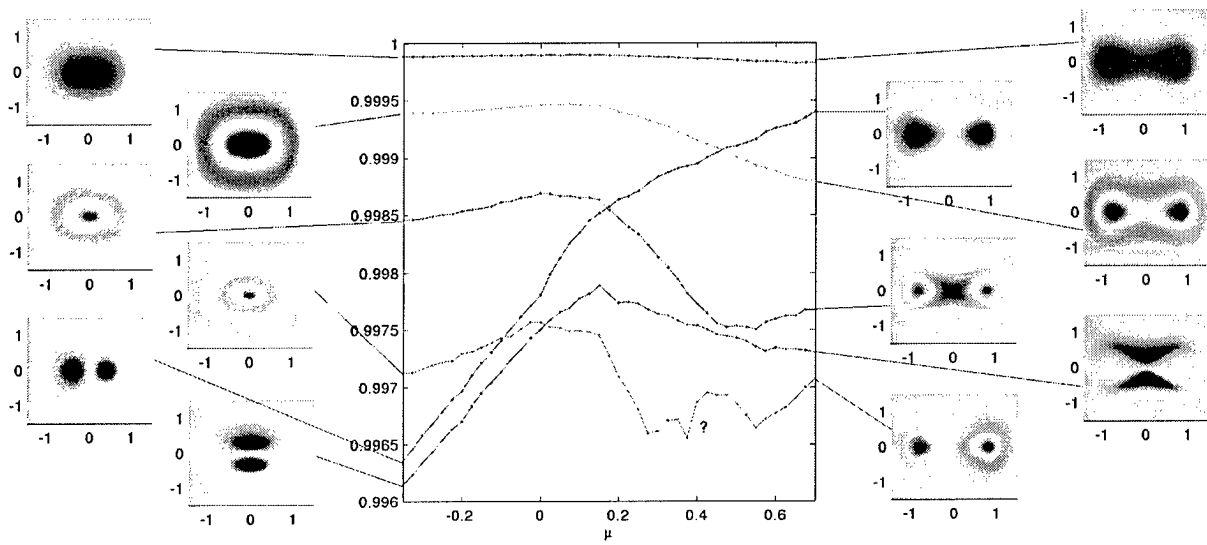
Fig. 8. Duffing: The six largest eigenvalues of the reversibilized discretized transfer operator in dependence of the bifurcation parameter μ, together with the corresponding eigenmodes ($\varepsilon = 0.1$, depth=14, $\delta = 0$).

Dynamics in Molecular Modelling and the Scope for Uncertainty Analysis by Dellnitz-Preis and Polynomial Chaos Methods.

Prasana Venkatesh.

August 29, 2003.

Abstract.

This report describes the form of the dynamical systems involved in computational chemistry and molecular modelling and points out the avenues where methods of uncertainty analysis and uncertainty propagation may be usefully applied. Specific possibilities include the quantification of uncertainty in the semi-empirical potential energy functions in classical molecular dynamics and the assessment of uncertainty in quantum molecular dynamics (Car-Parrinello molecular dynamics) due to the incomplete knowledge of the exchange correlation functional. These can have bearings on atomistic simulation in general. In relation to this, two example dynamical system definitions are given which may be starting points in the investigation of the Dellnitz-Preis and polynomial chaos methods in this area.

1. Introduction.

Experimental values of physical quantities of a many-particle system can be found as an ensemble average. Experimental systems are so large that it is impossible to determine this ensemble average by summing over all accessible states on a computer. There exist essentially two methods for determining these physical quantities as statistical averages over a restricted set of states: the molecular dynamics (MD) and Monte Carlo (MC) methods. Suppose we have a random sample of, say, 10^7 configurations of the system which are all compatible with the values of the system parameters. For such a large number we expect averages of physical quantities over the sample to be rather close to the ensemble average. It is unfortunately impossible to generate such a random sample; however, we can generate a sample consisting of a large number of configurations which are determined successively from each other and are hence correlated. This is done in molecular dynamics and Monte Carlo methods. Our focus in this report is on molecular dynamics.

Molecular dynamics is a widely used method for studying classical many-particle systems. It consists essentially of integrating the equations of motion of the system numerically. It can therefore be viewed as a simulation of the chemical or molecular system as it develops over a period of time. The system moves therefore in phase space along its physical trajectory as determined by the equations of motion. The great advantage of MD is that it not only provides a way to evaluate expectation values of static physical quantities; dynamical phenomena such as transport of heat or charge, or relaxation of systems far from equilibrium can also be studied.

The remainder of this report is organised as follows. Section 2 describes classical molecular dynamics and points out avenues for uncertainty analysis in such calculations. Section 3 describes quantum

molecular dynamics in the context of atoms in molecules. The verlet algorithm for classical and quantum molecular dynamics simulations, a symplectic integrator, is described for the situation with holonomic constraints. The importance of uncertainty analysis due to the inexact knowledge of the exchange correlation functional is emphasised a the most important problem to be tackled either by polynomial chaos or any other method of uncertainty propagation. Section 4 describes molecular systems, in particular the nitrogen molecule and the CS_2 trimer, which can be used as model cases to study different methods of uncertainty analysis - Dellnitz-Preis graph theoretic methods or stochastic galerkin methods.

2. Classical Molecular Dynamics.

Consider a collection of N classical particles. The particles interact with each other via an interaction potential which is the negative gradient of a force-field. If the internal force acting on particle i be denoted by $F_i(R)$ where R comprises the position coordinates r_i of all particles. In the absence of gravitational forces and other forces due to boundaries, the equations of molecular dynamics are

$$\frac{d^2}{dt^2} r_i(t) = \frac{F_i(R)}{m_i} \tag{1}$$

in which m_i is the mass of particle i. The solutions of the equations of motion describe the time evolution of a real system although the description of equation (1) is approximate for the following reasons:

(a.) It is a classical description as per Newton's laws of motion. The importance of quantum effects depends strongly on the particular type of system considered and on the physical parameters (temperature, density, etc.). In Section 3, quantum molecular dynamics is described in the context of density functional theory.

(b.) The forces between the particles are not known exactly; quantum mechanical calculations from which they can be determined are subject to systematic errors as a result of the neglect of correlation effects, as we have seen in previous chapters.Usually these forces are given in a parametrised form, and the parameters are determined either by *ab initio* calculations or by fitting the results of simulations to experimental data.

In a molecular dynamics simulation, one initialises a system, starts the simulation, and lets the system reach equilibrium. The number of particles and the form of the interaction are specified. The particles are assigned positions and momenta. If a Lennard-Jones potential, which is discussed below, is used, the positions are usually chosen as the sites of a Bravais face centered cubic (fcc) lattice [1], which is the ground state configuration of the Lennard-Jones system. The velocities are drawn from a Maxwell distribution at the specified temperature. The numerical solution of molecular dynamics is achieved by symplectic integrators such as the Verlet algorithm [2]. In Section 3.1 a description of the Verlet method in the presence of holonomic constraints is given.

The development of force fields is based on a judicious combination of accurate electronic structure calculations and some empiricism. The empiricism in the force fields results in some uncertainty whose propagation in the molecular dynamics simulation needs to be quantified. Over the years, a number of potentials such as bond-order potentials, embedded atom potentials, and simple pair potentials have been developed; as, e.g., see equations (5) - (10) in reference [3]; a full description of empirical potentials may be found in Chapter 4 of reference [4]. A famous force field is the Stillinger Weber potential used in the molecular dynamics calculations of Silicon and other semiconducting systems. The parameters in these force fields are determined by fitting to experimental structure, phonon spectra, and mechanical properties. Uncertainty in these fitted parameters can have an impact on the computed properties obtained from simulating equation (1). The use of polynomial chaos in order to assess the propagation of uncertainty in molecular dynamics with respect to the uncertain parameters in the interatomic potential of force-fields is an as yet uninvestigated research problem.

An example of an interatomic force-field is the negative gradient of a van der Waals potential function, the Lennard-Jones 12-6 function. The Lennard-Jones 12-6 function takes the following form

$$V(r) = 4\varepsilon\left[\left(\frac{\sigma}{r}\right)^{12} - \left(\frac{\sigma}{r}\right)^{6}\right] \tag{2}$$

where the two parameters are the collision diameter σ and the well-depth ε. The effect of uncertainty in σ and ε on molecular dynamics is worthy of investigation by polynomial chaos methods. Another challenging problem is the application of polynomial chaos methods to molecular dynamics in the context of the Stillinger-Weber potential; see equations (4.121) - (4.123) in reference [4].

3. Quantum Molecular Dynamics: Atoms in Molecules.

Given a diatomic molecule AB and its ground state electron density $\rho_{AB}(r)$ obtained by the standard Hohenberg-Kohn-Sham density functional theory (DFT) [5], we seek to solve the optimisation problem

$$\text{minimise } E_A(\rho_A; R_A) + E_B(\rho_B; R_B), \tag{3}$$

subject to

$$\rho_{AB}(r) = \rho_A(r) + \rho_B(r) \quad \forall r, \tag{4}$$

in order to determine $\rho_A(r)$ and $\rho_B(r)$; R_A and R_B, are held fixed, and are the respective nuclear coordinates of the atoms A and B for a given internuclear separation. E_A and E_B are the total energy functionals of atoms A and B. In terms of the effective single-particle orthonormal orbitals $\{\psi_i^A(r)\}$ and $\{\psi_i^B(r)\}$,

$$\rho_A(r) = \sum_k n_k^A \left| \psi_k^A(r) \right|^2 \tag{5}$$

and

$$\rho_B(r) = \sum_k n_k^B \left| \psi_k^B(r) \right|^2 \tag{6}$$

where n_k^A and n_k^B are the occupation numbers for the one-particle wave-functions $\psi_k^A(r)$ and $\psi_k^B(r)$ respectively. The Kohn-Sham total energy functional for each isolated atom is given by

$$E_A(\{\psi_i^A(r)\}, R_A) \equiv E_A(\rho_A, R_A) = \sum_k n_k^A \int (\psi_k^A(r))^* \left[-\frac{h^2}{8\pi m}\nabla^2 \right] \psi_k^A(r) dr - e^2 Z_A \int \frac{\rho_A(r)}{|r - R_A|} dr +$$
$$e^2 \iint \frac{\rho_A(r)\rho_A(r')}{|r - r'|} dr dr' + E_{xc}(\rho_A(r)) \tag{7}$$

and

$$E_B(\{\psi_i^B(r)\}, R_B) \equiv E_B(\rho_B, R_B) = \sum_k n_k^B \int (\psi_k^B(r))^* \left[-\frac{h^2}{8\pi m}\nabla^2 \right] \psi_k^B(r) dr - e^2 Z_B \int \frac{\rho_B(r)}{|r - R_B|} dr +$$
$$e^2 \iint \frac{\rho_B(r)\rho_B(r')}{|r - r'|} dr dr' + E_{xc}(\rho_B(r)) \tag{8}$$

where e is the electronic charge, h is Planck's constant, m the electronic mass, and Z_A and Z_B are the respective atomic numbers of A and B. E_{xc} is the exchange correlation functional. The spin orbitals must satisfy the orthonormality constraints

$$\langle \psi_k^A | \psi_l^A \rangle = \delta_{kl} \tag{9}$$

and

$$\langle \psi_k^B | \psi_l^B \rangle = \delta_{kl}. \tag{10}$$

The solution of the optimisation problem given by equations (2) and (4) may be achieved by quantum molecular dynamics via a slight modification of the dynamical simulated annealing method of Car and Parrinello [6]. This requires the construction of a dynamical Lagrangian which includes the electronic wave functions and their time derivatives as the variables with respect to a fixed internuclear separation. This leads to a classical mechanics problem with the sum of the energy functionals of equations (7) and (8) acting as a potential. If a friction term is then added to the equations of motion of this classical system, the degrees of freedom will come to rest after some time, with values corresponding to the minimum of the classical potential, which is the energy of the quantum system at the equilibrium configuration of the nuclei. It is also pos-

sible to set the frictional force to zero in order to simulate the system at nonzero temperature. The Lagrangian is given by

$$L(\{\psi_i^A(r)\}, \{\psi_i^B(r)\}; R_A, R_B) = \frac{\mu_A}{2}\sum_k (\dot{\psi}_k^A)^2 + \frac{\mu_B}{2}\sum_k (\dot{\psi}_k^B)^2 - \tag{11}$$

$$E_A(\{\psi_i^A(r)\}; R_A) - E_B(\{\psi_i^B(r)\}; R_B) + \sum_k \sum_l \Lambda_{kl}^A[\langle \psi_k^A|\psi_l^A\rangle - \delta_{kl}] +$$

$$\sum_k \sum_l \Lambda_{kl}^B[\langle \psi_k^B|\psi_l^B\rangle - \delta_{kl}] + \int V_{AB}(r)[\rho_A(r) + \rho_B(r) - \rho_{AB}(r)]dr$$

where μ_A and μ_B are small masses and M_A and M_B are the respective masses of the nuclei of A and B respectively. Λ_{kl}^A, Λ_{kl}^B, and $V_{AB}(r)$ are the Lagrange multipliers which enforce orthonormality and the atoms in molecule constraint of equation (4). There is no term in the Lagrangian of equation (11) that pertains to Coulombic repulsion between the nuclei of A and B because it is a constant at fixed internuclear separation. The details of the kinetic energy of the electrons do not matter; the fictitious masses μ_A and μ_B used in the kinetic energy term can be set to unity. If friction is included into the equations of motion, the particular values of the electronic and nuclear masses do not matter as the kinetic energy is zero at the minimum of the potential of the Lagrangian of equation (11). The Euler-Lagrange equations corresponding to the first variations of the functional of equation (11) are given by

$$\mu_A \ddot{\psi}_k^A = -\frac{\partial}{\partial \psi_k^A} E_A(\{\psi_i^A(r)\}, R_A) + \sum_l \Lambda_{kl}^A(t)\psi_l^A(r) + \int V_{AB}(r)\left[\frac{\partial}{\partial \psi_k^A}\rho_A(r)\right]dr \quad, \tag{12}$$

and

$$\mu_B \ddot{\psi}_k^B = -\frac{\partial}{\partial \psi_k^B} E_B(\{\psi_i^B(r)\}, R_B) + \sum_l \Lambda_{kl}^B(t)\psi_l^B(r) + \int V_{AB}(r)\left[\frac{\partial}{\partial \psi_k^B}\rho_B(r)\right]dr \quad. \tag{13}$$

The time integration of the quantum molecular dynamics equations (12) and (13) can be undertaken by the use of Verlet's method.

3.1 Verlet's Method for Constrained Dynamics.

Verlet's method is widely used for the simulation of many-particle dynamics in the computer simulation of liquids [2]. Suppose there are N particles with R denoting the position coordinates r_i of all the particles. Consider the dynamics

$$\frac{d^2}{dt^2}r_i(t) = F_i(R) \tag{14}$$

where F_i is a force-field. Verlet's method in the absence of any constraints on the particles is the recurrence relation

$$r_i(t+h) = 2r_i(t) - r_i(t-h) + h^2 F_i[r(t)] \tag{15}$$

which is accurate to $O(h^4)$ and wherein $r_i(t)$ is the position of the ith particle at time $t = nh$ where h is the time-step and n is an integer. Suppose M constraints, $\sigma_k(R) = 0, k = 1, ..., M$, are imposed upon the particles. The constraint force acting on the particle is

$$\sum_{k=1}^{M} \lambda_k \nabla_{r_i} \sigma(R) \tag{16}$$

where the $\{\lambda_k\}$ are the Lagrange multipliers to be determined. At time $t = nh$ we have at our disposal the positions at times t and $t-h$. First, one calculates new positions $\tilde{r}_i(t+h)$ ignoring the constraints according to

$$\tilde{r}_i(t+h) = 2r_i(t) - r_i(t-h) + h^2 F_i[r(t)] \tag{17}$$

and the corrected new positions are given by

$$r_i(t+h) = \tilde{r}_i(t+h) - \sum_{k=1}^{M} \lambda_k \nabla_{r_i} \sigma(R) \tag{18}$$

where the $\{\lambda_k\}$ are found by an iterative procedure. The iterations are numbered by an index l. In each iteration, a loop over the constraints k is carried out, and in each step of this loop, the Lagrange multiplier λ_k and all the particle positions are updated. The positions are updated according to

$$r_i^{new} = r_i^{old} - h^2 \lambda_k^{(l)} \nabla_{r_i} \sigma_k(R(t)) . \tag{19}$$

The parameter $\lambda_k^{(l)}$ is found from a first order expansion of $\sigma_k(R(t))$ and requiring that the latter vanishes:

$$\sigma_k(R^{new}) \approx \sigma_k(R^{old}) - \sum_i \nabla_{r_i}\sigma_k(R^{old})\nabla_{r_i}\sigma_k(R(t)) = 0 . \tag{20}$$

This leads to

$$\lambda_l^{(k)} = \frac{\sigma_k(R^{old})}{h^2\left\{\sum_i \nabla_{r_i}\sigma_k(R^{old})\nabla_{r_i}\sigma_k(R(t))\right\}}.$$

(21)

Each step will therefore shift the positions more closely to the point where they all satisfy the constraint. The iterations are stopped when all the constraints are smaller in absolute value than some small positive number.

3.2 Investigation of Uncertainty in the Exchange Correlation.

Using polynomial chaos to study the propagation of uncertainty in Car-Parrinello calculations is a good idea. But, it cannot be done without an understanding of the uncertainty in the density functional. We suggest that one considers using the semi-empirical density functionals that the chemists have constructed by fitting a guessed at form with parameters to the results of configuration interaction computations for small systems [4, 7]. This can be taken as a standard for comparisons. Then the various physically motivated functionals would deviate from that standard, and one could study the propagation of those deviations through the Car-Parrinello computation. It has become apparent to solid-state physicists that no functional or computational method that does not treat exchange exactly is to be taken seriously. This is an excellent problem for uncertainty analysis in molecular modelling.

4. Molecular Systems.

Interactions in molecular systems can be divided into intra-molecular and inter-molecular ones. The latter are often taken to be atom-pair interactions. The intra-molecular interactions, i.e., the interactions between the atoms of one molecule, are determined by chemical bonds and are therefore not only strong compared with inter-molecular interactions (between atoms of different molecules) but also include oriental dependence. A brief description of intra-molecular degrees of freedom and interactions is as follows.

First of all, the chemical bonds can stretch. The interaction associated with this degree of freedom is usually described in the form of a harmonic potential for the bond length l

$$V_{stretch}(l) = \frac{1}{2}\alpha_S(l-l_0)^2$$

(22)

where l_0 is the equilibrium bond length.

Now consider three atoms bonded in a chain-like configuration A-B-C. This chain is characterised by a bending or valence angle φ which varies around an equilibrium value φ_0 and the potential is described in terms of a cosine

$$V_{valence}(\varphi) = -\alpha_\beta[\cos(\varphi-\varphi_0) + \cos(\varphi+\varphi_0)]$$

(23)

where the equivalence of the angles φ_0 and $-\varphi_0$ is taken into account.

Finally there is an interaction associated with chain configurations of four atoms *A-B-C-D*. The plane through the first three atoms, *A, B,* and *C* does not in general coincide with that through *B, C,* and *D*. The torsion interaction is similar to the bend interaction, but the angle, denoted by θ, is now between these two planes

$$V_{torsion}(\theta) = -\alpha_T[\cos(\theta - \theta_0) + \cos(\theta + \theta_0)] \tag{24}$$

Characteristic vibrations associated with the different degrees of freedom distinguished here can be derived from the harmonic interactions - the frequencies vary as the square root of the α-coefficients. In general the bond length vibrations are the most rapid, followed by the bending vibrations. In order for molecular dynamics simulations to be accurate, the time step for integration should be chosen smaller than the fastest degree of freedom. But this degree of freedom will vibrate with a small amplitude, because of the strong potential, most of the computational time in molecular dynamics simulations will be consumed by those parts of the motion which are not expected to contribute strongly to the physical properties of the system. Moreover, if there is a clear separation between the time-scales of the various degrees of freedom of the system, energy transfer between the fast and slow modes is extremely slow, so it is difficult, if not impossible, to reach equilibrium within a reasonable amount of time. It is in such instances of molecular dynamics that graph-theoretic methods for the identification of almost invariant sets can simplify and accelerate convergence to equilibrium [8].

4.1 Direct Approach for the Nitrogen Molecule.

A good base case for investigating methods of uncertainty analysis is molecular dynamics of the nitrogen molecule N_2 in the context of the rigid molecule approximation. In this approximation molecules are treated as rigid bodies whose motion consists of translations of the centre of mass and rotations about this point. The forces acting between two rigid molecules are usually composed of atomic pair interactions between atoms belonging to different molecules. The total force acting on a molecule determines the translational motion and the torque determines the rotational motion. The N_2 molecule consists of two nitrogen atoms, each of mass 14 atomic mass units (amu) and whose separation *d* is kept fixed in the rigid approximation. The coordinates of the molecule are the three coordinates of the centre of mass and the two coordinates defining its orientation. The latter can be polar angles but here we shall characterise the orientation of the molecule by a unit normal pointing $\hat{n}$ from one atom to the other.

The motion of the centre of mass of the molecule is determined by the total force F_{tot} acting on the particular molecule. This force is the sum of all the forces between each of the two atoms in the molecule and in the remaining molecules. The atomic forces can be modelled by a Lennard-Jones interaction with the

appropriate atomic nitrogen parameters $\sigma = 3.72$ Angstroms and $\varepsilon/k_B = 37.3$ Kelvin [9] where k_B is the Boltzmann constant. The equation of motion for the centre of mass R_{cm} is then

$$\ddot{R}_{cm} = F_{tot} \tag{25}$$

which can be solved in exactly the same way as in an ordinary molecular dynamics simulation. The motion of the orientation vector $\hat{n}$ is determined by the torque τ with respect to the centre of the molecule which is given in terms of the forces $F^{(1)}$ and $F^{(2)}$ acting on atoms 1 and 2 respectively.

$$\tau = (d/2)\hat{n} \times (F^{(1)} - F^{(2)}). \tag{26}$$

The torque changes the angular momentum L of the molecule. This is equal to $I\omega$, where I is the moment of inertia equal to md^2 and ω is the angular frequency vector whose norm is the angular frequency and whose direction is the axis around which the rotation takes place. Note that τ is not necessarily parallel to ω. The equation of motion for the angular momentum is

$$\tau = I\dot{\omega} \tag{27}$$

and we note that the angular frequency ω is in turn related to the time derivative of the direction vector $\hat{n}$ as

$$\frac{d}{dt}\hat{n} = \omega \times \hat{n} \tag{28}$$

Combining equation (27) and (28), the molecular dynamics equation is

$$\frac{d^2}{dt^2}\hat{n} = \omega \times (\omega \times \hat{n}) + \tau \times \hat{n}/I = -\omega^2 \hat{n} + \tau \times \hat{n}/I \tag{29}$$

and this equation of motion leaves the norm of the direction vector $\hat{n}$ as it should.

For general molecules, there will exist an extra degree of freedom: the angle of rotation around a molecular axis - the third Euler angle, which is denoted as γ. The straightforward procedure for solving the equations of motion is to calculate the principal angular velocity ω in terms of the time derivatives of the Euler angles. The Euler equation of motion gives the rate of change in ω in terms of the torque. The time derivatives of the Euler angles can be found again from ω, and these can be used to calculate the new atomic positions. There is however, a problem when the Euler angle θ is zero, as in that case the transformation from ω to the time derivatives of the Euler angles becomes singular. The most efficient method is to use the quaternion representation which avoids the instability resulting from this singularity. In the quaternion method, the orientation of the molecule is represented in terms of a four-dimensional unit vector rather than three Euler angles [11].

4.2 The CS_2 Trimer.

A more complicated example is the trimer molecule CS_2 [12]. The linear geometry of this molecule is in principle imposed automatically by the correct bond constraints between the three pairs of atoms. However, the motion of this molecule is described by two positional degrees of freedom: two to define the orientation of the molecule and three for the center of mass position. The three atoms without constraints have three degrees of freedom and if three of these are eliminated using the bond constraints, we are left with six degrees of freedom instead of the five required. A procedure is to fix only the distance between the two sulphur atoms

$$\left| r_{S^{(1)}} - r_{S^{(2)}} \right|^2 = d^2 \tag{30}$$

and to fix the position of the C-atom by a linear vector constraint

$$(r_{S^{(1)}} + r_{S^{(1)}})/2 - r_C = 0 \tag{31}$$

adding up to the four constraints required. For a molecule, in general a number of atoms forming a backbone set is identified and these are fixed by bond constraints (the two sulphur atoms in this example). In the case of a planar structure we take three non-colinear atoms as a backbone. These atoms satisfy three bond constraints and the remaining atoms are constrained linearly. In a three-dimensional molecular structure, four backbone atoms are subject to six bond constraints and the remaining ones to a linear vector constraint each. In the constraint procedure, the degrees of freedom of the non-backbone atoms are eliminated so that the forces they feel are transferred to the backbone. This elimination is always possible for linear constraints such as those obeyed by the non-backbone atoms.

The equations of molecular dynamics for this system may be written down now by introducing Lagrange multipliers λ and μ for the bond and linear vector constraints respectively.

$$m_S \frac{d^2 r_{S^{(1)}}}{dt^2} = F_1 - 2\lambda(r_{S^{(1)}} - r_{S^{(2)}}) - \frac{\mu}{2} \tag{32}$$

$$m_S \frac{d^2 r_{S^{(2)}}}{dt^2} = F_2 + 2\lambda(r_{S^{(1)}} - r_{S^{(2)}}) - \frac{\mu}{2} \tag{33}$$

$$m_C \frac{d^2 r_C}{dt^2} = F_C + \mu \tag{34}$$

The linear constraint of equation (31) is now differentiated twice with respect to time and using the equations of motion

$$F_C + \mu = \frac{m_C}{2m_S}(F_1 + F_2 - \mu) \tag{35}$$

is obtained. We can thus eliminate the multiplier μ and obtain the equations of motion for the S-atoms

$$m_S \frac{d^2 r_{S^{(1)}}}{dt^2} = \left(1 - \frac{m_C}{2M}\right)F_1 + \frac{m_C}{2M}F_2 + \frac{m_C}{M}F_C - 2\lambda(r_{S^{(1)}} - r_{S^{(2)}}) \tag{36}$$

$$m_S \frac{d^2 r_{S^{(2)}}}{dt^2} = \left(1 - \frac{m_C}{2M}\right)F_2 + \frac{m_C}{2M}F_1 + \frac{m_C}{M}F_C + 2\lambda(r_{S^{(1)}} - r_{S^{(2)}}) \tag{37}$$

where $M - 2m_S + m_C$. It is not possible to eliminate the multiplier λ. Therefore, the molecular dynamics equations for CS2 involve integrating equations (36) and (37) subject to the constraint of equation (30). This is achieved by the modified Verlet algorithm of Section 3.1 with the atomic forces F_1 and F_2 being appropriately negative gradients of the interatomic potential [13].

Bibliography.

1. Ashcroft, N. W. and N. D. Mermin, **1976**, *Introduction to Solid State Physics*, Holt, Reinhart, and Wisnton, New York.

2. Allen, M. P. and D. J. Tildesley, **1989**, *Computer Simulation of Liquids*, Oxford University Press.

3. Rountree, C. L., Kalia, R. K., Lidorikis, E., Nakano, A., van Brutzel, L., and P. Vashishta, **2002**, *Annual Reviews of Materials Research*, 377-400.

4. Leach, A. R., **2001**, *Molecular Modelling - Principles and Applications*, Second Edition, Prentice Hall.

5. Kohn, W., **1999**, *Reviews of Modern Physics*, 71, 1253-1266.

6. Car, R. and M. Parrinello, **1985**, *Phys. Rev. Lett.*, 55, 2471.

7. Pople, J. A., **1999**, *Reviews of Modern Physics*, 71, 1267-1274.

8. Dellnitz, M. and R. Preis, **2002**, *Congestion and Almost Invariant Sets in Dynamical Systems*, and references therein.

9. Cheung, P. S. Y. and J. G. Powles, **1975**, *Molecular Physics*, 30, 921-949.

10. Evans, D. J., **1977**, *Molecular Physics*, 34, 317-325.

11. Evans, D. J. and S. Murad, **1977**, *Molecular Physics*, 34, 327-331.

12. Ciccotti, G., Ferrario, M., and J. P. Ryckaert, **1982**, *Molecular Physics*, 47, 1253-1264.

13. Goldstein, H., **1980**, *Classical Mechanics*, Addison-Wesley, Reading.

Symmetry-Breaking and Uncertainty Propagation in a Reduced Order Thermo-acoustic Model

Gregory Hagen   Andrzej Banaszuk

Abstract—We present a thermo-acoustic model on a cylindrical, or annular, geometry, capable of modeling instabilities of tangential acoustic modes. The model accounts for non-uniform density, damping, rotational flow, and heat-release coupling. It is shown that deliberately introducing spatial variations in some quantities has a similar effect to adding damping to the system. The effects of these symmetry-breaking concepts are evaluated on the model through linear analysis and the net amount of additional damping is computed. We show how various symmetry-breaking concepts are robust with respect to the uncertainty in the model parameters and we examine propagation of uncertainty with respect to a recently defined measure of uncertainty.

NOMENCLATURE

A	=	state space matrix
a	=	speed of sound
e	=	internal energy per unit volume
K	=	heat-release gains
p	=	pressure
q	=	volumetric heat-release
r, θ	=	radial, tangential (space) variables
R	=	mean radius
t	=	time
$\mathbf{u}$	=	velocity vector
u_r, u_θ	=	radial, tangential velocities
$\upsilon_2(\varpi)$	=	uncertainty metric
x	=	state vector in Galerkin truncated model
Y	=	acoustic boundary admittance
γ	=	ratio of specific heats (= 1.4)
ρ	=	density
ϕ	=	tangential (Fourier) basis function
ψ	=	radial basis function
ξ	=	damping constant
$\overline{(\cdot)}, (\cdot)'$	=	mean, perturbation quantities
$\tilde{(\cdot)}$	=	normalized quantities
$(\cdot)_0, (\cdot)_m$	=	spatially mean and m-periodic quantities

I. INTRODUCTION

Thermo-acoustic instabilities in gas turbine and rocket engines develop when acoustic waves in combustors couple with an unsteady heat-release field in a positive feedback loop. For a summary of active control of thermo-acoustic instabilities see [3]. Thermo-acoustic modeling and control is well-studied for axially extended combustion chambers, as in [5], [7], [14], [10], where the acoustic to heat-release coupling is dominated by longitudinal acoustic modes. However, comparably less attention has focussed on thermo-acoustic modeling in combustion chambers with annular, or cylindrical geometries. In the present work, we develop a low-order thermo-acoustic model on a circular geometry, somewhat similar to that of [1].

Often thermo-acoustic instabilities are dominated by a few natural acoustic modes, which can accurately be modeled with a low-dimensional model. Accurate heat-release models are difficult and time-consuming to implement. A low-order thermo-acoustic model, properly calibrated with acoustic data, can provide insight into the possibly deleterious acoustic-heat-release coupling and may provide a platform for fast evaluation of preliminary design concepts.

In this work we define **symmetry-breaking** as the deliberate introduction of spatial variations in the system parameters in order to change the stability properties. Recent work has focussed on analysis of heterogeneous distributed systems [6],[9],[11]. Symmetry-breaking is commonly refered to as mistuning in the literature regarding the dynamics of arrays of turbine blades on a disk. Studies of stability properties of turbine blade flutter through the introduction of spatial nonuniformities has appeared in [2], [16]. Optimal mistuning in arrays of bladed disks has appeared in [15], [17]. A study of the effects of asymmetry on compressor stall inception has appeared in [8].

As in the case of mistuning in arrays of bladed disks in turbines, this form of passive control is often more feasible than implementing an active control scheme. This may also be true for the case in combustion chambers, where high temperatures prohibit adequate sensing and may damage the actuators required for active control. Furthermore, symmetry-breaking can be a more cost-effective means of stability enhancement.

In the present work we develop a thermo-acoustic model capable of describing oscillations and passive control of tangential modes using symmetry-breaking concepts. The model is derived in section II, where we describe the parameters available for symmetry-breaking for stability enhancement. The low-order model is constructed by Galerkin projection and truncation. Linear analysis of stabilization via symmetry-breaking is discussed in section III. Parametric uncertainties are modeled as spatially varying components within the model. The propagation of these uncertainties

United Technologies Research Center, 411 Silver Lane, East Hartford, CT. 06108. Email: HagenGS@utrc.utc.com, BanaszA@utrc.utc.com

to the amplitude of pressure mode oscillations is described in terms of a recently defined measure of uncertainty [12], which is discussed in section IV.

II. MODEL DEVELOPMENT

We consider a combustor that has an annular shape and includes a circumferential array of bluff body flame holders, similar to that presented in [1]. Flameholders extend radially from inner to outer diameter of the annular combustor. A cut along a contant radius surface is shown in Figure 1. The thermo-acoustic system we consider is the linearized
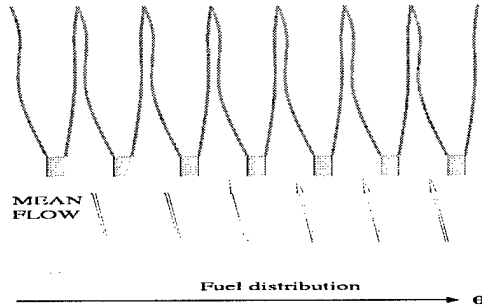

MEAN FLOW

Fuel distribution

θ

Fig. 1. A radial cross-section of a bluff body flameholder array in the tangential direction.

momentum and pressure dynamics as derived by Culick [4]. We now list the assumptions used throughout the rest of this work:

- Viscous effects are negligible.
- All quantities are periodic in θ.
- The acoustic medium is air and it acts as an ideal gas, with constant ratio of specific heats, γ.
- The flow is non-conducting (i.e. the other transport terms appearing in [4] are negligible).
- The steady density $\bar{\rho}(\theta)$, tangential velocity $\overline{u_\theta}(\theta)$, and boundary admittance $Y(\theta)$ are possibly spatially varying.
- All other steady, mean quantities are spatially uniform.
- The radial velocity perturbation u'_r is negligible on the interior of the domain.
- Variations in the axial direction are negligible.
- The heat-release and damping feedback are time-invariant.
- The heat-release feedback is a scalar operation that depends only on the tangential acoustic velocity.

We start with the inviscid transport equations written in cylindrical coordinates,

$$\frac{\partial \rho}{\partial t} + \nabla \cdot (\mathbf{u}\rho) = 0 \tag{1}$$

$$\rho \frac{\partial \mathbf{u}}{\partial t} + \rho \mathbf{u} \cdot \nabla \mathbf{u} = -\nabla p \tag{2}$$

$$\rho \frac{\partial e}{\partial t} + \rho \mathbf{u} \cdot \nabla e = -p \nabla \cdot \mathbf{u} + q. \tag{3}$$

By substitution of the ideal gas relation $e = \frac{1}{\gamma-1}\frac{p}{\rho}$ and (1) we obtain

$$
\begin{aligned}
(\gamma - 1) & \left[\rho \frac{\partial e}{\partial t} + \rho \mathbf{u} \cdot \nabla e \right] \\
&= \frac{\partial p}{\partial t} - \frac{p}{\rho}\frac{\partial \rho}{\partial t} + \mathbf{u} \cdot \nabla p - \frac{p}{\rho}\mathbf{u} \cdot \nabla \rho \\
&= \frac{\partial p}{\partial t} + \frac{p}{\rho}\nabla \cdot (\mathbf{u}\rho) + \mathbf{u} \cdot \nabla p - \frac{p}{\rho}\mathbf{u} \cdot \nabla \rho \\
&= \frac{\partial p}{\partial t} + p\nabla \cdot \mathbf{u} + \mathbf{u} \cdot \nabla p.
\end{aligned} \tag{4}
$$

Multiplying (3) by $(\gamma - 1)$ and applying (4) results in

$$\frac{\partial p}{\partial t} + \mathbf{u} \cdot \nabla p + \gamma p \nabla \cdot \mathbf{u} = (\gamma - 1)q. \tag{5}$$

The system (2,5) is the thermo-acoustic model that we focus on. Equations (2,5) are linearized about the steady pressure $\bar{p}$, density $\bar{\rho}(\theta)$, and tangential velocity $\overline{u_\theta}(\theta)$ where $\bar{p}$ is spatially uniform, and $\bar{\rho}(\theta)$ and $\overline{u_\theta}(\theta)$ are possibly spatially varying in the tangential direction. For notational convenience, we drop the arguments (θ) in the following equations. The linearized dynamics are

$$\bar{\rho}\frac{\partial u'_r}{\partial t} = -\frac{\overline{\rho u_\theta}}{r}\frac{\partial u'_r}{\partial \theta} + 2\frac{\overline{\rho u_\theta}}{r}u'_\theta - \frac{1}{r}\frac{\partial p'}{\partial r} \tag{6}$$

$$\bar{\rho}\frac{\partial u'_\theta}{\partial t} = -\frac{\overline{\rho u_\theta}}{r}\frac{\partial u'_\theta}{\partial \theta} - \frac{\bar{\rho}u'_\theta}{r}\frac{\partial \overline{u_\theta}}{\partial \theta} - \frac{\overline{\rho u_\theta}}{r}u'_r - \frac{1}{r}\frac{\partial p'}{\partial \theta} \tag{7}$$

$$
\begin{aligned}
\frac{\partial p'}{\partial t} &+ \frac{\gamma \bar{p}}{r}\frac{\partial u'_\theta}{\partial \theta} + \frac{\gamma p'}{r}\frac{\partial \overline{u_\theta}}{\partial \theta} + \frac{\gamma \bar{p}}{r}\frac{\partial r u'_r}{\partial r} \\
&= -\frac{\overline{u_\theta}}{r}\frac{\partial p'}{\partial \theta} + (\gamma - 1)q',
\end{aligned} \tag{8}
$$

For simplicity, we assume that u'_r is negligible on the interior of the domain, however, we retain that u'_r couples with the pressure on the outer boundary through a *static* boundary admittance relations (see e.g. [13])

$$u'_r = Y(\theta)p, \tag{9}$$

where the argument (θ) is included to indicate possible spatial variations in the boundary admittance. With the exception of the admittance relation (9), we assume that the contribution of the radial acoustic velocity coupling to the dynamics of the thermo-acoustic system is negligible, hence we will ignore (6). Note that further generalizations of this model can retain these dynamics. Also, note that a more general linear dynamic admittance condition could be easily handled by frequency domain techniques.

We will assume some generic, normalized mode shape in the radial direction, $\psi(r)$ which may be some weighted combination of Bessel functions, depending on the radial boundary conditions [4]. We assume that each quantity is written

$$X(r, \theta, t) := X(\theta, t)\psi(r).$$

We project the sysetm on to this radial mode. Integrating the term with u'_r in (8) results in

$$
\begin{aligned}
\int_{R_1}^{R_2} \psi(r)\frac{\partial r u'_r}{\partial r}\,dr &= \psi(R_2)R_2 u'_r(R_2) \\
&= \psi(R_2)R_2 Y p'(R_2) \\
&= \psi(R_2)^2 R_2 Y p'(\theta, t), \quad (10)
\end{aligned}
$$

where we have applied (9) and the assumption that $u'_r = 0$ on the interior. Equations (7) and (8) can be simplified to

$$\bar{p}\frac{\partial u'_\theta}{\partial t} = -\frac{\overline{pu_\theta}}{R}\frac{\partial u'_\theta}{\partial \theta} - \frac{\overline{pu'_\theta}}{R}\frac{\partial \overline{u_\theta}}{\partial \theta} - \frac{1}{R}\frac{\partial p'}{\partial \theta} \quad (11)$$

$$
\begin{aligned}
\frac{\partial p'}{\partial t} &+ \frac{\gamma\bar{p}}{R}\frac{\partial u'_\theta}{\partial \theta} + \frac{\gamma p'}{R}\frac{\partial \overline{u_\theta}}{\partial \theta} + \gamma\bar{p}\psi(R_2)^2 R_2 Y p'(\theta, t) \\
&= -\frac{\overline{u_\theta}}{R}\frac{\partial p'}{\partial \theta} + (\gamma - 1)q', \quad (12)
\end{aligned}
$$

where R is the mean radius. For notational convenienc we define the normalized quantities

$$\tilde{p} = \frac{p'}{\gamma\bar{p}}, \quad \tilde{q} = \frac{\gamma - 1}{\gamma\bar{p}}q', \quad \tilde{u} = u'_\theta, \quad (13)$$

$$\xi = \gamma\bar{p}\psi(R_2)^2 R_2 Y. \quad (14)$$

The speed of sound is given by

$$a^2 = \frac{\gamma\bar{p}}{\bar{p}}. \quad (15)$$

Because $\bar{p}$ is possibly spatially varying, the speed of sound is also spatially varying and we write $a^2 = a^2(\theta)$. Note that $\tilde{p}$ is now dimensionless and $\tilde{q}$ has dimensions of $[\frac{1}{\text{time}}]$. We scale θ as

$$\theta \to R\theta, \quad (16)$$

so θ now has dimensions of [length]. We apply (13-16) to (11,12) to result in the system

$$\frac{\partial \tilde{u}}{\partial t} = -\overline{u_\theta}\frac{\partial \tilde{u}}{\partial \theta} - \tilde{u}\frac{\partial \overline{u_\theta}}{\partial \theta} - a^2\frac{\partial \tilde{p}}{\partial \theta} \quad (17)$$

$$\frac{\partial \tilde{p}}{\partial t} = -\gamma\tilde{p}\frac{\partial \overline{u_\theta}}{\partial \theta} - \overline{u_\theta}\frac{\partial \tilde{p}}{\partial \theta} - \frac{\partial \tilde{u}}{\partial \theta} - \xi\tilde{p} + \tilde{q}, \quad (18)$$

for $\theta \in [0, 2\pi)$. Equation (17) has units of $[\frac{\text{length}}{\text{time}^2}]$ and equation (18) has units of $[\frac{1}{\text{time}}]$.

Spatially Varying Parameters

We expand all of the quantities in terms of Fourier modes $\{\phi\}_n$ where

$$\phi_n(\theta) = \frac{1}{\sqrt{2\pi}}e^{in\theta}.$$

So the pressure is expanded as

$$\tilde{p} = \sum_n p_n, \quad p_n = \langle \tilde{p}, \phi_n \rangle \quad (19)$$

where $\langle \cdot, \cdot \rangle$ is the standard inner product on $L_2(0, 2\pi)$. The coefficients $(\cdot)_n$ are defined similarly with respect to all of the other parameters in the model. We assume that the spatially varying parameters have period m around the circle in addtion to some mean quantity. Thus, we define

$$
\begin{aligned}
\overline{u_\theta}(\theta) &:= \overline{u_\theta}_0 + \overline{u_\theta}_m[\phi_m(\theta) + \phi_{-m}(\theta)] \quad (20) \\
\xi(\theta) &:= \xi_0 + \xi_m[\phi_m(\theta) + \phi_{-m}(\theta)] \quad (21) \\
a^2(\theta) &:= a_0^2 + a_m^2[\phi_m(\theta) + \phi_{-m}(\theta)]. \quad (22)
\end{aligned}
$$

We assume that the heat-release feedback is given by $q(\tilde{u}) = K\tilde{u}$. The case where $q(\tilde{u})$ is nonlinear will be examined in section IV. The spatially varying heat-release gain is given by

$$K(\theta) := K_0 + K_m[\phi_m(\theta) + \phi_{-m}(\theta)]. \quad (23)$$

Galerkin Projection

We are interested in the stability of the first tangential mode, and therefore we apply a Galerkin projection of the system (17, 18) on to the first Fourier modes $+1, -1$. We have $[\phi_m + \phi_{-m}][\phi_1 + \phi_{-1}] = \phi_{m+1} + \phi_{m-1} + \phi_{-m+1} + \phi_{-m-1}$. Since we are focussing on the stability of the first mode only, we take $m = 1$ in the (20-23). This produces additional cross-coupling between mode $+1$ and mode -1.

The Galerking truncation of the system (17, 18) is

$$\dot{x} = Ax. \quad (24)$$

where $x = [u_1, u_{-1}, p_1, p_{-1}]^T$ and

$$A = \begin{bmatrix} -i\overline{u_\theta}_0 & -i\overline{u_\theta}_2 & -ia_0^2 & ia_2^2 \\ i\overline{u_\theta}_2 & i\overline{u_\theta}_0 & -ia_2^2 & ia_0^2 \\ K_0 - i & K_2 & -i\overline{u_\theta}_0 - \xi_0 & i\overline{u_\theta}_2(1-\gamma) - \xi_2 \\ K_2 & K_0 + i & -i\overline{u_\theta}_2(1-\gamma) - \xi_2 & i\overline{u_\theta}_0 - \xi_0 \end{bmatrix}. \quad (25)$$

III. LINEAR ANALYSIS OF SYMMETRY-BREAKING

In this section we present some computational results that evaluate effect of various symmetry-braking concepts on the eigenvalues of (25). In the following computational results, nominal values, $\xi_0 = 0.2, \overline{u_\theta}_0 = 0.05, a_0^2 = 1, K_0 = 0.5$ were used. In the following analysis, variations in the mean tangential flow had little effect on the stability of the system.

Damping Variation

Figure 2 shows the maximum real parts of the stable eigenvalues of A resulting from differenct combinations of ξ_0 and ξ_2. A value of zero in the figure indicates that all of the eigenvalues are in the right half of the complex plane. For a fixed value of uniform damping ξ_0, increasing ξ_2 decreases the overall damping of the system. Therefore, uniform damping is more effective than spatially varying damping.
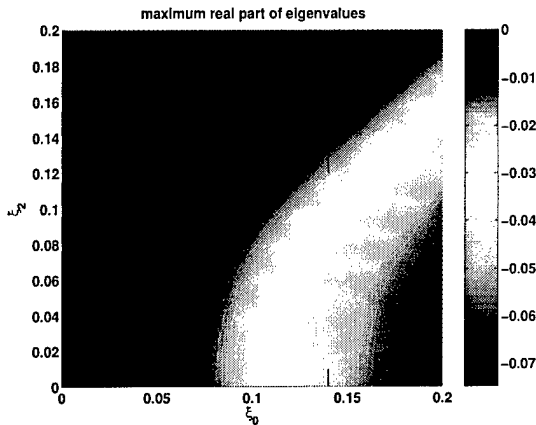

Fig. 2. Maximum real parts of stable eigenvalues for varying ξ_0 and ξ_2. A value of zero indicates that the linear system is unstable.

Speed of Sound Variation

Variation in the speed of sound is equivalent to changing the local resonance frequency. The results summarized in [2] show that such variations can be optimized to increase damping. Figure 3 shows the maximum real parts of the stable eigenvalues of A resulting from differenct combinations of a_0^2 and a_2^2. The figure shows that increasing the spatial variation of the speed of sound has a comparable effect to increasing ξ_0 (Compare with Figure 2). We see that changes in a_2^2 on the order of 10% of a_0^2 have a significant effect on the stability of A.

Heat-Release Gain Variation

Spatial variations in the heat-release coupling is an example of dynamic symmetry-breaking in the system. In other words, it may be possible to change the dynamic heat-release coupling, while maintaining mean quantities, such as temperature, density, etc. Figure 4 shows a root locus plot of the eigenvalues resulting from variations in K_2 and K_0. We see that increasing the spatial variation of the heat-release gain moves two eigenvalues to the left and moves the other two eigenvalues to the right. A contour plot similar to Figure 3 can be obtained for general combinations of K_2 for a constant K_0.
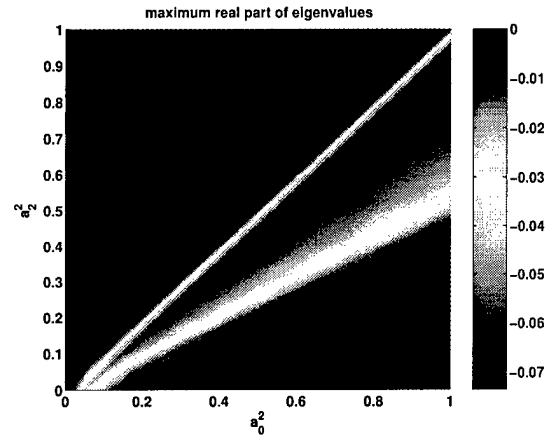

Fig. 3. Maximum real parts of stable eigenvalues for varying a_0^2 and a_2^2. A value of zero indicates that the linear system is unstable.
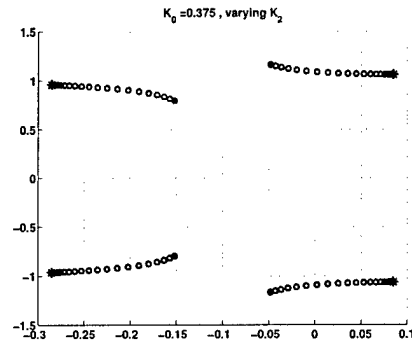

Fig. 4. Root locus plot showing eigenvalues for varying values of K_2. Eigenvalues corresponding with $K_2 = 0$ are shown in blue, and eigenvalues corresponding with $K_2 = 0.5$ are shown in blue.

IV. UNCERTAINTY PROPAGATION

We analyze uncertainty propagation with respect to the uncertainty measure, denoted by $v(\cdot)$, recently defined in [12]. For the present study, the output observable of interest is the amplitude of oscillation of the first tangential pressure mode. We denote by $\varpi(p)$ the resulting probability distribution of the pressure amplitude which results from a given distribution of uncertain model parameters. The uncertainty measure is therefore denoted by $v(\varpi)$. For the case of no uncertainty (all model parameters are exactly known) the resulting probability distribution will be a dirac-delta function and the resulting uncertainty metric will be $v(\varpi) = 0$.

As an example, we examine uncertainty propagation with respect to the measure $\varpi(p)$, that results from uncertain spatially varying sound speed, a_2^2 with different, fixed and certain, values of mean heat-release gain K_0. Similar results can be obtained for all of the other combinations of model parameters. Figure 5 shows the maximum real parts of the stable eigenvalues of A, with nominal values $a_0^2 = 1, \xi_0 =$

0.2. We examine cases with K_0 varying from 0.1 to 0.35 where a_2^2 is uncertain and may be up to 20% of a_0^2.

We compute the resulting uncertainty metric as defined in [12],

$$v_2(\varpi) = \min_{z \in \mathbb{R}} |\varpi - \delta_z|_2,$$

where $| \cdot |_2$ denotes the L^2-norm on the space $\mathcal{M}$ of probabilistic measure on $\mathbb{R}$. It is convenient to use the cumulative distribution function F_ϖ to compute the uncertainty measure. In this case, since $F_\varpi(p)$ is continuous, it can be shown that the uncertainty measure can be computed by

$$v_2(\varpi) = \left(\int_{-\infty}^{\infty} \left| \frac{1}{2} - \left| F_\varpi(x) - \frac{1}{2} \right| \right|^2 dx \right)^{\frac{1}{2}}. \quad (26)$$

We present the results of Monte-Carlo simulations of the PDE system (17, 18) where the heat-release coupling includes a saturation effect. From the analysis of the truncated model and Figure 5, we see that as K_0 increases, the system approaches the linear stability boundary, and hence, the amplitude should increase.
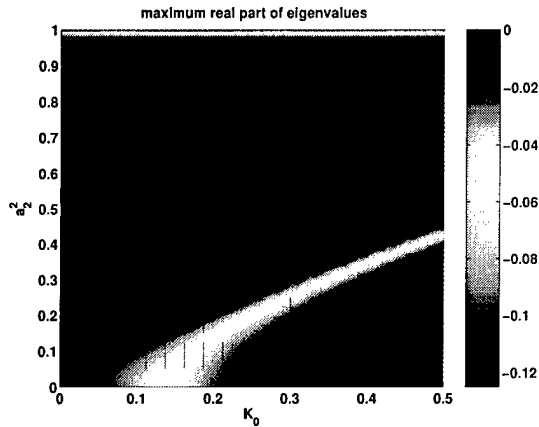

Fig. 5. Maximum real parts of stable eigenvalues. A value of zero indicates that the linear system is unstable.

The resulting distributions $\varpi(p)$ (shown as bars) and the respective normalized cumulative distribution functions $F_\varpi(p)$ (shown as lines) of the pressure amplitude are shown in Figure 6, for the nominal heat-release gain K_0 ranging from 0.1 to 0.35. For small vales of K_0 the system is linearly stable and therefore, all of the resulting amplitudes are zero. Therefore, the distribution of amplitudes for these cases is a delta function at zero. Because of this, the uncertainty propagation in terms of the metric (26) is also zero. As K_0 increases, the system approaches the linear stability limit, and the resulting distribution of amplitudes has a wider range. Therefore the uncertainty propagation corresponding with these cases is larger. When K_0 increases beyond the stability limit, the system enters a limit-cycle
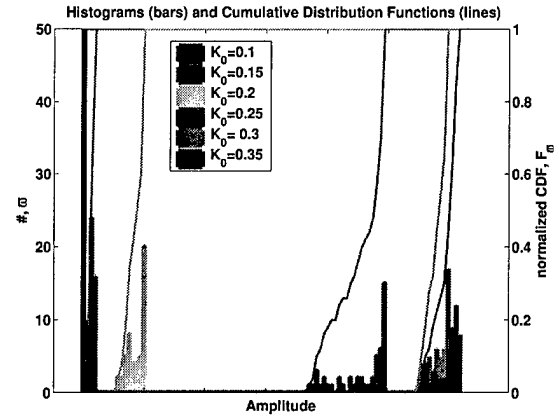

Fig. 6. Histograms and cumulative distribution functions of resulting amplitudes of oscillation for varying K_0 and uncertainty in a_2^2.

where the amplitude of oscillation is determined by the saturation nonlinearity and the amount of damping.

Figure 7 shows the values of the uncertainty metric based on the observable of pressure amplitude corresponding with different values of K_0 and uncertainty in a_2^2 up to 20% of a_0^2. We see that the lowest amount of uncertainty in the amplitude correspond with the highly stable cases. The uncertainty measure increases as the system approaches the stability boundary. The highest amount of uncertainty occurs near the linear stability boundary of A. However, for high values of K_0, the uncertainty propagation of a_2^2 to the pressure amplitude is actually decreased. We conjecture that the increased stability of the limit cycle explains the reduced uncertainty measure for the limit-cycling cases. An analytic study to investigate the relationship between a measure of hyperbolicity of the dynamics and the measure of uncetrainty is currently in progress.
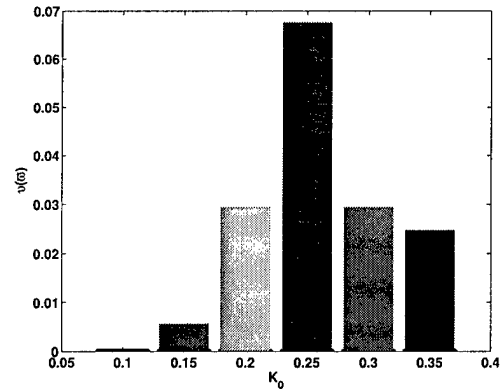

Fig. 7. Uncertainty metric $v(\varpi)$ versus K_0.

V. Conclusion

We have presented a simple one-dimensional thermo-acoustic model that is adequate for modeling oscillations of tangential acoustic modes. The model has been derived allowing for some spatially-varying parameters. We have investigated the effects of symmetry-breaking, or the deliberate introduction of spatial-variations in system parameters, on the system's linear stability properties. It was found that spatial variations in the steady tangential flow and damping do not enhance stability. Variations in the local speed of sound and the heat-release coupling gains significantly affects system damping. An example of uncertainty propagation through this system was presented in the context of spatially varying, uncertain, speed of sound, with varying levels of mean heat-release coupling. In this example, the uncertainty propagation given in terms of an uncertainty measure depending on the resulting distribution of the pressure amplitude, was the lowest for the limit-cycling case. An analytic study to investigate the relationship between a measure of hyperbolicity of the dynamics and the measure of uncetrainty is currently in progress.

Acknowledgements

References

[1] A. Banaszuk, G. Hagen, P. Mehta, and J. Oppelstrup. A linear model for control of thermoacoustic instabilities on an annular domain. *Proceedings of the IEEE Conference on Decision and Control*, 2003.

[2] O. O. Bendiksen. Localization phenomena in structural dynamics. *Chaos, Solitons, and Fractals*, 11:1621–1660, 2000.

[3] S. M. Candel. Combustion instabilities coupled by pressure waves and their active control. *Fourth International Symposium on Combustion, The Combustion Institute*, pages 1277–1296, 1992.

[4] F. E. Culick. Nonlinear behavior of acoustic waves in combustion chambers, parts I and II. *Acta Astronautica*, 3:715–757, 1976.

[5] A. P. Dowling. Nonlinear self-excited oscillations of a ducted flame. *Journal of Fluid Mechanics*, 346:271–290, 1997.

[6] G. Dullerud and R. D'Andrea. Distributed control of inhomogeneous systems with boundary conditions. *Proceedings of the 38th IEEE Control Conference on Decision and Control*, pages 186–190, 1999.

[7] M. Fleifil, A. M. Annaswamy, Z. A. Ghoneim, and A. F. Ghoniem. Response of a laminar premixed flame to flow oscillations: A kinematic modal and thermoacoustic instability results. *Combustion and Flame*, 106:487–510, 1996.

[8] M. B. Graf, T. S. Wong, E. M. Greitzer, F. E. Marble, C. S. Tan, H. W. Shin, and D. C. Wisler. Effects of nonaxisymmetric tip clearance on axial compressor performance and stability. *Transactions ASME Journal of Turbomachinery*, 1998.

[9] G. Hagen. Absolute stability of a heterogeneous semilinear dissipative parabolic pde. *Submitted to the 43rd IEEE Conference on Decision and Control*, 2004.

[10] C. A. Jacobson, A. I. Khibnik, A. Banaszuk, J. Cohen, and W. Proscia. Active control of combustion instabilities in gas turbine engines for low emissions. part 1: Phisycs-based and experimentally identified models of combustion instability. *AVI*, 2000.

[11] M. R. Jovanovic, B. Bamieh, and M. Grebeck. Parametric resonance in spatially distributed systems. *Proceedings of the 2003 American Control Conference, Denver, CO.*, pages 119–124, 2003.

[12] I. Mezić and T. Runolfsson. Uncertainty analysis of complex dynamical systems. *To appear in Proceedings of the 2004 American Control Conference*, 2000.

[13] P. M. Morse and K. U. Ingard. *Theoretical Acoustics*. Princeton University Press, 1968.

[14] A. Peracchio and W. Proscia. Nonlinear heat release/acoustic model for thermo-acoustic instability in lean premixed combustors. *ASME paper 98-GT-269*, 1998.

[15] E. P. Petrov, R. Vitali, and R. T. Haftka. Optimization of mistuned bladed discs using gradient-based response surface approximations. *AIAA-2000-1522*, 2000.

[16] A. J. Rivas-Guerra and M. P. Mignolet. Local/global effects of mistuning on the forced response of bladed disks. *Journal of Engineering for Gas Turbines and Power*, 125:1–11, 2003.

[17] B. Shapiro. A symmetry approach to extension of flutter boundaries via mistuning. *Journal of Propulsion and Power*, 14(3):354–366, 1998.

Workshop on Design of Dynamical Systems Robust to Uncertainty
January 15-16, 2004

United Technologies Research Center
Technical Education Center, Room A
411 Silver Lane
East Hartford, Connecticut

Organizers: Andrzej Banaszuk, Mark Myers, UTRC, Igor Mezic, UCSB, Jerrold Marsden, Caltech

Thursday, January 15

7:30 am: Registration and Continental Breakfast

Opportunities & Challenges in Design of Dynamics in the Presence of Uncertainty

8:00 am: Introduction to UTRC, Dr. Jean Colpin, Director, UTRC

8:30 am: Opening Remarks, Dr. Carey Schwartz, Program Manager, DARPA

9:00 am: Analytical Systems Engineering, Dr. Clas Jacobson, Director, Systems Dept, UTRC

9:30 am: Design of Robust Dynamical Systems: Key Principles and Workshop Overview
Andrzej Banaszuk, Pratt & Whitney Program Office, UTRC

10:00 am Break

Uncertainty Propagation in Dynamical Systems

10:30 am: Uncertainty in Analysis & Design: Dynamical Systems Perspective
Igor Mezic, Professor, Dept. Mechanical & Environmental Engineering, UCSB

11:30 am: Uncertainty and networks of dynamical systems
Jerrold Marsden, Professor, Control & Dynamical Systems, Caltech

12:30 pm: Working Lunch

1:30 pm: Uncertainty Propagation in networks of Dynamical Systems
Tamas Kalmar-Nagy, Mihai Huzmezan, UTRC

Decompositions of Large Networks of Dynamical Systems

2:00 pm: Analysis and Computational Methods for Dynamical Systems on Graphs
Sanjay Lall, Stanford and Matthew West, UC Davis

3:00 pm: On The Approximation of Complicated Dynamics, Michael Dellnitz, Department Chair, Applied Mathematics, University of Paderborn

4:00 pm: Break

4:30 pm: Graph Decomposition Methods
Robert LaBarre, Subbarao Varigonda, UTRC

5:00 pm Propagation of Invariant Measures in Interconnected Dynamical Systems
Leonid Bunimovich, Professor, Georgia Institute of Technology

6:00 pm: Dinner

Friday, January 16

7:30 am: Continental Breakfast

Iterative Methods for Dynamical Systems

8:00 am: Spectral Balance: Frequency Domain Framework for Analysis and Control of Dynamical Systems in Presence of Disturbances
Andrzej Banaszuk, Pratt & Whitney Program Office, UTRC

9:00 am: Newton Iterations for Persistent Periodic Oscillations in Dynamical Systems (KAM Theory), Umesh Vaidya, UCSB

9:30 am: Break

Design Of Robust Dynamical Systems

10:00 am: Symmetry vs Robustness of Dynamical Systems, Prashant Mehta, UTRC

10:30 am: Aeroengine Combustion Stabilization, Gregory Hagen, UTRC

11:00 pm: Coordinated Control of UAVs, Troy Smith, Shawn Shadden, California Institute of Technology

11:30 pm: DNA example, Igor Mezic, Professor, UCSB, Igor Fedichenia, UTRC

12:00: Working Lunch

1:00 pm: Coarse Methods Analysis of Complex Systems
Yannis Kevrekidis, Professor, Dept. Chemical Engineering, Princeton University